This is to certify that the
thesis entitled

ESTIMATION OF EUGENOL DIFFUSION COEFFICIENT IN LLDPE
USING FTIR-ATR FLOW CELL AND HPLC TECHNIQUES

presented by

Gaurav Dhoot

has been accepted towards fulfillment
of the requirements for the

Masters degree in Packaging

Major Professor's Signature

12/12/08

Date

# ESTIMATION OF EUGENOL DIFFUSION COEFFICIENT IN LLDPE USING FTIR-ATR FLOW CELL AND HPLC TECHNIQUES

By

Gaurav Dhoot

A THESIS

Submitted to:
Michigan State University
in partial fulfillment of the requirements
for the degree of

Master of Science

Packaging

2008

## ABSTRACT

ESTIMATION OF EUGENOL DIFFUSION COEFFICIENT IN LLDPE USING FTIR-ATR FLOW CELL AND HPLC TECHNIQUES

By

Gaurav Dhoot

A time-resolved Fourier transform infrared-attenuated total reflectance spectroscopy (FTIR-ATR) technique was set up and used to study the diffusion of eugenol through linear low density polyethylene (LLDPE) at 16, 23 and 40°C. The 1514 $cm^{-1}$ peak for eugenol (aromatic -C=C- stretching) was monitored over time to estimate the diffusion coefficient (*D*). The Fickian model was found to fit well to the experimental data and the *D* value of eugenol through LLDPE was estimated to be between 1.05±0.01 and 13.23±0.18 x $10^{-10}$ $cm^2$/sec for temperature range of 16 to 40°C. The FTIR-ATR results were compared with one and two side diffusion process and quantified by high performance liquid chromatography (HPLC) technique. Eugenol sorbed in LLDPE samples at different times, was extracted in methanol and the concentration determined by HPLC. The diffusion coefficient by both two-sided and one-sided HPLC system was found to be approximately three times higher than the FTIR-ATR values although they were in the same order of magnitude of $10^{-10}$ $cm^2$/sec. The difference between the FTIR-ATR and HPLC results was mainly attributed to difference between the two measuring techniques. Eugenol diffusion in ethylene vinyl acetate (EVA) films was also studied. The EVA film swelled as soon as it came in contact with eugenol. The FTIR-ATR technique enabled to detect hydrogen bonding interactions between eugenol and EVA.

**Acknowledgement**

This thesis is the result of two years of research work at School of Packaging, Michigan State University. In these two years, I had opportunities to work with many people who have directly or indirectly contributed towards this work. It is a pleasure to convey my gratitude to them all in my humble acknowledgment.

Firstly, I would like to express my gratitude to Dr. Rafael Auras for his supervision, advice, and guidance from the very early stage of this research. He not only gave me the opportunity to work in the field of my interest, but also made me a part of a number of important industry projects, the experience of which would prove very crucial in my career. Above all and the most needed, he provided me unflinching encouragement and support in various ways. His truly scientific approach to problems, his knack of managing resources and people, and his ultimate passion and hardworking nature have exceptionally inspired and enriched my growth as a student and a researcher. I am truly thankful to him in many more ways than I can express in words.

I wish to express my warm and sincere thanks to Dr. Maria Rubino, who has introduced me to many of the core packaging subject. I am grateful to her for her guidance, advice and motivation for this project. I gratefully acknowledge Dr. Herlinda Soto-Valdez for her advice, supervision, and crucial contribution, which made her a backbone of this research and so to this thesis. I would specially like to mention the pains she had taken to help me with the laboratory work. The perfection she puts in her work and her humble nature have always motivated me. I would like to express my sincere

thanks to Dr. Kirk Dolan for his help and guidance in this project. The motivation and encouragement he provided fuelled in me the passion to strive for the best.

I would like to extend my acknowledgement to Dr. Susan Selke, Dr. Twede, Dr. Bruce Harte, Dr. Eva Almenar and all other faculty members for the knowledge they have granted me during the last two years. I would also like to thank the staff members Linda, Colleen, April and Kelby for their assistance in the department office and laboratory. I am also grateful to the CFPPR members for funding this project.

I wish to thank Dharmendra Mishra and Shantanu Kelkar for all the efforts and help they have provided me with developing the MATLAB codes for this thesis. I am indebted to all the past and present graduate students in the research group- Turk, Sukeewan, Sung Wook, Hayati, Praveen, Kang, Pankaj Kumar and Santosh Medival for all their help with my research work and all the fun and joy that we have shared together. I owe my thanks to all my friends at MSU for making this two year endeavor full of fun, joy and happiness.

I am grateful to my parents for taking all the efforts and pains to send me to the US to undertake this study. I am thankful to them for their unconditional and endless love and support. I would like to express gratitude towards my brother-in-law Hemant Mundra, my sister Sapana and my cute niece 'Gondu'- Rhea for all the love and affection I have received from them.

Finally, I dedicate this thesis to all the souls who have strived to leap beyond the matrix of illusion, to take our entire reality to a new level of consciousness.

Gaurav Dhoot

## Table of Contents

## List of Tables

## List of Figures

## Nomenclature

| | |
|---|---|
| $D$ | Diffusion coefficient |
| $\mu$ | Chemical potential |
| $z$ | Distance in the polymer film |
| $L$ | Polymer film thickness |
| $C$ | Permeant concentration |
| $C_{eqb}$ | Permeant concentration at equilibrium |
| $t$ | Time during diffusion process |
| $T_g$ | Glass transition temperature |
| $m$ | Number of terms in the infinite series |
| $M_t$ | Mass gain of permeant at time $t$ |
| $M_{eqb}$ | Mass gain of permeant at equilibrium |
| $E$ | Electric field amplitude |
| $E_0$ | Initial electric field amplitude |
| $\gamma$ | Evanescent wave decay coefficient |
| $d_p$ | Depth of penetration of evanescent field |

| | |
|---|---|
| $n$ | Refractive index |
| $n_1$ | Refractive index of the polymer film |
| $n_2$ | Refractive index of the ATR crystal |
| $n_{12}$ | Ratio of $n_1$ to $n_2$ |
| $\theta$ | Incident angle of infrared beam |
| $\theta_c$ | Critical angle of penetration of infrared beam |
| $\alpha$ | Absorption coefficient |
| $I$ | Reflected infrared intensity |
| $I_0$ | Incident infrared intensity |
| $n'$ | Complex refractive index |
| $k$ | Attenuation index |
| $N$ | Number of reflections of infrared beam in ATR crystal |
| $T$ | Thickness of ATR crystal |
| $l$ | Length of ATR crystal |
| $d_e$ | Effective thickness/effective depth of penetration of IR beam |
| $e$ | Molar extinction coefficient |
| $\lambda$ | Wavelength of infrared radiation |
| $A$ | Infrared absorbance of infrared radiation |
| $A_t$ | Infrared absorbance of permeant at time $t$ |
| $A_{eqb}$ | Infrared absorbance of permeant at equilibrium |

| | |
|---|---|
| $\theta_{eff}$ | Effective angle of penetration of infrared beam |
| $\theta_{face}$ | Face angle of the ATR crystal |
| $E_D$ | Activation energy |
| $\delta$ | A very small value to cause small increment in $D$ for sensitivity analysis |

# Chapter 1

# Introduction

## 1.1 Background

From a humble growth in 1930-40's, when plastics like polyethylene were invented, today, plastics due to their versatility have found applications in many different fields. One application which has undergone a revolution by use of plastics is packaging. While 40% of plastics in Europe are utilized for packaging applications, nearly 50% of food is packaged in plastic packaging [1]. In the US, plastics are projected to outpace paper as packaging material of choice in the food sector, with a forecasted growth of 3% per year through 2010 [2]. There are various advantages of plastics that have made them the most popular materials for food packaging applications, like [1]-

- they can be melted and molded into different rigid shapes or into films
- they are generally chemically inert
- they are cost effective in meeting market needs
- they are lightweight
- they provide choice in respect of transparency, color, heat sealing, heat resistance and barrier.

However, polymeric materials being semi-crystalline are not completely impermeable like glass or metals and have an inherent disadvantage which allows the transfer of gases, liquids, polymeric processing additives, other volatile/non-volatile compounds across their boundary layers. Such transfer of compounds is also known as mass transfer.

Mass transfer has been subject of study in polymer science with applications in many varied fields. One of the important areas affected by mass transfer phenomena is packaging. Aroma, flavor loss due to scalping, migration of undesired compounds, permeation of gases through package walls leading to organoleptic alterations in food, are some of the common problems that need to be addressed by packaging material scientist [3, 4].

The two major mechanisms of mass transfer in packaging materials are diffusion and sorption. While diffusion relates the rate of transfer of a compound across the package wall, sorption is related to the mass uptake of the compound by the packaging material. The extent of diffusion and sorption are measured by diffusion and solubility coefficient, respectively. While solubility coefficient measures the rate of mass uptake by the package material, the partition coefficient defined as ratio of concentration of compound in the product (food) and the polymer (package wall), actually governs the overall sorption that would occur [5, 6].

Mass transfer processes in packaging systems are usually classified as migration, scalping/sorption and permeation. Migration is the release of compounds like polymeric processing aids (plasticizers, UV stabilizers etc.) from the package walls into the food, while scalping can be described as the sorption of flavor/aroma compounds by packaging material from food e.g. limonene sorption from orange juice. Permeation is the process resulting from diffusion and sorption/de-sorption of compound (permeant), and it is often expressed as the product of diffusion and solubility coefficients [5]. Permeation occurs in steady and unsteady state. The rate of concentration change of the permeant across the polymeric package wall varies in the unsteady state, before it finally becomes constant in

the steady state. Both sorption and diffusion are important factors in the unsteady state, but in the steady state, diffusion takes over and sorption reaches a dynamic equilibrium [6]. Since diffusion is an important mechanism governing mass transfer processes, it plays a vital role in determining the barrier properties of polymeric films and hence also the shelf life of packaged product.

On other hand, another packaging technique going beyond barrier to enhance product shelf life is active packaging. It is a technique employing active substances to interact with the product environment and sometimes the product itself to bring an increase in the product shelf life [7]. Various active packaging techniques have been developed such as oxygen scavenging, moisture scavenging, ethylene scavenging, ethanol release, odor scavenging, aroma release, flavor release, carbon dioxide release, pesticides release, antimicrobials, and antioxidants release [7, 8]. Antioxidants are usually added to polymers to protect them from oxidation, but, there are also packages where the release of the antioxidant like butylated hydroxytoluene (BHT) from the polymer films is used to improve the product shelf life. Hence, mass transfer is an important phenomenon in active packaging too. In order to study the rate of release of these active substances and to tailor make the package according to the food product requirement, it is essential to carry out the diffusion analysis of these substances. Hence, diffusion kinetics is an important field of study in packaging science.

### 1.2 Motivation

Many iso-static and quasi-iso-static techniques have been developed to study the diffusion process based on the use of permeation cells (non condensable gases) with gas

chromatography (GC) or high performance liquid chromatography (HPLC) systems (includes use of chromatography for separation of compounds and UV, IR etc. detection techniques) and gravimetric techniques (usually for condensable gases) [5]. Many other techniques that have been explored are based on microscopy, inverse gas chromatography using capillary columns [9], nuclear magnetic resonance (NMR) spectroscopy [10], proton-induced X-ray emission (PIXE) or proton-induced gamma-ray emission (PIGE) [11]. The use of Infrared Spectroscopy (IR) in various modes like transmission Fourier transform spectroscopy (FTIR) [12], FTIR imaging [13] and FTIR- ATR (attenuated total internal reflectance) imaging [14], and FTIR – ATR spectroscopy [15-35] for diffusion analysis has been studied widely by many research groups.

FTIR-ATR system has various advantages over other conventional immersion techniques, in which the polymer sample is first immersed in the permeant (in case of liquids) for different time lengths, and then the permeant sorbed in the polymer quantified by weight or concentration in gravimetric instrument or by chromatography, respectively. Unlike in these techniques, with FTIR-ATR, it is possible to monitor the diffusion process over the entire length until the equilibrium condition is reached, the experiment times are sometimes shorter than conventional techniques, the permeant and polymer chemical interactions can be monitored [16, 28, 32], and the change in polymer conformational regularity [36], crystallinity [16] and swelling can be observed as the diffusion proceeds [16, 33]. There have been studies where it has been used successfully for determining the diffusion coefficients in multi-component systems [15, 17, 27] and in case of polymer – polymer inter-diffusion [18] and monomer - polymer diffusion [34]. In the medical field, FTIR ATR technique has been valuable in studying controlled release

of drugs from suspensions [22]. The low penetration depth of attenuated infrared radiation helps determine the mass transfer in ultra-thin films [23] and polymer membranes [27, 37].

In earlier studies involving FTIR-ATR, most of the systems consisted of a polymer film sandwiched between a stationary permeant reservoir and an ATR crystal. In these cases, optimum contact between the polymer film and the crystal was ensured by solution or melt casting, or hot pressing the film over the crystal. However, this meant that the morphological properties of such a film would be different from commercially available film, and hence it would be difficult to correlate their mass transfer properties. Another problem was the possibility of loss of contact between the film and the crystal in cases where the permeant would cause swelling in the film [15]. To overcome this problem, many groups used the flow pressure of gas or liquid permeant over the polymer film to ensure good contact with the ATR crystal [15, 27, 35, 36], although the experimental conditions to obtain proper contact and successful fitting of the experimental data are not always detailed and explained. Very few researchers like Yi et al, [35] have actually evaluated the change in diffusion coefficient caused by change in permeant flow pressure. Until now most studies involved polymer/permeant systems with distinct IR absorbance peaks. These however restrict the choice of polymer/permeant system that can be analyzed using this technique.

### 1.3 Goal and Objectives

The goal of this study was to design and implement a FTIR-ATR based technique for diffusion analysis of organic compound from packaging material.

The objectives of this study are:

- To configure and setup an FTIR-ATR based equipment for its application in determining the diffusion coefficient.
- To determine various factors affecting the outcome of the technique and to optimize the conditions as per the chosen polymer/permeant system.
- To determine the diffusion coefficient of eugenol in LLDPE film at different temperatures.
- To compare the results from FTIR-ATR based technique with HPLC based technique.

# Chapter 2

## Literature Review

The growing use of plastics in food packaging is posing a great challenge, especially in preserving the quality of food in terms of its sensory characteristics like flavor and aroma. Polymers being organic compounds are very often susceptible to interactions with organic flavor and aroma compounds in food. Diffusion of these compounds through the packaging material not only limits the shelf life of such foods, but any interaction products of such compounds may lead to off-flavors and even potentially dangerous reaction compounds. Hence, as the variety of food products in the market and their complexity in terms of flavor and aroma is increasing, it is a challenging task for packaging scientists to evaluate, develop and manufacture a package with tailor-made barrier property.

There are various techniques that are used for determining the barrier properties in packaging materials. Some of these are listed in section 1.2. Although, the fundamentals of the diffusion process remain the same, different techniques have different permeant detection methods, and hence work by different principles. Since, the current study deals with use of FTIR-ATR and HPLC based techniques for diffusion measurement, it is essential to know the theory and the previous work performed with these techniques.

In this chapter, after a brief discussion on diffusion analysis model, the method of Fourier Transform Infrared (FTIR) Spectroscopy and HPLC is described. HPLC has long been used in migration analysis in different polymers. A section of this chapter is dedicated to the review of this technique for mass transfer analysis. Though FTIR-ATR

has been in use since 1950's, its use in diffusion analysis is more recent. It wasn't until 1990's that a theoretical model of FTIR-ATR diffusion analysis was developed based on theory of diffusion applied in special case of attenuated radiation in ATR mode. A detailed theory and mathematical approach is discussed in this review. In order to understand the versatility of the FTIR-ATR technique, a brief review of the previous work using this technique is presented.

Eugenol was chosen as the organic permeant in this study. This chapter also reviews some of the important properties of eugenol which marks its potential in food application.

## 2.1 Theory of Diffusion

The fundamental driving force causing a molecule to transfer within the polymer, or between a polymer and a surrounding phase, is the tendency to equilibrate the chemical potential of the molecules (permeant). Since the packaging materials separate the aroma/flavor compounds in food from the outside atmosphere and vice versa, there is always a tendency for these compounds and atmospheric gases to reach a thermodynamic equilibrium. This transfer of permeant molecules across the polymer film is also known as diffusion. Diffusion can also be defined as the process in which components are transported from one part of a mixture to another by random molecular motions [38, 39].

In a typical mass transfer process, the permeant first gets sorbed by the polymer surface at the higher concentration side ($C_1$), then, diffuses through the film before being desorbed at the low concentration side ($C_2$), as shown in Figure 2.1 [5].

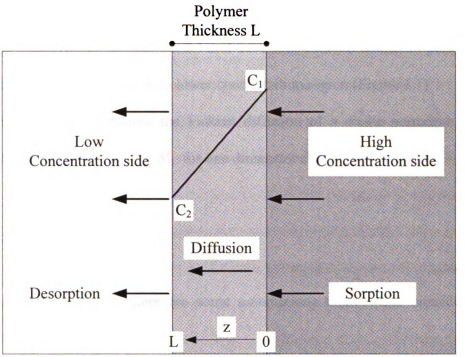


**Figure 2.1** Mass transfer involving sorption, diffusion and de-sorption

According to Fick's law, in a diluted, unidirectional, isotropic polymeric phase, the rate of transfer of the diffusing permeant $F$, per unit area, is given by equation 2.1.

$$F = -D\frac{\partial \mu}{\partial z} \tag{2.1}$$

where $D$ is the thermodynamic transport coefficient, $\mu$ is the chemical potential of the diffusing permeant and $z$ is the diffusion distance. For a single component/permeant, and for dilute system, the chemical potential can be replaced by concentration $C$ [38].

$$F = -D\frac{\partial C}{\partial z} \tag{2.2}$$

where $C$ is the permeant concentration and $D$ is now called the permeant diffusion coefficient. The negative sign in equation 2.1 and 2.2 indicates the direction of permeant flow from higher concentration region to lower concentration region (Figure 2.1).

For unsteady state diffusion, the Fickian diffusion of a single permeant in a polymer film as described by Crank [38], for one dimensional continuity equation:

$$\frac{\partial C}{\partial t} = D\frac{\partial^2 C}{\partial z^2} \tag{2.3}$$

where $t$ is the time. However, there are some assumptions made while considering equations 2.2 and 2.3.

1. The value of $D$ is assumed to be independent of both, the permeant concentration and the polymer relaxation.
2. The diffusion process through the polymer material is unidirectional (direction z) and perpendicular to the flat surface of the polymer film and negligible amount diffuses through the film edges.
3. Solutions to diffusion equations are obtained for particular cases derived from the corresponding boundary and initial conditions.

Diffusion mechanisms differ at temperatures above and below the glass transition temperature ($T_g$), of the polymer. At temperatures $T > T_g$, polymers are called 'rubbery' and in this case the polymers respond quickly to physical change induced by the diffusing permeant. The polymer chains relax and reach new state of equilibrium faster than the time required for the diffusing permeant to pass through the polymer matrix. In the case

of 'glassy' polymers when $T < T_g$, the polymer chains being stiff, do not have enough time to relax and reach new state of equilibrium before the advance of the diffusing permeant.

Hence it can be summarized that [40]:

- In rubbery polymers diffusion is generally described by Fickian behavior, except in cases where sorption equilibrium cannot be achieved at polymer interfaces.
- In case of glassy polymers diffusion process is more complex and may be described by three mechanisms:

1. Case I or Fickian diffusion, where relaxation of polymer-permeant system is faster than diffusing permeant.
2. Case II diffusion, where relaxation of polymer-permeant system is slower than diffusing permeant.
3. Anomalous diffusion behavior, where the polymer-permeant system has relaxation rates comparable with the diffusing permeant and the diffusion process is predominantly affected by 'holes' and 'micro cavities' in the polymer matrix.

As seen in Figure 2.1, a diffusion model developed for diffusion in plane sheet, for constant surface concentrations can be given as follows [38]:-

Boundary conditions are:

$$C = C_1,\ z = 0,\ t \geq 0, \tag{2.4}$$

$$C = C_2,\ z = L,\ t \geq 0, \tag{2.5}$$

$C = f(z),\ 0<z<L,\ t = 0,$ (2.6)

The solution of equation 2.3 with boundary conditions of equation 2.4 and 2.5, and initial conditions of equation 2.6, in the form of trigonometrical series is –

$$C = C_1 + (C_2 - C_1)\frac{z}{L} + \frac{2}{\pi}\sum_{m=1}^{\infty}\frac{C_2\cos m\pi - C_1}{m}\sin\frac{m\pi z}{L}\exp\left[\frac{-Dm^2\pi^2 t}{L^2}\right] + \frac{2}{L}\sum_{m=1}^{\infty}\sin\frac{m\pi z}{L}\exp\left[\frac{-Dm^2\pi^2 t}{L^2}\right]\int_0^L f(z')\sin\frac{m\pi z'}{L}dz' \quad (2.7)$$

In case of sorption by a membrane, in case of uniform initial concentration, i.e if the region $-L<x<L$ is initially at concentration $C_0$ and surfaces are kept constant concentration $C_1$, equation 2.7 becomes,

$$\frac{C - C_0}{C_1 - C_0} = 1 - \frac{4}{\pi}\sum_{m=0}^{\infty}\frac{(-1)^m}{2m+1}\exp\left[\frac{-D(2m+1)^2\pi^2 t}{4L^2}\right]\cos\left[\frac{(2m+1)\pi z}{2L}\right] \quad (2.8)$$

If $M_t$ denotes the mass of diffusing permeant, which has entered the sheet at time $t$ and $M_{eqb}$ is the corresponding mass at infinite time, then we obtain the Fickian mass uptake equation 2.9. The following equation is obtained after performing mathematical operations similar to equation 16 in Appendix F.

$$\frac{M_t}{M_{eqb}} = 1 - \frac{8}{\pi^2} \sum_{m=0}^{\infty} \frac{1}{(2m+1)^2} \exp\left[\frac{-D(2m+1)^2 \pi^2 t}{4L^2}\right] \tag{2.9}$$

The details of the method employed in this study, to solve this equation are given in Chapter 3 in sections 3.6 and 3.7.

## 2.2 High Performance Liquid Chromatography (HPLC)

The first work in chromatography is attributed to the work done by a Russian scientist, Mikhail Tswett in the early 20$^{th}$ century [41]. His work involved separation of mixture of different plant pigments by placing the extracts in glass column filled with calcium carbonate particles. Different color bands were observed as different pigments got adsorbed on the solid particles and moved through the columns at different speeds, this resulting in their separation. Hence, this technique was coined 'chromatography', a Greek word for 'color writing' [41].

Some of the defining properties of the chromatographic process are:

1. The stationary and mobile phases are immiscible.
2. The mixture of analytes to be separated is passed through one side of the column containing the stationary phase.
3. Mobile phase flows from one end of analytes deposition towards the other.
4. Different rates or ratios of separation of analytes from the mixture, takes place multiple times along the length of the column.
5. The separated analytes eluting at different rates, can be detected by different detection methods and their qualitative and quantitative analysis can be done.

In HPLC the mobile phase is a single or a mixture of liquids. The HPLC market today is much larger than gas chromatography (GC) because of some disadvantages with the latter technique, like limitation of the analytes to relatively low molecular weight and low polarity, and thermally stable. However, a vast number of bio-chemically important analytes fall beyond this category. The partitioning of the analytes between non polar mobile phases and silica particles with adsorbed water is called 'normal phase' chromatography. The more popular method is to flow more polar mobile phase containing the analyte mixture through non polar covalent bonded organic groups, known as 'reverse phase'. The stationary phase in HPLC consists of an organic monomolecular layer chemically bonded to the free silanol groups on the silica particle surface. The most common free group is a long-chain n-C18 hydrocarbon (octadecyl silyl group, ODS) [41].

### 2.3 A brief review of the use of HPLC in packaging for mass transfer determination

Migration from packaging materials is an important subject in food and packaging industry, because the migrant compound may cause a change in organoleptic properties and may also induce toxicity within the food. Although, the food contamination can be induced both by external-environment/package interface and the internal interface, migration is mainly defined as transfer of migrants from package to the food. The process of migration is strongly affected not only by the thermodynamic equilibrium (solubility or partition coefficient) but also the kinetics of mass transfer (diffusion coefficient). Hence it is also desirable to determine the diffusion parameters for a migrant in package-

food simulant system [5]. There are many techniques that can be employed in measuring migration, and HPLC is one of the most widely used techniques [42].

In 1982, Snyder and Breder [43] described the HPLC method for determination of 2,4- and 2,6- Toluenediamine in aqueous extracts of food contact boil in bag and retort pouches. The aqueous extracts were obtained by filling the boil in bag and the retort pouch with pure water, then sealing them and then exposing the bags to water bath (212°F) and the retort pouches to retorting process (212°F, 15 psi). An acetonitrile: water (10% v/v) mobile phase and UV detector was used in this study. Later in 1985, Snyder and Breder [44] evaluated a new FDA migration cell for studying the migration of components of plastic food packaging materials into various food simulating solvents. The study involved migration of styrene from polystyrene at 40 and 70°C in food simulating solvents: water; 3% acetic acid; 8, 20, 50, and 100% ethanol; corn oil; HB-307; heptane; hexadecane; and decanol. Diffusion coefficient values determined for styrene migration from polystyrene at 40 and 70°C were $3 \times 10^{-13}$ and $4 \times 10^{-12}$ $cm^2/sec$, respectively.

Jenke in 1992 [45], examined the migration of several low molecular weight model solutes through a polypropylene/polyolefin blend via a permeation-cell experimental design. A reverse phase HPLC technique using Supelcosil LC8-DB stationary phase and mobile phase of methanol:water (1:1) with small amount of trifluoroacetic acid was used to determine phthalate and paraben mixture concentrations. The analytes were detected using 220 nm wavelength of UV. Nerin et al. [46] studied a new method to determine antioxidants and UV stabilizer content of polymer film. A procedure consisting of connecting in series two different HPLC columns, one for size-

exclusion chromatography (SEC) and the second one a normal-phase (silica) column was developed. An automatic three-way switching valve was placed between the two columns. Through the valve, the polymer was drained whereas the rest of the compounds, a group of antioxidants and UV stabilizers, were separated and analyzed in the second column.

In 1998, Morelli-Cardoso et al. [47] determined the migration of di(2-ethylhexyl) phthalate (DEHP) from poly(vinyl chloride) (PVC) cling films into various food simulants. A Nucleosil $C_{18}$ guard column was used for the HPLC analysis. The mobile-phase was methanol:water (96:4 v/v), at a flow rate 0.7 ml/min; oven 30°C and UV detector (254 nm).

O'Brien et al. [48] in 1999, compared the experimental migration data to the theoretical migration models for high density poly(ethylene) (HDPE). The migration experiments were performed using single side cells, by exposing only one surface to the fatty food simulant olive oil. The test conditions selected were of 10 days at 40°C, for 2 and 6 hours at 70°C. Concentrations of two UV stabilizers, 2-Hydroxy-4-*n*-octyloxy benzophenone and 2-(2-Hydroxy-3-*t*-butyl-5methylphenyl)-5-chlorobenzotriazole were determined using HPLC. In a later study, similar work was done to compare the results of theoretical migration model with the experimental values for polypropylene (PP) [49]. A review of the migration of substances from food packaging mentioned the use of HPLC by FDA (Food and Drug Administration) and EC (European Commission) researchers. The studies using HPLC techniques for migration involved determination of Bisphenol – A (BPA) in epoxy resins and diglycidyl ether of BPA (DGEBA) migration from plastic films [50].

A reverse phase HPLC based technique was used by Caner and Harte to determine the Irganox 1076 migration concentration from PP film exposed to high-pressure processing [51]. The results showed that there was no significant difference in the concentration of Irganox 1076 migrating from PP, and into the food simulant liquid (FSL) for pressure-treated vs non-treated samples. The phthalates (endocrine disrupters) released from food-contacted plastics into aqueous solution during microwave conditioning were measured by Jen and Liu [52] in 2006. The released phthalates in aqueous solution were diffused through a cellular dialysis membrane into the perfusion stream and thus enriched prior to HPLC analysis. The dimethyl phthalate (DMP), diethyl phthalate (DEP) and dibutyl phthalate (DBP) were well separated by a C-18 column and eluted gradient from 40 to 90% aqueous acetonitrile (at pH 6.0) and 1.0 to 1.5 ml/min flow-rate. Detection was carried out with an UV detector at 225 nm.

In 2008, Silva et al. [53] studied the migration of the model migrant 1,4-diphenyl-1,3-butadiene (DPBD) from LDPE film into two representative aqueous foodstuffs i.e orange juice and tomato ketchup. The simulants were put into contact with the additive loaded plastic inside a migration cell. After exposure to different time-temperature conditions, the extraction was carried out with hexane and acetonitrile. The extracted DPBD was detected by HPLC at 330 nm. Migration was not detectable in tomato ketchup and effective diffusion coefficients of DPBD determined in the polymer-orange juice system were $2.9 \times 10^{-12}$, $3.7 \times 10^{-12}$, and $7.5 \times 10^{-12}$ $cm^2/sec$ at 5, 25 and 40°C, respectively.

Thus, from this review, we can see that HPLC based methodology has been widely used since many years, by several research groups for mass transfer studies. Also,

the fact that this technique has been used by FDA and EC researchers further reinforces the reliability of this conventional technique.

## 2.4 Fourier Transform Infrared (FTIR) Spectroscopy

The infrared (IR) wavelength region can be divided into near infrared (13,300 to 4000 $cm^{-1}$), mid infrared (4000 to 400 $cm^{-1}$) and far infrared region (400 to 40 $cm^{-1}$) [41]. Molecules absorb IR radiation when a chemical bond in the molecule vibrates at the same frequency as the incident radiation. Only molecules that undergo change in dipole moment during vibration absorb IR radiation. Hence, elements like $H_2$, $O_2$, etc. with symmetrical diatomic molecules are IR inactive, while molecules like HCl, CO etc. with asymmetrical diatomic molecules have a dipole moment and are therefore IR active. IR spectrogram is a spectrum displaying absorption peaks at different wavelengths and with different intensities based on the chemical group present in the substrate. Chemical groups undergo various vibrations like stretching, bending, rocking at scissoring at characteristic wavelength, hence an IR spectrogram of a particular chemical compound becomes a characteristic finger print unique to that compound.

Along with the applications, the FTIR machines too evolved, the double beam dispersive grating spectrometers were replaced by FTIR machines based on Michelson interferometer in 1980's. The Michelson interferometers, as the name suggests makes use of the fact that two beams of light i.e, one from the movable mirror (possible to change path length) and one from the fixed mirror (same path length) when brought together may undergo a destructive or constructive interference depending on the difference in their phases. Hence, depending on the velocity of the movable mirror it is possible to achieve a wide wavelength of IR radiation even when the IR source is monochromatic. Such a system enabled higher speed, better signal to noise ratio and precision than their

predecessors. Hence, they are now being used widely in qualitative and quantitative analsyis of many organic compounds [41].

## 2.5 FTIR-ATR (Fourier Transform Infrared–Attenuated total reflectance) Spectroscopy

Much credit in development of internal reflection spectroscopy is given to work done by N.J. Harrick in Philips Laboratories and Fahrenfort in Dutch Shell Laboratories in 1950 – 60's, who proposed and developed the technique independently. Internal reflection spectroscopy is a technique of recording the optical spectrum of sample material that is in contact with denser transparent medium and then studying the wavelength dependence of reflectivity of this interface by introducing light into the denser medium. The reflectivity measured depends upon the interaction of the evanescent wave with the sample material and hence is characteristic to the sample material [54].

Infrared radiation traveling from denser medium undergoes total internal reflection at the interface with the rarer medium only when the incident angle $\theta$ exceeds critical angle $\theta_c$.

$$\theta_c = \arcsin\left(\frac{n_1}{n_2}\right) \tag{2.10}$$

where $n_1$ and $n_2$ represent the refractive indices rarer medium (polymer) and dense (ATR crystal), respectively.

Some of the properties of the evanescent field are as follows [55]:

1. The field intensity in the rarer medium is not zero and the instantaneous normal component of energy flow in this medium has time average zero. Hence, there is no loss of energy and the propagating radiation in the denser medium is totally internally reflected.

2. The evanescent field in the rarer medium is non-transverse wave and has components in all spatial orientations.

3. The evanescent field is confined to the surface of the rarer medium and decreases in intensity with distance normal to the surface in this medium.

4. A nonzero energy flow in the direction parallel to the surface results in displacement of the incident and reflected waves, also known as Goos – Hanchen shift.

The evanescent wave produced at the interface of the crystal and the polymer looses its magnitude as it travels further in the polymer matrix (Figure 2.2). Its magnitude can be expressed as:

$$\frac{E}{E_o} = e^{(-\gamma z)} \tag{2.11}$$

where $E/E_o$ is the relative loss in the electric field strength compared to its value at the interface. $\gamma$ and $z$ are the evanescent wave decay coefficient and the distance from the reflecting surface. The depth of penetration of the evanescent field is given by $d_p$. The use of $d_p$ in ATR studies goes back to work by done Popov and Lavrent'ev in 1980 [56].

$$d_p = \frac{1}{\gamma} \quad \text{and} \quad \gamma = \frac{2n_2\pi\sqrt{\sin^2\theta - \left(\frac{n_1}{n_2}\right)^2}}{\lambda} \tag{2.12}$$

where

$\gamma$ is reciprocal of depth of penetration

$\lambda$ is wavelength of interest

Depth of penetration is a parameter that occurs when $E$ decays to a value $E_o\ exp(-1)$. However, $E$ is not zero at $d_p$, since $d_p$ has been historically defined to be the depth at which the electric field amplitude $E$ is half its value at the surface ($z = 0.693/\gamma$). Hence as $E$ is 37% of amplitude at surface at $d_p$, depth is actually greater than $d_p$ and almost three times $d_p$ [57].

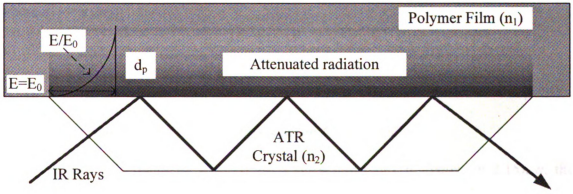


**Figure 2.2** Attenuated radiation in FTIR-ATR spectroscopy

In conventional transmission spectroscopy, if the reflection losses are neglected, transmission follows a simple exponential law $I/I_o = exp(-ad)$, where $I$ is the reflected IR

intensity, $I_o$ is the incident IR intensity, $d$ is the layer thickness and $\alpha$ is the absorption coefficient. For low absorptions $I/I_o = (1-\alpha d)$. By analogy, in internal reflection spectroscopy, reflection for bulk materials or thin films can be written as $R^N = (1-\alpha d_e)^N$, where $N$ is the number of reflections and $d_e$ is the effective thickness, which is defined as the film thickness required to give the same absorption as that obtained from the transmission measurement. For thin films or bulk materials with low absorption $d_e$ becomes independent of $\alpha$ [57].

The effective depth of penetration $d_e$ in case of low absorption case is given by Equation 2.13 and the number of reflections $N$ can be calculated with Equation 2.14 [58].

$$d_e = n_{12} E_0^2 d_p / 2\cos\theta \tag{2.13}$$

where $n_{12} = n_1/n_2$.

$$N = (l/T)\cot\theta \tag{2.14}$$

where $l$ is the length and $T$ is the thickness of the ATR crystal.

In dielectric materials with complex refractive index n' (equation 2.15), $\alpha$, the absorption coefficient can be related to this complex refractive index by equation 2.16.

$$n' = n(1 - ik) \tag{2.15}$$

$$\alpha = 4\pi nk / \lambda \tag{2.16}$$

where $k$ is the attenuation index and $\lambda$ is the wavelength of the IR radiation.

Sampling depth experiments performed with various methods showed that polymers and other organic compounds are weakly absorbing, so we can assume the depth of penetration for zero absorption case, i.e. Equation (2.12). Mirabella performed experiments with polypropylene ($n_1$ =1.5) and found that low absorption assumption is valid because values of $\alpha$ = 288 $cm^{-1}$ and $k$ = 0.013 were lower than $\alpha \leq 10^4$ and $k \leq 0.1$, values above, which zero absorption approximation is not valid [55].

The refractive index undergoes a change with wavelength. For materials absorbing energy, in the region (wavelength) of IR absorption, the refractive index changes and increases with increase in wavelength or decrease in wavenumber. This is also known as dispersion of the refractive index. Mirabella studied the effect of dispersion in polypropylene. In ATR spectroscopy, the absorption peak is influenced not only by the extinction (attenuation) coefficient *(k)* but also the refractive index *(n)*, giving rise to more complex refractive index *n'*. Another anomaly is the fact that changing refractive index also changes the critical angle and penetration depth [58].

$$n' = n(1 + ik) \qquad (2.17)$$

Such optical effects are much greater in reflection spectroscopy than in transmission method. This was confirmed by difference in band position for $Al_2O_3$ in grazing angle reflection spectroscopy and transmission spectroscopy [59]. Graf et al. [60] used Kramers Kronig transformation to find accurate values for optical constants of polystyrene taking into account the optical dispersion. Tickanen et al. [61] used variable angle FTIR-ATR and Kramers Kronig transformation (KKT) to find the optical constants

*n* and *k*. Huang et al. [62] did a study of the ATR spectrum of polyethylene and found difference in the peak intensity ratios of the 720 and 730 $cm^{-1}$ peaks in the ATR spectrum and the true spectrum obtained after performing KKT and Fresnel reflectivity analysis.

## 2.6 FTIR-ATR diffusion model

The absorbance of the IR light by a medium and its concentration can be related by the Beer Lambert law, in differential form as [21]-

$$dI = -eCIdz \tag{2.18}$$

where $e$ is molar extinction coefficient, $C$ is concentration of absorbing species and $z$ is the position in the absorbing medium.

Intensity ($I$) can be related to absorbance as-

$$dI = I_0 dA \tag{2.19}$$

From equation (2.18) and (2.19) ATR absorbance can be related to concentration.

$$A = \int_0^L eC\frac{I}{I_0}dz \tag{2.20}$$

The expression is related to the evanescent wave as -

$$I=E^2 \tag{2.21}$$

From equations 2.18, 2.19, and 2.20

$$A = \int_0^L NeCE_o^2 \exp(-2\gamma z)dz \tag{2.22}$$

where $N$ is the number of reflections of the IR beam in ATR crystal.

Now for a polymer with thickness $L$ exposed to constant surface concentration of solute, we take the initial and final boundary conditions as:

$$C=C_0 \text{ at } t = 0 \text{ and } 0<z<L \tag{2.23}$$

$$C=C_{eq} \text{ at } t \geq 0 \text{ and } z = L \tag{2.24}$$

$$\frac{\partial C}{\partial z} = 0 \text{ at } t \geq 0 \text{ and } z = 0 \tag{2.25}$$

where $z = L$ is the interface between the solute and the polymer, and $z=0$ is the interface between the ATR crystal and the polymer.

Considering equation 2.8 by Crank [21], and the boundary conditions (equations 2.23, 2.24 and 2.25) and considering the theory of FTIR-ATR (equation 2.22), we obtain equation 2.26. A detailed derivation of the FTIR-ATR model is given in Appendix F.

$$\frac{A_t}{A_{eqb}} = 1 - \frac{8\gamma}{\pi(1-\exp(-2\gamma L))} \sum_{m=0}^{\infty} \frac{\exp(g)[(-1)^m 2\gamma + f\exp(-2\gamma L)]}{(2m+1)(4\gamma^2 + f^2)} \tag{2.26}$$

where

$$g = \frac{-D(2m+1)^2\pi^2 t}{4L^2} \qquad f = \frac{(2m+1)\pi}{2L}$$

where $A_t$ and $A_{eqb}$ are the absorbance values at time $t$ and equilibrium respectively, and $L$ is the thickness of the polymer.

The details of the method employed in this study, to solve this equation are given in Chapter 3 in sections 3.6 and 3.7.

## 2.7 A brief review of the earlier studies utilizing FTIR-ATR technique for mass transfer determination

FTIR-ATR has been widely used for characterization of materials for many years [55, 63]. Some of the earlier studies of mass transport phenomena by using ATR spectroscopy, go back to the work done by Lavrent'ev et al.[64] and Remizov et al. [65]. They quantified small molecule diffusion in polyethylene and Kausch and Jud quantified the inter-diffusion of PMMA and styrene-acrylonitrile [66]. However, these studies did not take into consideration the exponential decay of the evanescent field, which led to errors in the quantification [66]. The technique was also used by Vorenkamp et al. [67] in 1989, but this study involved only the observation of poly(methyl methacrylate) (PMMA) and poly(vinyl chloride) (PVC) inter-diffusion but did not quantify it.

First studies, taking into consideration the sensitivity of the evanescent waves in the Fickian model were those done by Brandt et al. [66]. The study involved small molecule diffusion of ethyl acetate, benzene, methyl ethyl ketone (MEK), acetone, methanol and water in poly(ethylene) [17]. The results from these experiments compared reasonably with the conventional techniques.

Schlotter and Furlan [68] studied the diffusion of n-decyl alcohol in hydrogenated polybutadienes. The study focused on finding the influence of branch content on crystallinity and the diffusion of n-decyl alcohol. A nonlinear relation was observed between the equilibrium sorption of decyl alcohol and density (crystallinity) of

hydrogenated polybutadienes and could not be predicted by two phase model. It was concluded that this behavior existed due to the presence of large fraction of intermediate mass that acted in manner intermediate to fully accessible amorphous region and fully restricted crystalline region [69]. Xu and Balik [70, 71] studied the rate of loss of $CaCO_3$ filler in latex paint as function of pH of the aqueous solution they were exposed to. Their results using FTIR-ATR technique compared favorably well with conventional weight loss technique at lower pH values. Their later study involved simultaneous measurement of water diffusion, swelling, and calcium carbonate removal in a latex paint [72]. The water sorption in the paint however, could not be described by a simple Fickian model.

Van Alsten and Coburn [73] studied the effect of polyimide morphology on diffusion of heavy/deuterated ($D_2O$) water. The morphology of the polymer was changed by changing cure time, which in turn changed the polymer crystallinity, density and orientation. The diffusivity of water generally decreased with increase in chain backbone stiffness, and the activation energy for diffusion generally increased with backbone stiffness. For a given backbone composition, the diffusivity seemed to markedly increase as the density of the amorphous phase decreased. The spectrum also showed bimodal distribution of water, representing free and clustered water molecules. In 1995, Van Alsten [66] reviewed the FTIR-ATR technique for measurement of molecular transport in macromolecular systems.

Banerjee et al. [74] studied the breakthrough time and diffusion rate of a chemical warfare agent, Sulfur Mustard (SM) or 1,1-dichloroethane which was well known vesicant used in Iran-Iraq conflict in early 1990's. FTIR-ATR method was used to observe SM transport in butyl rubber by monitoring the 1120 $cm^{-1}$ C-O-C bond in SM

and showed good correlation with mass gain experiment results. Semwal et al. [75] used the FTIR-ATR technique to measure the breakthrough time and diffusion coefficient of SM and Oxygen mustard (OM) in polypropylene and biaxially oriented polypropylene. The results were obtained at different temperatures and showed good correlation with mass gain experiments. In 1995, Hellstern and Hoffman [23] presented a formula to calculate the attenuated total reflectivities of films of any thickness. Most studies [64, 76] till date assumed that at given time the concentration of permeant in the film can be assumed to be constant in region of evanescent field. However, this assumption hold true only when the film thickness was more than five times the evanescent radiation penetration depth [63]. So, based on the reflectivity formula by this group diffusion coefficient of gases as well as thickness of films from 10 nm up to the penetration depth could be determined.

Fieldson and Barbari [21] in 1993 developed an analytical solution to the problem of one-dimensional Fickian diffusion with constant surface concentration. They integrated the concentration profile with the intensity of the evanescent field to obtain this solution. The study involved measuring water diffusion in poly(acrylonitrile) (PAN) and examination of water clustering in the polymer by observing the O-H stretching at different stages of diffusion process. A detailed error analysis was performed to examine the validity of the technique and it was hence suggested for use in cases of liquid and gas diffusion measurement. Unlike in case of infinite permeant reservoir, a permeant in liquid mixture may not have the same concentration at the liquid/polymer surface as that in the bulk liquid. So, in 1995 they further developed the FTIR-ATR Fickian diffusion model by incorporating the effect of adjacent mass transfer boundary layer and the equilibrium

partition coefficient [20]. This model could be used in cases where a polymer sorbs a single permeant from a liquid mixture. A model for studying Case II diffusion in polymers using FTIR-ATR spectroscopy was also derived. Fieldson and Barbari used a simple case of constant surface concentration and constant velocity front, and used Heaviside function to describe the concentration profile and integrate in the FTIR-ATR absorbance theory. Diffusion of acetone in polypropylene, methanol in polystyrene, and methanol in PMMA was studied. Although, acetone in polypropylene and methanol in polystyrene followed a Fickian model, methanol in PMMA followed a Case II diffusion model [20]. The models developed by this group were used widely by many other research groups.

Diffusion of ethanol in glycerogelatin films was studied in 1995 by Tralhao et al. [77] by using FTIR-ATR spectroscopy. The results for ethyl alcohol-d showed good agreement with previous studies. However, using this technique gave additional advantage of being able to study time-dependent changes in composition of glycerogelatin films during the diffusion process. It could be concluded that hydrophilic components like glycerol diffused out of these films when in contact with ethanol and ethyl alcohol-d.

Farinas et al. [19] used FTIR-ATR technique to study urea diffusion in silicone polymer. Urea absorption band at 1650 $cm^{-1}$ was monitored over time to find its diffusion coefficient in silicone polymer and the results were in good comparison with tracer method based on use of radiolabeled $^{14}C$-urea. Balik and Simendinger [15] in 1997 described the design of ATR cell that could be used for diffusion analysis of commercially available films. In their cell design, the polymer film was sandwiched

between a liquid permeant reservoir at the top and ATR crystal at the bottom. A pressurized $N_2$ gas let into the cell exerted pressure on the liquid reservoir, which in turn exerted pressure on the polymer film to ensure good contact with the ATR crystal. They compared amyl acetate diffusion in poly(ethylene), and $CO_2$ diffusion in poly(styrene) (PS) by FTIR-ATR and gravimetric technique based on an electrobalance. The diffusion coefficient for amyl acetate in poly(ethylene) by FTIR-ATR was 3.05 x $10^{-9}$ $cm^2$/sec, while by gravimetric technique it was 9.1 x $10^{-9}$ $cm^2$/sec, which is three times of ATR results.

Hajatdoost and Yarwood [78] used the technique to test the effect of repetitive sorption and desorption (cycling) on water transport process in poly(ethersulfone) (SPEES/PES) films. Dual mode sorption model for diffusion in glassy polymers was used to study the diffusion and the OH stretching bond from 2700 to 3800 $cm^{-1}$ was used to monitor the concentration of diffusing water. It was seen that the sorption kinetics were not dramatically affected by cycling, but the desorption process considerably slowed, to an extent which depended on the sulfonation level of the films. Their further work in 2000 involved the study of diffusion and perturbation of different of water in presence of different ions, through polyelectrolyte (SPEES/PES) thin films [33]. Pereira and Yarwood [79] also worked with this system to study the diffusion of water into sulfonated poly(ethersulfone) films as a function of film thickness, preparation solvent and degree of sulfonation.

Hong et al. [80] successfully demonstrated the technique's use for measuring penetrant diffusion coefficients in polymers from the vapor phase. MEK sorption in

polyisobutylene was studied simultaneously by FTIR-ATR (carbonyl bond absorbance) and quartz spring microbalance and very similar diffusion coefficients were obtained. The diffusion coefficients obtained from both methods showed excellent correlation as the function of temperature and concentration, using Vrentas and Duda free-volume theory. The same group, a year later, demonstrated the power of the technique for measuring multicomponent diffusion of MEK/toluene mixtures at different compositions [81]. The data obtained on monitoring the C=O bond in MEK and aromatic C-C bond in toluene was fit to multicomponent diffusion model derived for use with ATR method.

Sammon et al. [82] studied the sorption of water and methanol in poly(ethylene terepthalate) (PET) of varying crystallinity. Diffusion of water in PET followed Fickian kinetics and showed significant decrease in the diffusion coefficient with increase in the polymer crystallinity. The diffusion coefficient ranged from 8.57 to 0.52 x $10^{-9}$ $cm^2$/sec for a crystallinity range of 4-25%. The relation between the polymer crystallinity and diffusion coefficient was found to be non linear, and it was implied that the spherulitic crystal size in polymer may play a important role in diffusion process. Methanol sorption in PET however, deviated from Fickian, and followed Case II and anamolous diffusion kinetics. A dual sorption model was used to fit the data for methanol sorption. This model gives two diffusion coefficients, one for rapid absorption in the surface sites and other for subsequent diffusion in the bulk material. Methanol diffusion in PET was accompanied by swelling, and it was seen that increase in crystallinity decreased the swelling, which may due to reduction in the polymer free volume. Evidence of the presence of free and hydrogen bonded methanol in PET was seen in the OH stretching region of the spectrum. Sammon et al. [83] also compared water transport in PET with that in PVC films. It was

found that incase of PVC, the plasticizer content (hence the glass transition temperature) had considerable influence on the sorption, swelling process and on the equilibrium content and state of water.

Laity and Hay [24] in 1999 utilized the FTIR-ATR technique in studying diffusion of water in swollen cellophane film. Cellophane film soaked in water containing some heavy/deuterated water ($D_2O$) was placed over another film sample which was swollen by normal water ($H_2O$) and held over the ATR crystal. $D_2O$ concentration in the film was measured by monitoring the 2505 $cm^{-1}$ O-D stretching band. Diffusion coefficient of $0.56x10^{-5}$ $cm^2/sec$ was similar to previous literature values, but was significantly different from their previous work using NMR technique.

Permeant characteristics strongly influence the transport phenomena in polymer membranes. Murphy et al. [27] demonstrated the effect of permeant size, shape and the multi-component effect on the diffusion coefficient in Teflon membranes, using the FTIR-ATR technique. Diffusion coefficient was seen to decrease with permeant molecular size (cis-1,2-dichloroethylene, trichloroethylene and tetrachloroethylene) and followed a exponential relationship. Permeant shape seemed to have greater effect on the diffusion coefficient due to the presence of bulkier side groups. Linear, flexible and symmetrical molecules (1-chloropentane) showed greater mobility and faster diffusion compared to the rigid structured molecules of same the molecular size (chlorocyclopentane). In multi-component system, it was observed that faster moving mobile permeant diffused faster in presence of the slower moving permeant, but the rate of diffusion of the slower permeant was unaffected.

Although, permeant flow cells were now widely used in FTIR-ATR study, no group had published any data on the effect of flow pressure of the permeant on the mass transfer results. A detailed study in this regards was undertaken by Yi et al. [35] They studied the diffusion of acetone in poly(propylene) at various flow pressures and found that the diffusion coefficient values did not vary above a threshold flow pressure of >230 kPa. They found that practice of using the reference band (polymer band) to correct the uncertainties in absorbance of permeant bands (band ratioing) yielded inconsistent results. A correction for scaling the absorbance value of the permeant band by dividing it by the polymer absorbance value obtained when stable contact between the polymer and crystal is achieved was also discussed.

One of the powerful application of FTIR-ATR technique was displayed by Elabd and Barbari [84] when they used the technique to characterize the diffusion of acetic acid in poly(isobutylene). The diffusing acetic acid was divided into two populations: linear (1726 $cm^{-1}$ C=O stretching) and cyclic dimers (1715 $cm^{-1}$ C=O stretching), and the diffusion coefficient of each population was determined. Further, to study solute-polymer binding effect on diffusion process MEK diffusion in vinyl alcohol/vinyl butyral copolymer was performed [85]. A diffusion-solvation model was developed which accounted for solute-polymer binding (binding costant $K$) to obtain effective diffusion coefficient $D_{eff}$ ; $D_{eff} = D/(1+K)$, where $D$ is the true (without binding) diffusion coefficient. The results had good comparison with diffusion of similar size molecule of methylene chloride. Solute-solute and solute-polymer interactions were studied by Elabd and Barbari [86] by studying diffusion of MEK/butanol in poly(isobutylene). Three different diffusing species (free MEK, self associated butanol and MEK-butanol

complex) were indentified by monitoring the deconvoluted peak of carbonyl and hydroxyl bonds with time. The value of $D_{eff}$ was found to be higher for free MEK followed by MEK-butanol complex and lowest for butanol cluster. In 2003, Elabd et al. [17] described the emergence of FTIR-ATR technique over the previous two decades and reviewed the work done by many research groups, especially Yarwood and Barbari groups who have widely used the technique. Their work mentioned the advantages and shortcomings of the techniques and suggested recommendations for future advancement of this technique in use for diffusion measurement.

A very unique application of this technique was explored by O'Callaghan et al. [49] while evaluating a polymer sample chemical protective clothing (latex, neoprene or nitrile rubber) for their resistance to various chemicals like acetone, acetone/water mixtures, naphthalene and commercial pesticide based on malathion. The polymer/ATR crystal contact was ensured by using gas pressure on 0.6 atm. A simple method of calculating diffusion coefficient was employed by using lag time method formula *(Lag time=$L^2$/6D)*. This simple form though does not take into account the evanescent field decay, the results obtained by using it have shown good correlation with results from other methods [19, 74, 75]. The technique was especially useful in determining the breakthrough times as in earlier studies [74]. Another novel application was to determine the diffusion of diallyl terepthalate (DAT) monomer in poly(DAT) films. The diffusion coefficient of DAT in 120 μm thick poly(DAT) film was found to range from 2 to 30 x $10^{-10}$ $cm^2$/sec at temperature range of 21 to 50°C [34].

In 2004, Philippe et al. [31] studied the sorption and transport of water and corrosion inhibitor anions in the corrosion protective epoxy coatings. Water transport was described by dual sorption model. First step resulted due to the rapid sorption of strongly hydrogen bonded water at the polymer sites and second due to the sorption in micro-voids in the cured polymer network. $HPO_4^{2-}$ ions too followed same transport kinetics as water both in terms of the nature and the rate of diffusion. Doppers et al.[16] in 2006 monitored acetone/water mixture diffusion in poly(vinyl alcohol) (PVOH). It was seen that acetone did not diffuse in dry PVOH, but diffused in moist film. Water diffusion in PVOH swelled it rapidly after the resistance for very short times. Hence, it followed case II diffusion process. Also, water entering the polymer lowered its glass transition temperature and made it like a gel. The fall in the polymer crystallinity was also studied by monitoring the spectrum over time, indicating that water was able to break the polymer-polymer intermolecular hydrogen bonding.

Ohman et al. [87] successfully determined water and electrolyte diffusion in aluminium/polymer interface by using Kretschmann configuration with FTIR-ATR system. In this configuration, when the crystal in coated with thin layer of metal, the evanescent field still passes through the metal layer into the rarer medium (polymer film). The method employed proved useful in studying changes in polymer coated metal surface, like oxidation (aluminium oxide/hydroxide) and surface film formation on the metal.

**2.8 Eugenol as an antimicrobial and antioxidant**

For food products entering the market, in order to be termed as "fresh" and "natural", use of synthetic additives for food preservation should be limited. For example,

Butylated hydroxytoluene (BHT) cannot be used in products labeled "fresh", "natural" or no "preservative" [88]. Also, the perception of growing health effects due to food additives has made general public conscious of consuming food with synthetic additives. People today want same quality food with good shelf life, but with minimum or no synthetic food additives [89]. Some experiments, which have proved the carcinogenic effect of BHA in animals, have put in question the use of synthetic antioxidants like BHT, BHA (Butylated hydroxylanisole), TBHQ (tert-butylhydroxyhyydroquinone), PG (Propyl gallate) in food products [90]. Therefore, many packaging materials manufacturing industries interested in developing natural food additives, which can be used with existing polymeric packaging structures.

There are various natural antioxidants that have been recognized to have good antioxidant properties, like the extracts from rosemary, white pepper, black pepper, sage, coriander, nutmeg, marjoram, clove, cinnamon, turmeric, red paprika, caraway, peppermint, thyme, oregano, cumin, fennel, parsley, garlic, and ginger [91]. 'Eugenol' is a clear to pale yellow oily liquid extracted from certain essential oils especially from clove oil, nutmeg and cinnamon. It is slightly soluble in water and soluble in organic solvents. It has a pleasant, spicy, clove-like odor.

Lipid oxidation of food products is a big problem for food and pharmaceutical applications. Oxidation is responsible for decreasing the nutrition value of products, generates rancidity, and to produce off- flavors in products; thus affecting the product shelf life. Oxidative processes in foods also produce deterioration in texture and color by lipid and protein degradation [90]. Eugenol acts by trapping chain growing peroxy radical

by donation of phenolic hydrogen atom as shown in equation 2.27. This reaction is faster than the attack of peroxy radicals in equation 2.28 [92].

$$ROO^{\cdot} + ArOH \rightarrow ROOH + ArO^{\cdot} \quad (2.27)$$

$$ROO^{\cdot} + RH \rightarrow ROOH + R^{\cdot} \; (O_2 \rightarrow ROO^{\cdot}) \quad (2.28)$$

$$2ROO^{\cdot} \rightarrow \text{INERT PRODUCTS}$$

In 2006, Phoopuritham et al. [90] concluded that clove and cinnamon oils showed a strong antioxidant and radical scavenging activity, better than thyme, ginger and rosemary oils. Clove oil proved to be far more effective at lower concentrations for inhibition of DPPH (2,2-diphenyl-1-picryhydrazyl radical) radical than pure eugenol, BHT, BHA. DPPH radical scavenging technique is widely used to find the antioxidant activities in relatively shorter time. This oil shows enough potential to be used as natural preservative to prevent oxidation and can be used even at the later stages of lipid oxidation [93].

Eugenol has been used as a natural antimicrobial and it is very effective against micro organisms like *L.monocytogenes, L innocua, S. enteritidis, S.Typhimurium, Micrococcus, V.vulnificus, C. botulinum, B. subtilis*. Its potential food applications include marinade and sauces (poultry, pork, beef, seafood), salads and sauces (celery, lettuce, parsley, radish, mushroom, cabbage, fennel, spinach, bean sprouts, cucumber), cheese, bakery products and seasonings [94]. Eugenol presence showed significant increase in total antioxidant activity (TAA) and reduction in nutritional, sensory and

functional losses of grapes. Also the microbial spoilage was significantly reduced, thus increasing the shelf life of the table grapes [95].

Remmal et al. [96] in 2003 studied the bactericidal effects of clove oil and eugenol against *Escherichia coli* strain obtained from colibacillosis affected hen and *Bacillus subtilis* strain obtained from poultry meat. Clove oil and eugenol both showed a minimum inhibitory concentration (MIC) of 0.05% (v/v) for *E. coli* and 0.033% (v/v) for *Bacillus subtilis*. Minimum inhibitory concentration is defined as the minimum concentration resulting in significant decrease in test organism.

# Chapter 3

# Materials and Methods

## 3.1 Introduction

This chapter describes the FTIR-ATR setup and methodology employed for finding the diffusion of eugenol in LLDPE. The major challenge in this research was to configure the FTIR-ATR equipment and all the parts required for achieving continuous flow system for eugenol. Further, the use of HPLC based technique in determining the diffusion when permeant eugenol has one-sided and two-sided contact with the film is described.

A MATLAB® program was used to evaluate the data and proved very useful to study residuals in the experimental and theoretical diffusion profiles. Sensitivity of the theoretical equations was also evaluated to actually see the region in the diffusion profile which most affects the diffusion coefficient.

## 3.2 Materials

The commercial polymer film used in this study was LLDPE film ($n_1$=1.5, thickness L = 25±4 μm, obtained from Flexopak, Attiki, Greece). The permeant used in this study was eugenol (≥ 98% from Sigma Aldrich, St. Louis, MO, USA). LLDPE was chosen because it is one of the most commonly used food contact polymer, and also the simple spectrum of LLDPE provides a wide region for detecting the permeant IR absorbance peak. Ethylene vinyl acetate (EVA) polymer film ($n_1$=1.5, thickness L = 20±3 μm) obtained from Borden Inc., (Columbus, OH) was also used in this study.

Figure 3.1 shows the chemical structure for eugenol and the constitutional unit of LLDPE and EVA.

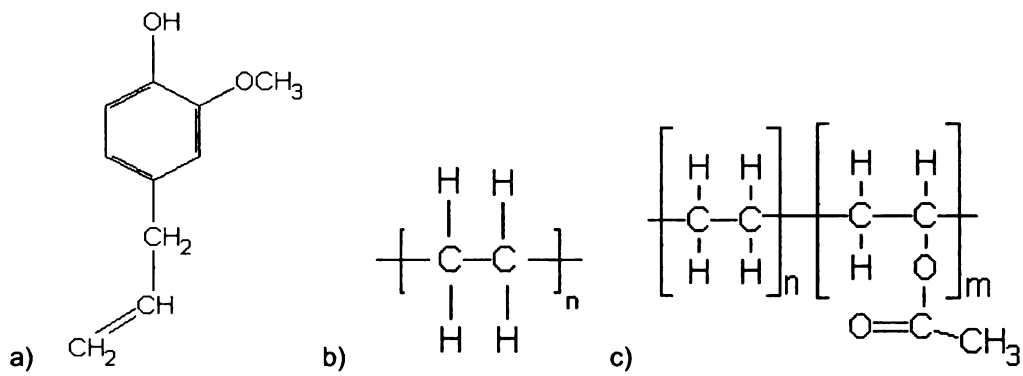


**Figure 3.1** Chemical structure a) Eugenol b) LLDPE and c) EVA

### 3.3 FTIR-ATR Flow Cell Setup

A Shimadzu IR Prestige–21 spectrophotometer from Shimadzu Scientific Instruments (Columbia, MD, USA) with an attenuated total reflection accessory ATR MAX II and a liquid jacketed flow cell assembly from Pike Technologies (Madison, WI, USA) were used. A 56 x 10 x 4 mm ZnSe crystal ($n_2$= 2.43, 45° bevel angle) from Pike Technologies was used with the ATR accessory. Figure 3.2 shows the ATR cell design used in this study.

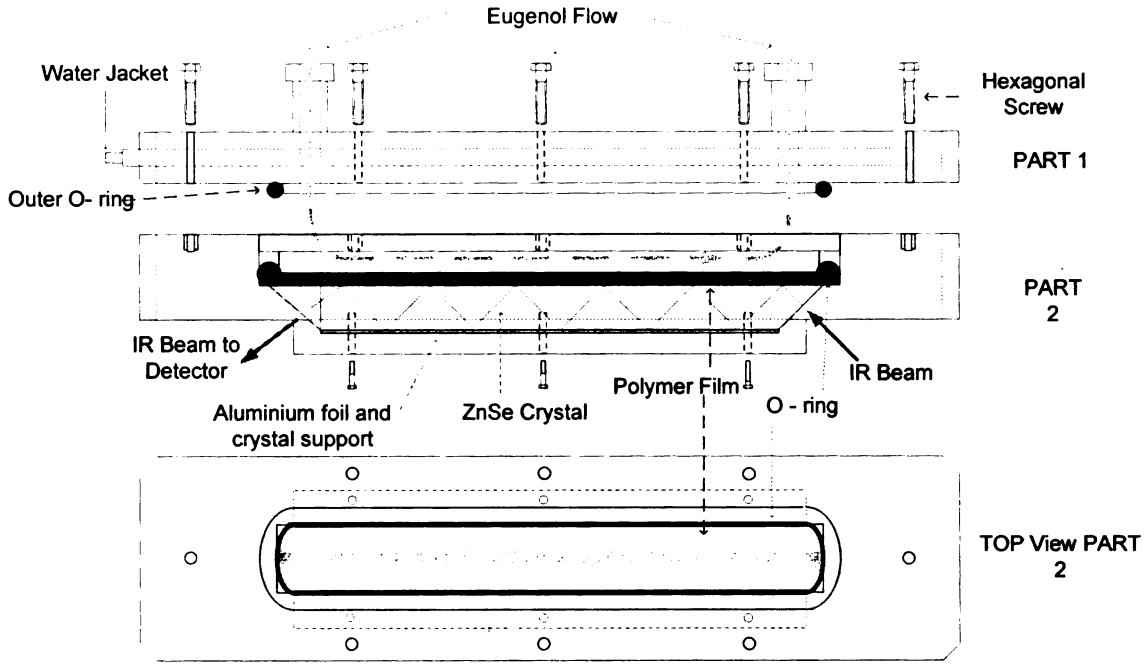


**Figure 3.2** FTIR-ATR Flow cell design (adapted from Pike Technologies)

The cell is mainly divided into two parts. The top part provides the eugenol inlet and outlet, and also includes a water jacket for cell temperature control. In the bottom half the LLDPE film is placed on the ATR crystal and sealed in place with an O-ring and Aluminum laminated plastic support. The two halves are then screwed together, and the seal is achieved with the help of an outer O-ring.

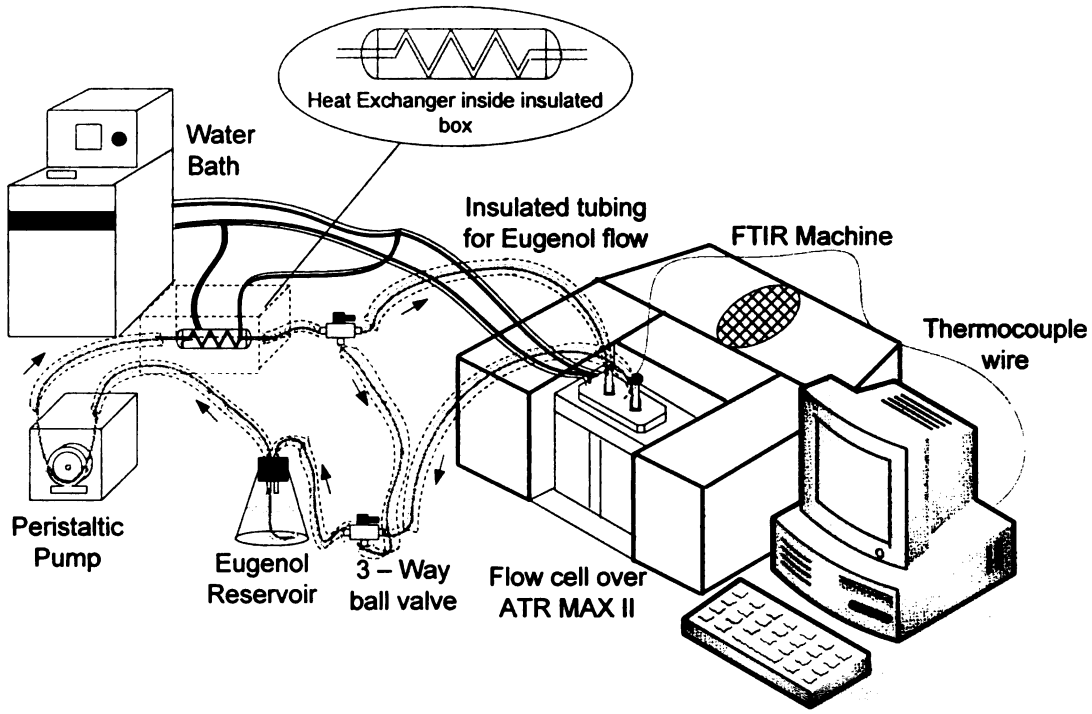


**Figure 3.3** FTIR-ATR experimental setup.

Figure 3.3 shows the entire flow circuit of eugenol. Insulated platinum cured silicone tubing and a Masterflex C/L pump from Cole Parmer Instrument Company (Vernon Hills, IL, USA) were used to pump eugenol at different flow rates. A small glass tube was used to connect the tubing with the flow cell inlet and outlet. A 5 litre water bath (Neslab Instruments Inc., Newington, NH, USA) was used for controlling the temperature of eugenol and the flow cell. A thermocouple at the outlet of the flow cell was used to continuously monitor eugenol temperature. To maintain the temperature of liquid eugenol in the reservoir constant, an outer loop was created by using two 3-way ball valves. Temperature controls for the cell and eugenol were achieved with precisions of less than ± 0.5°C.

### 3.4 FTIR-ATR Measurement Procedure

The FTIR-ATR experiment was performed by first taking the background scan of air and then placing the sample on the ATR crystal in the flow cell for 30 min to equilibrate with the cell temperature. Then 30 infrared scans at every 2 min and 4 $cm^{-1}$ resolution were taken to obtain the absorbance data. The spectrum was analyzed using IR Solution software from Shimadzu Scientific Instruments (Columbia, MD, USA).

#### 3.4.1 FTIR-ATR Preliminary experiments

The first step in FTIR-ATR measuring technique was to determine the characteristic eugenol peak which can be monitored over time for the diffusion process. Table 3.1 shows the eugenol and LLDPE characteristic IR peaks and their corresponding functional group assignment. Figure 3.4 shows the overlapped spectrum of LLDPE and eugenol. The LLDPE spectrum is shown in dotted lines, while the Eugenol spectrum is a solid line. It can be seen that eugenol has a very complex spectrum and overlaps all the LLDPE peaks. To find the best suitable peak for studying eugenol diffusion process, initially preliminary pilot experiments were performed. Eugenol was flown at 6 ml/min through the flow cell and eugenol absorbance peaks at 1637, 1514 and 1033 $cm^{-1}$ were monitored over time.

**Table 3.1** Main IR absorption peaks for LLDPE and eugenol.

| **Wavenumber $cm^{-1}$** **Vibration mode** | **Chemical Functional groups** | |
|---|---|---|
| | **Eugenol** | **LLDPE** |
| 2870 (sym), 2960 (asym) stretching | Methyl ($-CH_3$) | - |
| 1370 (sym), 1450 (asym) bending | Methyl ($-CH_3$) | Methyl( $-CH_3$) |
| 2860 (sym), 2930 (asym) stretching | Methylene ($-CH_2-$) | Methylene ($-CH_2-$) |
| 1465, 720 bending | Methylene ($-CH_2-$) | Methylene ($-CH_2-$) |
| 3000, 3040 stretching | C=C→ H | - |
| 1033 stretching | -C-O-C- | - |
| 650 – 1000 bending | C=C↘H | - |
| 910, 990 bending | Vinyl $C = CH_2$ | - |
| 1514, 1608, 1637 stretching | Aromatic C = C | - |
| 3300 – 3550 stretching | Phenol CO→ H | - |
| 1300 – 1400 bending | CO↘H | - |

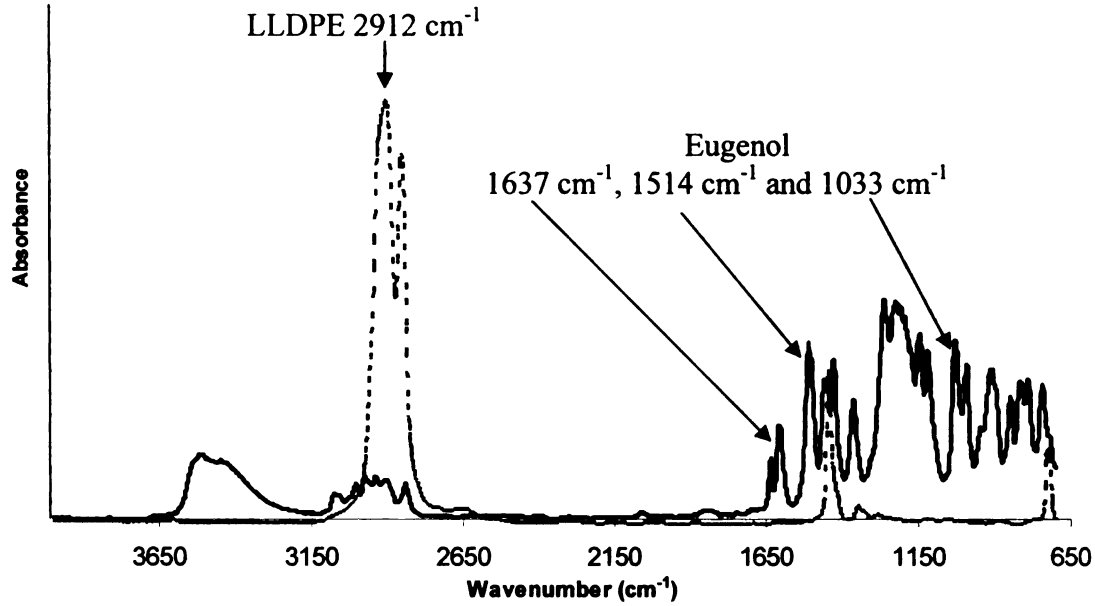


**Figure 3.4** Overlapped FTIR-ATR spectrum of eugenol and LLDPE

To verify the exact absorbance peak locations, a second order derivative of the absorbance spectrum, obtained from IR Solution software as shown in figure 3.5, was obtained. A Savitsky-Golay method with degree of polynomial 2 and number of convolution points as 5 was used to determine the derivative form. Each absorbance peak in its derivative form has downward and upward pointing feature. The central frequency of the band exactly corresponds to the downward feature in the derivative form [97]. The change in absorbance of these peaks, measured by change in absorbance peak height was studied over time. Figure 3.6a shows the absorbance of these characteristic eugenol peaks over time. Figure 3.6b shows the short time absorbance data of these characteristic peaks.

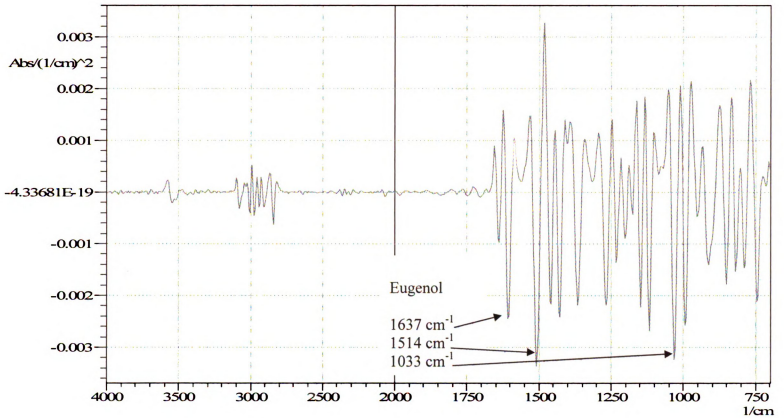


**Figure 3.5** Second derivative of eugenol absorbance spectrum helped identify exact peak locations from IR Solution software.

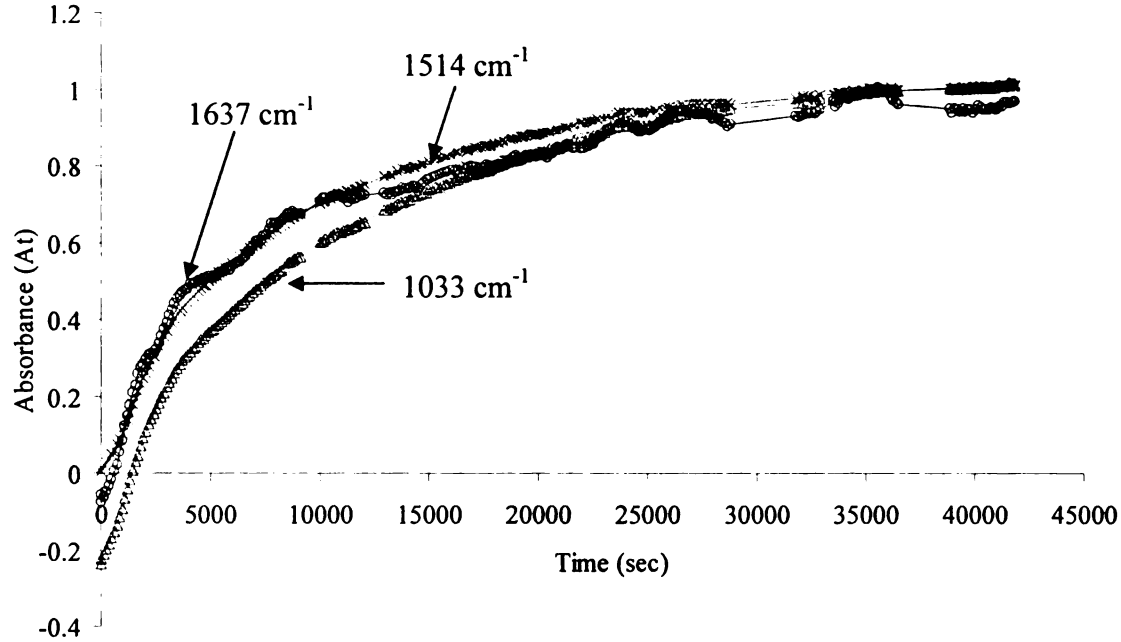


a)

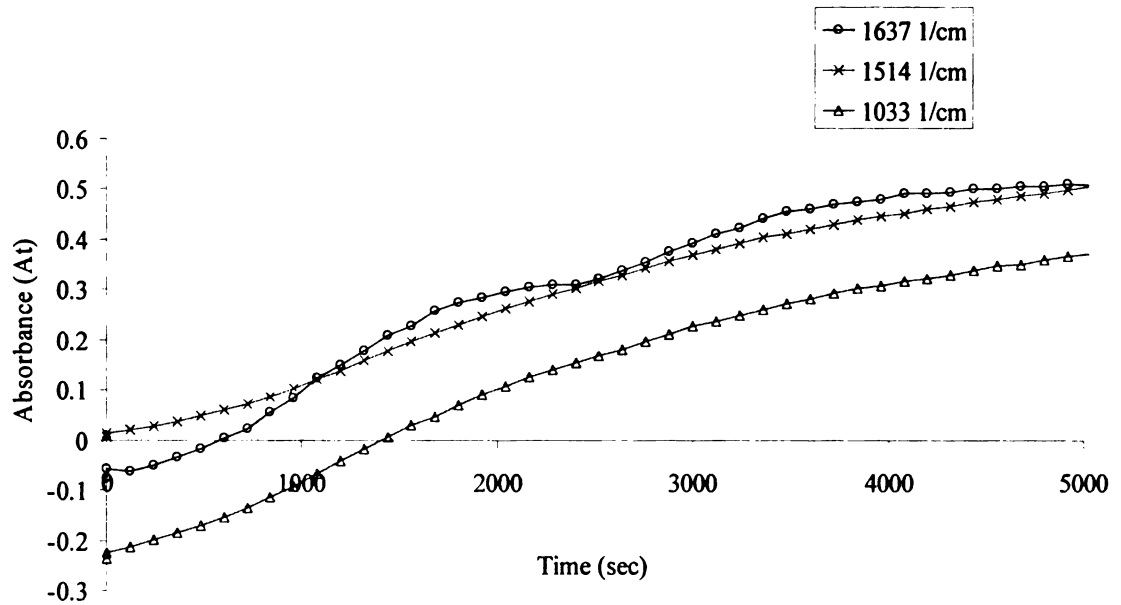


b)

**Figure 3.6** Absorbance of eugenol peaks in LLDPE at a) longer times b) at shorter times.

Although, absorbance of these peaks were very close at higher times (>20000 sec), at times <20000 sec 1033 $cm^{-1}$ deviated from the other two peaks. The peak at 1033 $cm^{-1}$ represents the C-H stretching in C=C-H bond in eugenol (Table 3.1). As in Figure 3.4 it can be seen that C-H stretching region in eugenol spectrum is a wide region. Hence 1033 $cm^{-1}$ peak is not sharp (wide absorbance region) and may have been influenced by the adjacent peaks, thereby not providing reliable change in absorbance peak height. On other hand, 1637 $cm^{-1}$ being low in overall intensity showed quite low intensity in the shorter times (<5000 sec) and showed a unstable (wavy) absorbance pattern. At shorter times, when eugenol concentration is low, the region of 1637 $cm^{-1}$ which falls in low intensity, shows very low absorbance change and was very close to the noise found in the spectrum. Hence detection of this peak also became unreliable at shorter times.

To find the equilibrium time at three different temperature conditions 16, 23 and 40°C preliminary runs were carried out at eugenol flow of 8 ml/min. Steady state was considered when the absorbance values deviated by less than 1% over time period of 30 min. A small constant increase in the absorbance value of the eugenol peak, during the steady state was observed as eugenol permeated through the film and settled over the crystal. Figure 3.7 shows the normalized absorbance ($A_t/A_{eqb}$) over time (sec), for the preliminary runs at three temperatures. Based on these runs equilibrium time for the three temperatures was found to be ~ 85000 sec or 23.61 h for 16°C, ~ 35000 sec or 9.72 h for 23°C, and 20000 sec or 5.55 h at 40°C.

Also, to find if there is any change in eugenol 1514 $cm^{-1}$ absorbance peak over time, eugenol was flown at 8 ml/min for 24 h over the ATR crystal and the absorbance values noted (Figure 3.8). Absorbance values were collected every 8 mins. Since, the background scan in this case was that of pure eugenol, the absorbance values deviated around zero absorbance. The values deviated uniformly between ±0.0003 (absorbance value $A_t$), which is considered as very low value compared to the absorbance values of the order of $10^{-1}$ for pure eugenol ($A_{bkg}$), thus giving an maximum % deviation (($A_{bkg} - A_t$) x 100 /$A_{bkg}$) of 0.35.

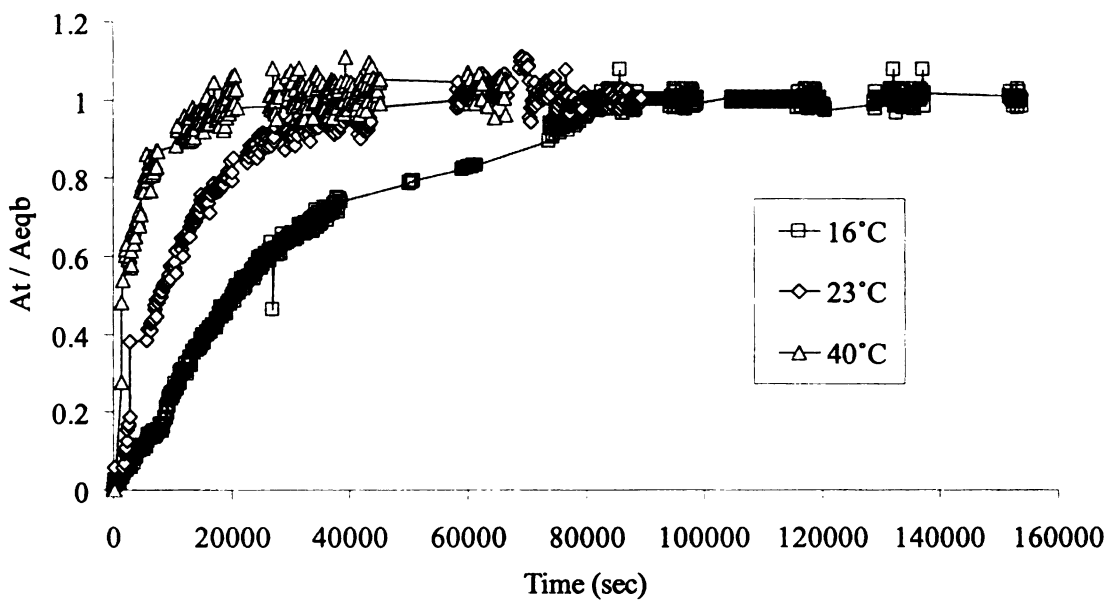


**Figure 3.7** Preliminary runs for equilibrium time measurement at 16, 23 and 40°C.

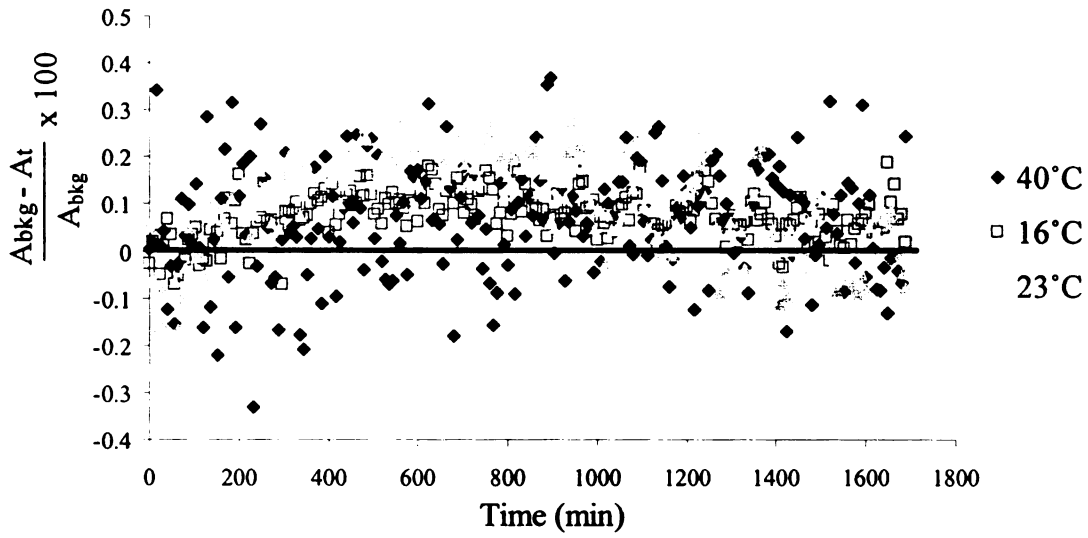


**Figure 3.8** Deviation of pure eugenol absorbance flown over the ATR crystal at different temperatures. The black line indicates zero deviation of eugenol values.

### 3.4.2 Eugenol/LLDPE FTIR-ATR experiments

Although the refractive index of the substrate in the absorbing region of the spectrum, in ATR spectroscopy undergoes a complex change [55], like many other earlier studies using this technique [15-20, 24, 28, 31-35], we assumed constant refractive index at the 1514 $cm^{-1}$ peak. Since peak ratioing could not be performed, we had to assume constant refractive index only at one absorption peak (1514 $cm^{-1}$), thus reducing the error that would have been involved with monitoring of two peaks (polymer and penetrant) separated by some wavenumber range. However, inability to measure polymer peak meant we could not monitor the changes in polymer/crystal contact and had to rely on the eugenol flow pressure to achieve optimum contact with the crystal. Hence, experiments were performed at four different flow conditions; 0, 6, 8 and 11 ml/min. For the study at 0 ml/min condition, one side of the LLDPE film was heated on a hot plate at 50°C for 30

sec and then placed on the ATR crystal. Eugenol was then injected into the closed cell. The conditions of 6, 8 and 11 ml/min flow were set by adjusting the flow control knob of the peristaltic pump and simultaneously measuring the eugenol volume coming out of the outlet of the flow cell by standard measuring cylinder. The study was further conducted by changing the depth of penetration of the IR radiation, by changing the angle of penetration of incident IR beam in the ATR crystal. The angle was changed using AutoPRO™ software from Pike Technologies. The experiments were carried at 45° in the preliminary runs and for experiments with variable flow rates. To increase the depth of penetration, angle of 39° was chosen because it enabled the highest depth of penetration. The effective angle $\theta_{eff}$ used to achieve a penetration angle $\theta$ =39°, is given by Equation 3.1 [98].

$$\theta_{eff} = \theta - \sin^{-1}\left[\frac{\sin(\theta - \theta_{face})}{n_2}\right] \tag{3.1}$$

where $\theta_{face}$ = 45° (face angle of the crystal) and $n_2$= 2.43 (crystal refractive index) and

It was also assumed that the diffusing permeant (eugenol) did not cause any change in the refractive index of the polymer (LLDPE), and hence the depth of penetration of the IR radiation was constant. Since most organic compounds are considered as weakly IR absorbing [55], eugenol may have caused zero or minimal change in the refractive index. This assumption may be valid also because no interaction was observed between eugenol and LLDPE through the diffusion process as established by the lack of chemical interaction or swelling of LLDPE which could lead to change in

refractive index. All the experiments were performed in triplicates at temperatures of 16, 23 and 40°C. Table 3.2 summarizes all the different experiments performed at the different temperature, eugenol flow and penetration angle conditions.

**Table 3.2** Overview of FTIR-ATR based LLDPE/Eugenol experiments

| Temperature (°C) | 16 | 23 | 40 |
|---|---|---|---|
| Flow (ml/min) | 8 | 0, 6, 8, 11 | 8 |
| Penetration angle ($\theta$ °) | 45 | 39, 45 | 45 |

### 3.4.3 Eugenol/EVA experiments

In case of EVA film, since the film is sticky, it had very good contact with the ATR crystal. Hence, the experiment was performed by flowing eugenol through the flow cell at low flow rate of 4 ml/min. Because of the swelling observed in this film, experiment was restricted to only one temperature of 23 °C.

## 3.5 Eugenol/LLDPE HPLC experiments

To compare the results obtained from the FTIR-ATR experiment a more conventional diffusion analysis technique using one-sided and two-sided permeation experiment, monitored by HPLC, was used.

The eugenol detection methodology by HPLC was same in case of both one-sided and two-sided experiments. An HPLC equipment (Waters 2695) coupled with a UV detector (Waters 2487) and equipped with a Nova-Pak® C18 (4 μm) column (all from Waters Corporation, MA, USA) at 25°C were used to quantify eugenol. A 10μl injection volume and an isocratic elution of 1ml/min flow with methanol: water (85:15) was used.

The data was collected at 280 nm and the retention time for eugenol was found to be 1.5 min (Appendix Figure E1). A calibration curve (Appendix Figure E2) was generated by injecting eugenol standard (99% pure from Sigma Aldrich, MO, USA) solutions in methanol (0.20 to 10 μg/ml). The peak area response was collected in triplicates for each standard solution and a calibration curve of area response (A.U.) vs concentration (μg eugenol/ml methanol) was plotted ($R^2$=0.9996).

### 3.5.1 Eugenol/LLDPE Two-sided experiment

Round samples (area 3.14 $cm^2$) were cut from the LLDPE film and placed in 40 ml vials containing 30 ml eugenol (Figure 3.8a). The film samples were introduced in the vials and extracted at variable time intervals until equilibrium was reached at each temperature. Four replications were included in each vial. The experiment was performed at 16, 23, and 40°C with maximum of 0.5°C variation. After taking the film samples from the eugenol vials, excess eugenol was first wiped off from the film surface. Then the films were immersed in 10 ml methanol (HPLC grade) for 10 sec to ensure no eugenol was left on the film surface. Finally, each film sample was placed in 20 ml methanol and continuously stirred for 24 h at room temperature for eugenol extraction. In pilot trial run by HPLC, the film sample after the initial extraction was placed again in 10 ml methanol and second extraction performed for more 24 h at room temperature and with continuous stirring. Unable to detect eugenol this time, we could confirm from the second extraction that 99.99% of the eugenol extraction took place within the first 24 h.

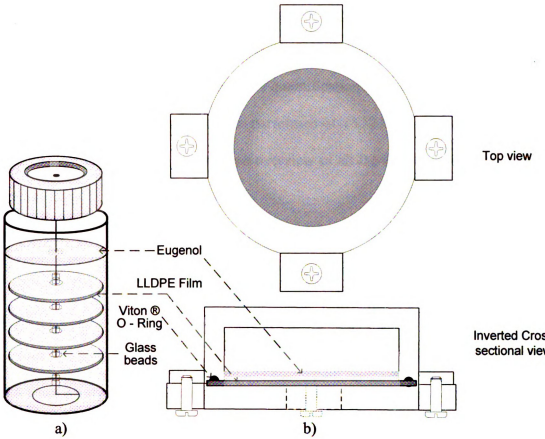


**Figure 3.9** a) vial for two-sided b) permeation cell for one-sided, HPLC experiment.

### 3.5.2 Eugenol/LLDPE One-sided experiment

In one-sided HPLC experiment, LLDPE film was placed in the permeation cell built from Aluminum alloy 2024 with eugenol reservoir on just one side (Figure 5b). The entire assembly was sealed using Viton® O-Rings. The film area of 15.2 $cm^2$ was exposed to eugenol on one side. The other side was open to atmosphere. The film was taken out of the cell at variable time intervals until equilibrium was reached at each temperature. Excess eugenol on the film surface was wiped out. Four circular samples of 1.53 $cm^2$ were cut from the exposed film area and their surface cleaned in methanol (HPLC grade). The films were weighed and placed in 10 ml methanol for 24 h and at

room temperature for extraction. The weight of eugenol extracted was subtracted from the film weight to finally normalize the amount of eugenol sorption per mg of the film sample. All other parameters for eugenol quantification were same as the two side HPLC experiment. These experiments were performed at 16, 23 and 40°C with maximum of 0.5°C variation. Table 3.3 provides an overview of all the HPLC experiments performed in this study.

**Table 3.3** Overview of HPLC LLDPE/Eugenol experiments

| Temperature (°C) | 16 | 23 | 40 |
|---|---|---|---|
| HPLC two-sided | ✓ | ✓ | ✓ |
| HPLC one-sided | ✓ | ✓ | ✓ |

### 3.6 Data Analysis

The absorbance data obtained from IR Solution® software was exported in form of a notepad file. An export retrieval program (Appendix A1) was used to retrieve the data into a spreadsheet (Excel™). Negative numbers were obtained at shorter times because of lower absorbance values. A scaling factor or the lowest absorbance value was added to all other values to get them in a positive scale (Appendix A2). The data in the form of absorbance values and corresponding time were loaded in MATLAB® R2008 (MathWorks, Natick, MA, USA) program (Appendix B1-B3).

In case of FTIR-ATR, data obtained was tested to fit the Fick's model expressed by Equation 2.26, where $A_t$ and $A_{eqb}$ are the absorbance values of eugenol sorbed at time $t$ and equilibrium, respectively. A predicted or theoretical diffusion curve was obtained based on fixed parameters as polymer and ATR crystal refractive indices (1.5 and 2.43,

respectively), wavelength of the permeant peak studied (6.60 x $10^{-4}$ cm or wavenumber of 1514.12 $cm^{-1}$), polymer thickness $L$ (LLDPE 25±4 cm), absorbance value $A_t$ at given time $t$ (sec) and variable parameters like $D$ and $A_{eqb}$ which were estimated by performing non linear regression (details in section 3.7) and with the value of $m$ = 100.

Incase of HPLC experiments, data obtained was tested to fit the Fick's model expressed by Equation 2.9, for sorption of permeant having constant $D$ in plane sheet [38], where $M_t$ and $M_{eqb}$ are concentration weight (μg of eugenol per mg LLDPE) of eugenol sorbed at time $t$ (sec) and equilibrium, respectively. A predicted or theoretical diffusion curve was obtained based on fixed parameters like polymer thickness $L$ (LLDPE 25±4 cm), $M_t$ at time $t$ and variable parameters like $D$ and $M_{eqb}$ which were estimated by performing non linear regression (details in section 3.7) and with the value of $m$ = 100. This diffusion model was used for the one-sided and two-sided diffusion process. In the case of two-sided sorption, $L$ was replaced by $L/2$, taking into account the change in boundary conditions.

### 3.7 Statistical Analysis

The best overall fit $D$ and $M_{eqb}$ values for four replications for the HPLC runs, the best overall fit $D$ and $A_{eqb}$ values for three runs for the FTIR-ATR experiments, the prediction interval for the observed experimental values, and the confidence intervals for best fit values were calculated by using non linear regression (nlinfit) function in MATLAB. Significant differences between the $D$ values were determined by using

Tukey's test. Calculations for least significance difference (LSD) were performed in MATLAB using student's t distribution table [99]. In order to determine the goodness of the fit of the theoretical curve and the observed data, root mean squared error (RMSE) and standard residuals were found by MATLAB for all the experimental runs.

Sensitivity coefficient helps determine the optimum range of times to estimate a parameter. The optimum time to estimate parameter $D$ is the time where the sensitivity coefficient is maximized [100]. The scaled sensitivity coefficient of $D$ is the product of $D$ and the derivative of the dependent variable with respect to $D$ (Equation 3.2), and the derivative was evaluated numerically:

$$D\frac{\partial Y_i}{\partial D} \approx D\frac{Y_i(D+\delta D) - Y_i(D)}{\delta D} \tag{3.2}$$

where $\delta D$ was a small value = $0.000001D$, and $Y_i = A_t/A_{eqb}$ from equation 2.26 and $M_t/M_{eqb}$ from equation 2.9. The scaled sensitivity coefficient of $D$ was plotted vs. time.

# Chapter 4

## Results and Discussion

In this chapter, the results are presented starting from the effect of eugenol flow rate and IR penetration angle on diffusion in LLDPE, the FTIR-ATR results and HPLC based results for the eugenol/LLDPE system at three different temperatures, and finally results for EVA/LLDPE system. A detailed discussion is done to better understand the different factors influencing these results.

### 4.1 FTIR-ATR Change in depth of penetration

Depth of penetration $d_p$ in Equation 2.12 shows that $d_p$ is influenced by different parameters like polymer and crystal refractive indices ($n_1$ and $n_2$), angle of penetration $\theta$, and wavenumber or reciprocal of wavelength ($1/\lambda$). As, $n_2$ is constant and $n_1$, though complex can be assumed constant, $d_p$ would vary with $\theta$ and the incident $\lambda$. Figure 4.1 shows $\theta$ dependence of $d_p$. The value of $d_p$ varies from 0.82 to 3.53 μm for $\theta$ varying from 55° to 39°. The value of $d_p$ is lower at higher wavenumber and vice versa. $d_p$ at 1514 $cm^{-1}$ was found to be 1.25 μm (Figure 4.2).

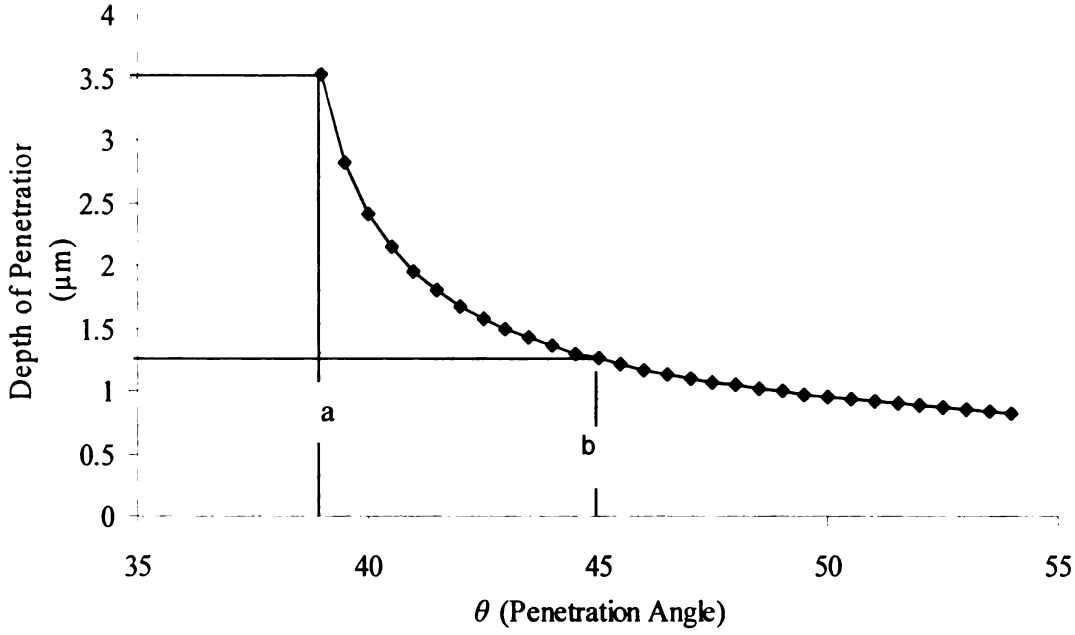


**Figure 4.1** Change in depth of penetration $d_p$ with angle of penetration $\theta$

**Note**: Line 'a' indicates $\theta$ =39° and line 'b' indicates $\theta$ =45°

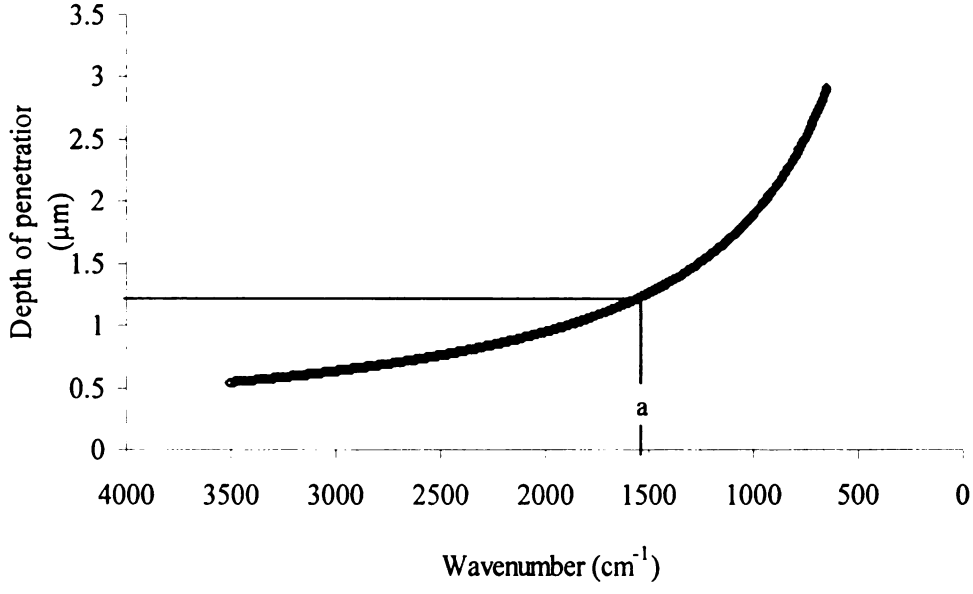


**Figure 4.2** Change in depth of penetration $d_p$ with wavenumber

**Note**: Line 'a' indicates wavenumber = 1514 $cm^{-1}$.

### 4.2 FTIR-ATR Effect of eugenol flow rate

Figure 4.3 shows the normalized absorbance data for eugenol at 1514 $cm^{-1}$ at 23°C as fitted by equation 2.26, and obtained at these four flow rates. The plots show the experimental values of normalized absorbance of all three-replication runs. The center line is the best predicted theoretical curve based on the Fickian model (Equation 2.25). The 95% confidence interval lines are very close to the predicted best fit curve, hence not clearly visible in Figure 4.3. The outer lines indicate the 95% prediction interval of the observed values. The figures below show the corresponding standard residual errors between the experimental and predicted values. Values along the dark line i.e zero residual, indicate exact match with the predicted values. Higher standard residuals, up to 4 standard residual, were observed at initial times (below $0.5 \times 10^4$ sec or 1.4 h) under all the four flow conditions. However, the number of experimental data points with higher residuals was limited and hence do not truly affect the value of *D,* the details of which are addressed later. This initial residual may be due to the initial instability of the LLDPE film and crystal contact. After the initial part of diffusion process, the experimental values deviated uniformly by 2 standard residuals from the zero line, which can be considered as good fit.

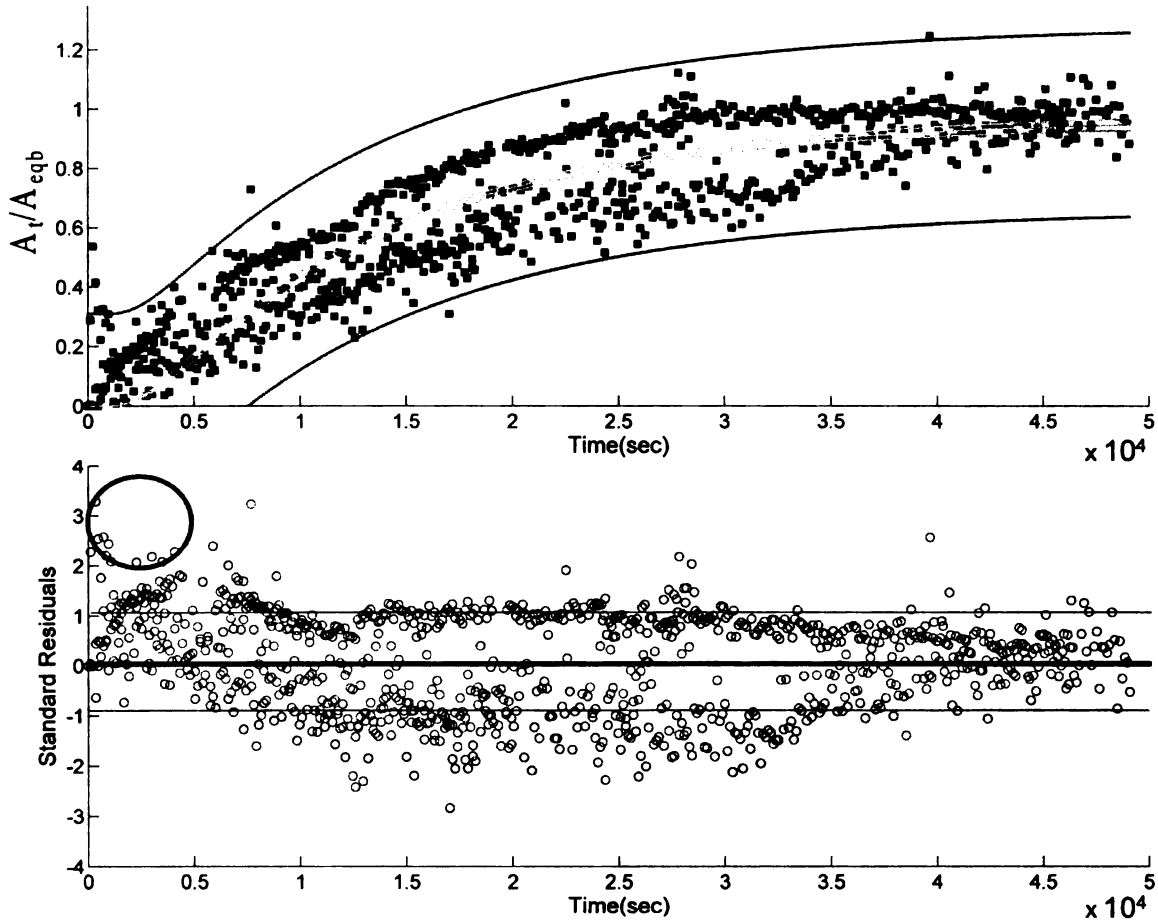


**Figure 4.3a** Normalized eugenol (1514 $cm^{-1}$) absorbance vs time at 'no flow' or 0 ml/min eugenol flow condition at 23°C.

**Note:** The central line shows the best fit to the dotted experimental values of all the three replications. The outer lines show the prediction interval for the observed experimental values. The confidence interval of the best fit is very narrow to the fitted curve and not clearly visible in the figures. The standard residuals are shown in the graph below with dark line indicating zero residual. The red oval indicates the higher residuals.

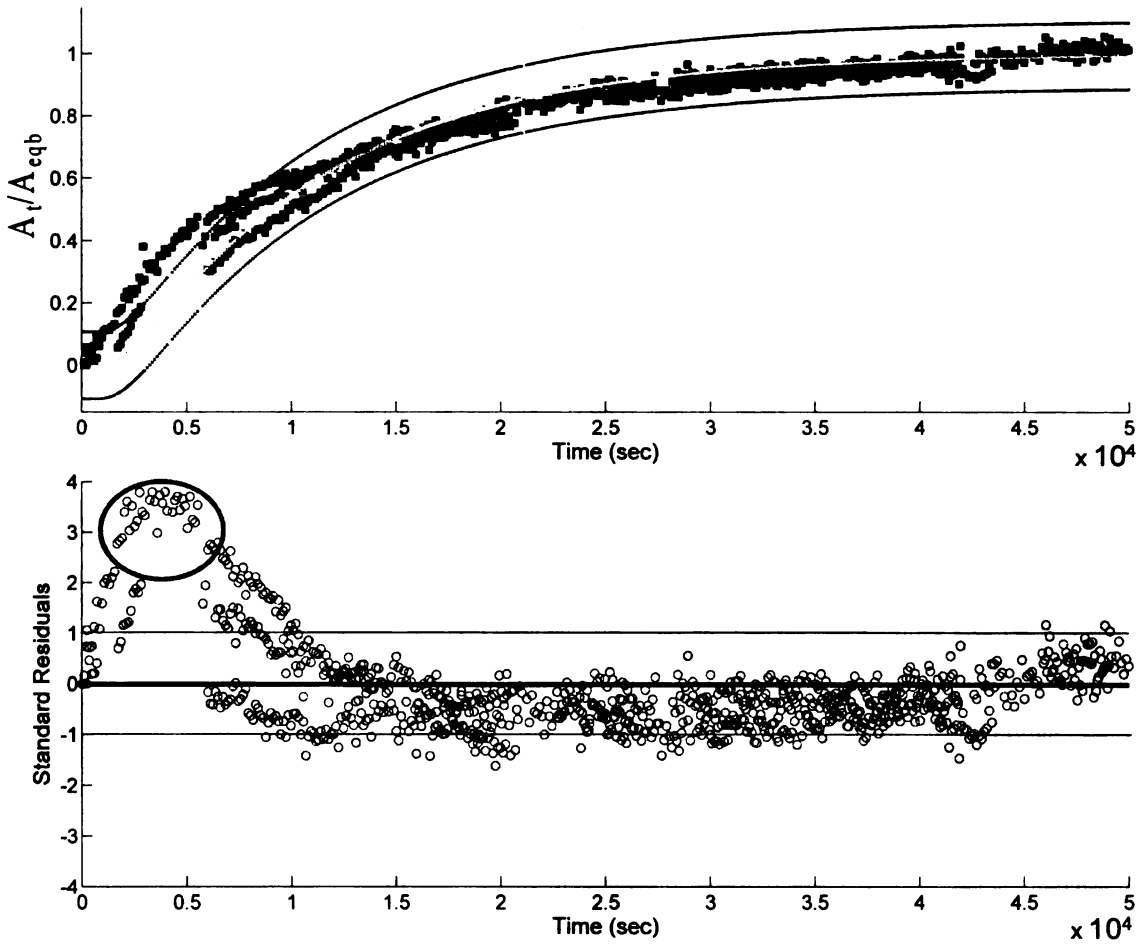


**Figure 4.3b** Normalized eugenol (1514 $cm^{-1}$) absorbance vs time at 6 ml/min eugenol flow condition at 23°C.

**Note:** The central line shows the best fit to the dotted experimental values of all the three replications. The outer lines show the prediction interval for the observed experimental values. The confidence interval of the best fit is very narrow to the fitted curve and not clearly visible in the figures. The standard residuals are shown in the graph below with dark line indicating zero residual. The red oval indicates the higher residuals.

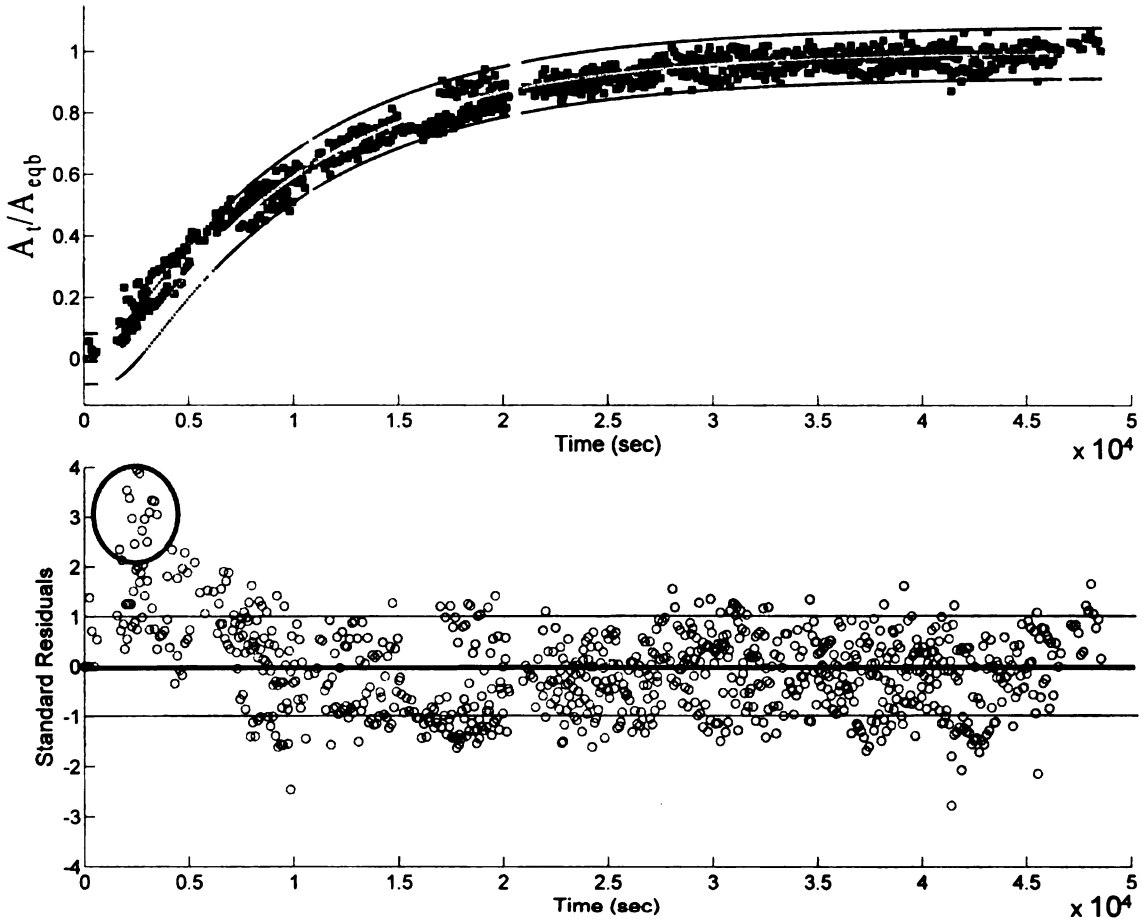


**Figure 4.3c** Normalized eugenol (1514 $cm^{-1}$) absorbance vs time at 8 ml/min eugenol flow condition at 23°C.

**Note:** The central line shows the best fit to the dotted experimental values of all the three replications. The outer lines show the prediction interval for the observed experimental values. The confidence interval of the best fit is very narrow to the fitted curve and not clearly visible in the figures. The standard residuals are shown in the graph below with dark line indicating zero residual. The red oval indicates the higher residuals.

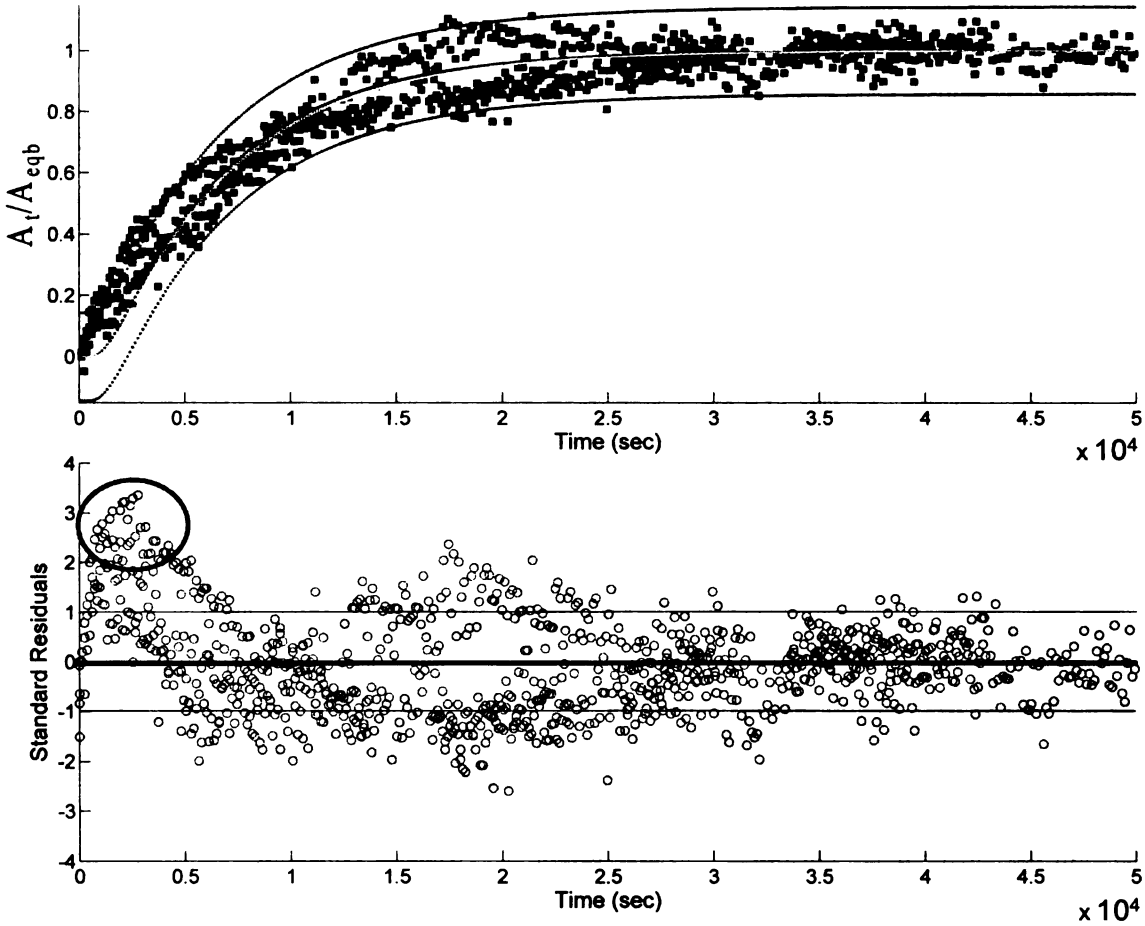


**Figure 4.3d** Normalized eugenol (1514 $cm^{-1}$) absorbance vs time at 11 ml/min eugenol flow condition at 23°C.

**Note:** The central line shows the best fit to the dotted experimental values of all the three replications. The outer lines show the prediction interval for the observed experimental values. The confidence interval of the best fit is very narrow to the fitted curve and not clearly visible in the figures. The standard residuals are shown in the graph below with dark line indicating zero residual. The red oval indicates the higher residuals.

Table 4.1 shows the $D$ values and the root mean square error (RMSE) involved in the measurements at the four flow rates. The values of $D$ at 0, 6 and 8 ml/min are close at $2.45 \times 10^{-10}$, $2.91 \times 10^{-10}$ and $3.37 \times 10^{-10}$ $cm^2/sec$ respectively, while the $D$ at 11 ml/min is very high at $4.90 \times 10^{-10}$ $cm^2/sec$. The transport of the permeant across the polymer film doest not depend only on diffusive transport but also on bulk flow induced by the pressure of the permeant flow system. However, bulk flow becomes a predominant mechanism in case of high degree of membrane swelling [101]. Hence, as we did not observe any swelling in the polymer film, bulk flow might not be the significant factor responsible for the rise in $D$ with flow rate. One reason for the increase in $D$ may be due to the faster increase in the absorbance due to more rapid achievement of efficient contact between the film and the crystal, which could not be accounted for by performing peak ratioing. Hence, the best flow rate was decided on the basis of RMSE values. The error values decreased with increased flow rate up to 8 ml/min, but were higher at 11 ml/min possibly due to some instability in film contact that may have occurred at high flow rate due to higher turbulence in the flow cell. Hence, all further experiments were performed at 8 ml/min.

**Table 4.1** Diffusion coefficient ($D$) and error by FTIR-ATR at different eugenol flow rates and at 23°C.

| **0 ml/min** | | **6 ml/min** | | **8 ml/min** | | **11 ml/min** | |
|---|---|---|---|---|---|---|---|
| ***$D$ x $10^{-10}$ ($cm^2$/sec)** | **RMSE** | ***$D$ x $10^{-10}$ ($cm^2$/sec)** | **RMSE** | ***$D$ x $10^{-10}$ ($cm^2$/sec)** | **RMSE** | ***$D$ x $10^{-10}$ ($cm^2$/sec)** | **RMSE** |
| $2.45 \pm 0.05_{a}$ (2.34 to 2.56) | 0.1266 | $2.91 \pm 0.02_{b}$ (2.87 to 2.95) | 0.0603 | $3.37 \pm 0.01_{c}$ (3.34 to 3.41) | 0.0448 | $4.90 \pm 0.04_{d}$ (4.82 to 4.99) | 0.0684 |



* values are expressed as best fit values for three replications ± standard error and ( 95% asymptotic confidence interval ).

RMSE = root mean square error

**Note**: different subscripts letter between columns and rows indicate statistically significant different values. ($\alpha = 0.05$)

### 4.3 FTIR-ATR Effect of angle of penetration of IR radiation

Figure 4.4 shows the normalized increase in eugenol absorbance with increase over time at 45° and 39° angle of penetration, respectively. Increasing depth of penetration (i.e., lower angle) meant getting close to the critical angle (~37° based on constant refractive index assumption). As seen in Figure 4.4b, highly variable data was obtained at 39°, which may have been the result of the spectrum distortion. As we approach the critical angle, the depth of penetration becomes indefinitely large, and the electric field amplitude changes abruptly, thus distorting the spectrum [55]. Table 4.2 shows the $D$ and the error involved in the experimental and predicted values at the two angles. Since the 45° incident angle resulted in lower RMSE, all experiments were performed at 45°.

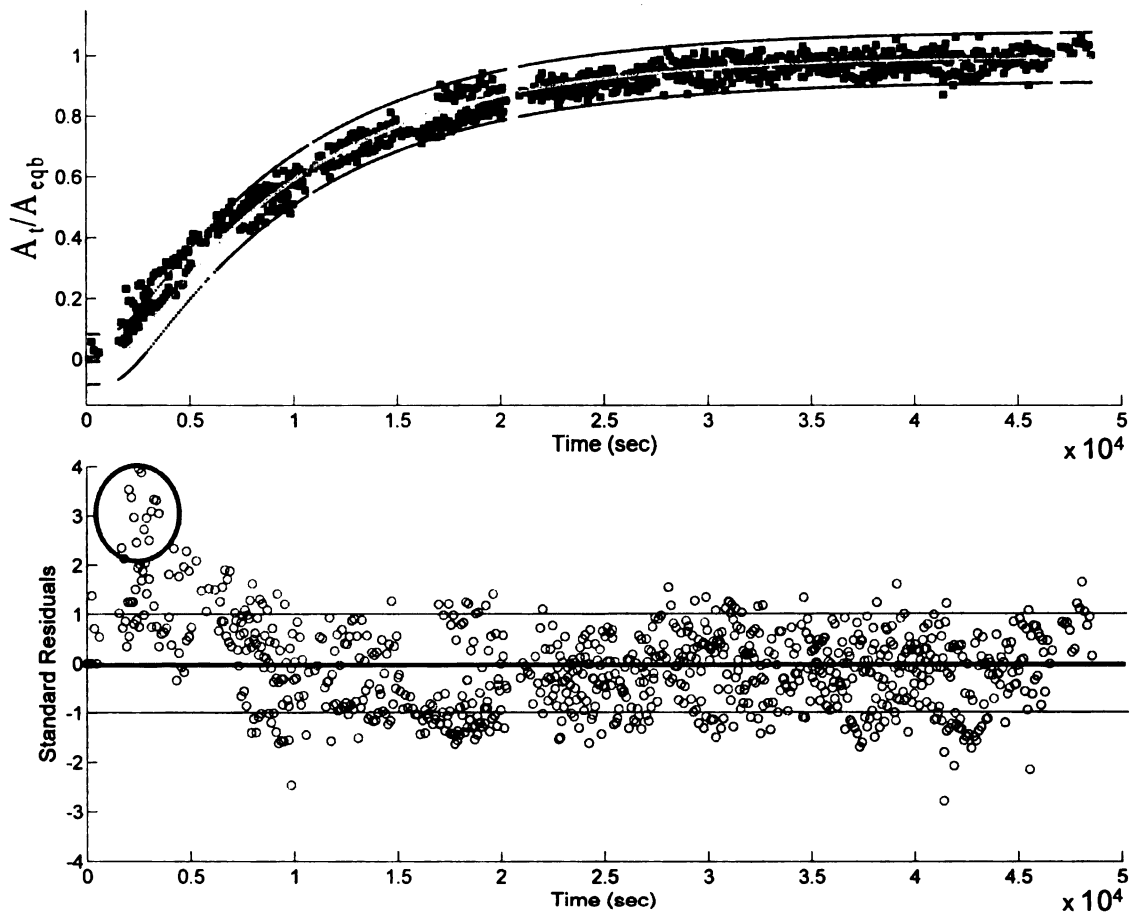


**Figure 4.4a** Normalized eugenol (1514 $cm^{-1}$) absorbance vs time at 45° IR penetration angle.

**Note:** The central line shows the best fit to the dotted experimental values of all the three replications. The outer lines show the prediction interval for the observed experimental values. The confidence interval of the best fit is very narrow to the fitted curve and not clearly visible in figure. The standard residuals are shown in the graph below with dark line indicating zero residual. The red oval indicates the higher residuals.

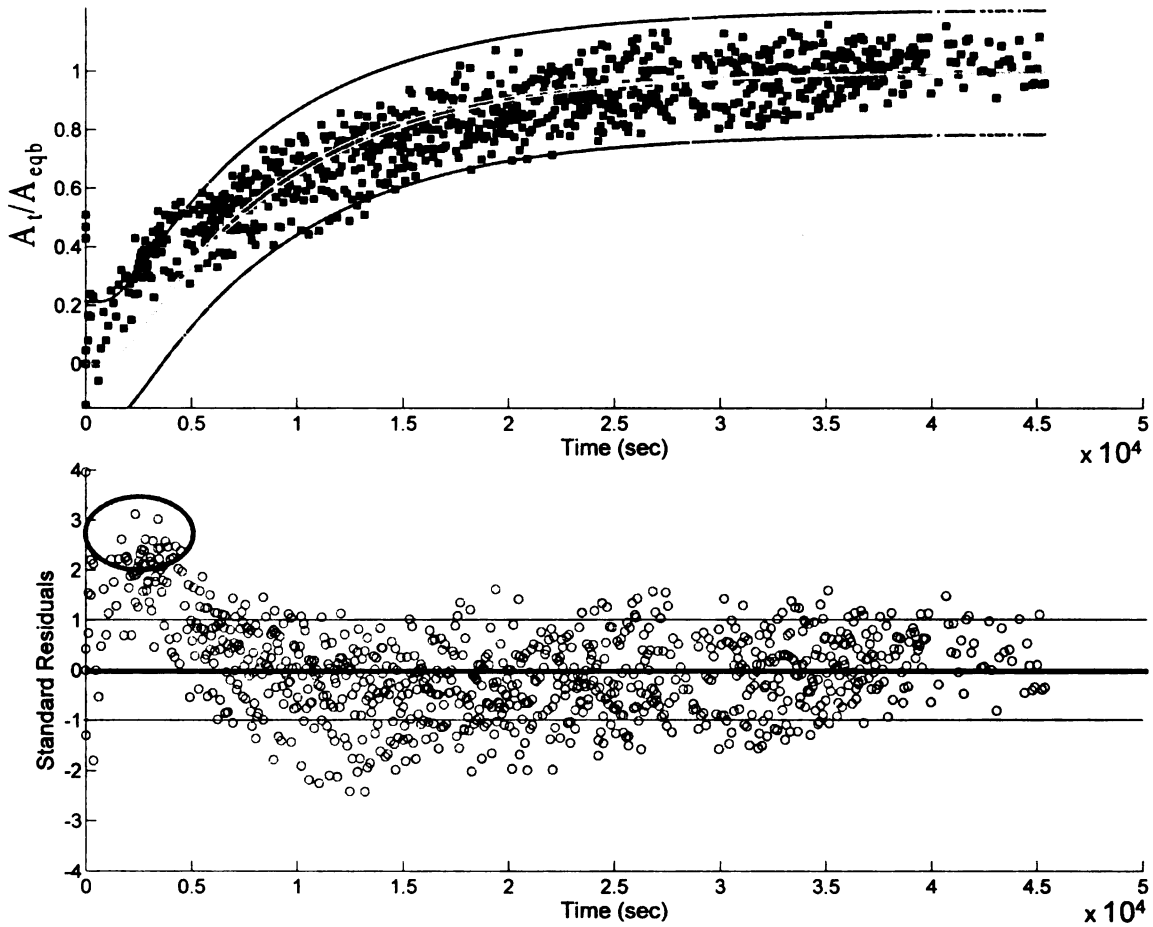


**Figure 4.4b** Normalized eugenol (1514 $cm^{-1}$) absorbance vs time at 39° IR penetration angle.

**Note**: The central line shows the best fit to the dotted experimental values of all the three replications. The outer lines show the prediction interval for the observed experimental values. The confidence interval of the best fit is very narrow to the fitted curve and visible in small region due to higher variation in data. The standard residuals are shown in the graph below with dark line indicating zero residual. The red oval indicates the higher residuals.

**Table 4.2** Diffusion coefficient (*D*) by FTIR- ATR at 45° and 39° incident angle and at 23°C.

| 45° | | 39° | |
|---|---|---|---|
| $*D \times 10^{-10}$ ($cm^2/sec$) | RMSE | $*D \times 10^{-10}$ ($cm^2/sec$) | RMSE |
| $3.37 \pm 0.01_{a}$ (3.34 to 3.41) | 0.0448 | $4.10 \pm 0.06_{b}$ (3.98 to 4.23) | 0.1278 |

* values are expressed as best fit values for three replications ± standard error and ( 95% asymptotic confidence interval ). RMSE = root mean square error

**Note**: different subscripts letter between columns and rows indicate statistically significant different values. ($\alpha = 0.05$)

### 4.4 FTIR-ATR based eugenol/LLDPE diffusion analysis at three different temperatures

The normalized eugenol absorbance over time at three different temperatures 16, 23 and 40°C are shown in Figure 4.5. The increase of eugenol absorbance at 40°C was much faster than at 23 and 16°C, taking only $1x10^4$ sec (2.8 h) to reach steady state. Higher residuals at the initial times can be seen in the plot of standard residuals for all the three temperatures, which could be mainly due to the inefficient contact between the LLDPE film and the crystal. The diffusion coefficients of individual sample runs and their equilibrium absorbance values at the three temperatures are shown in Appendix C1.

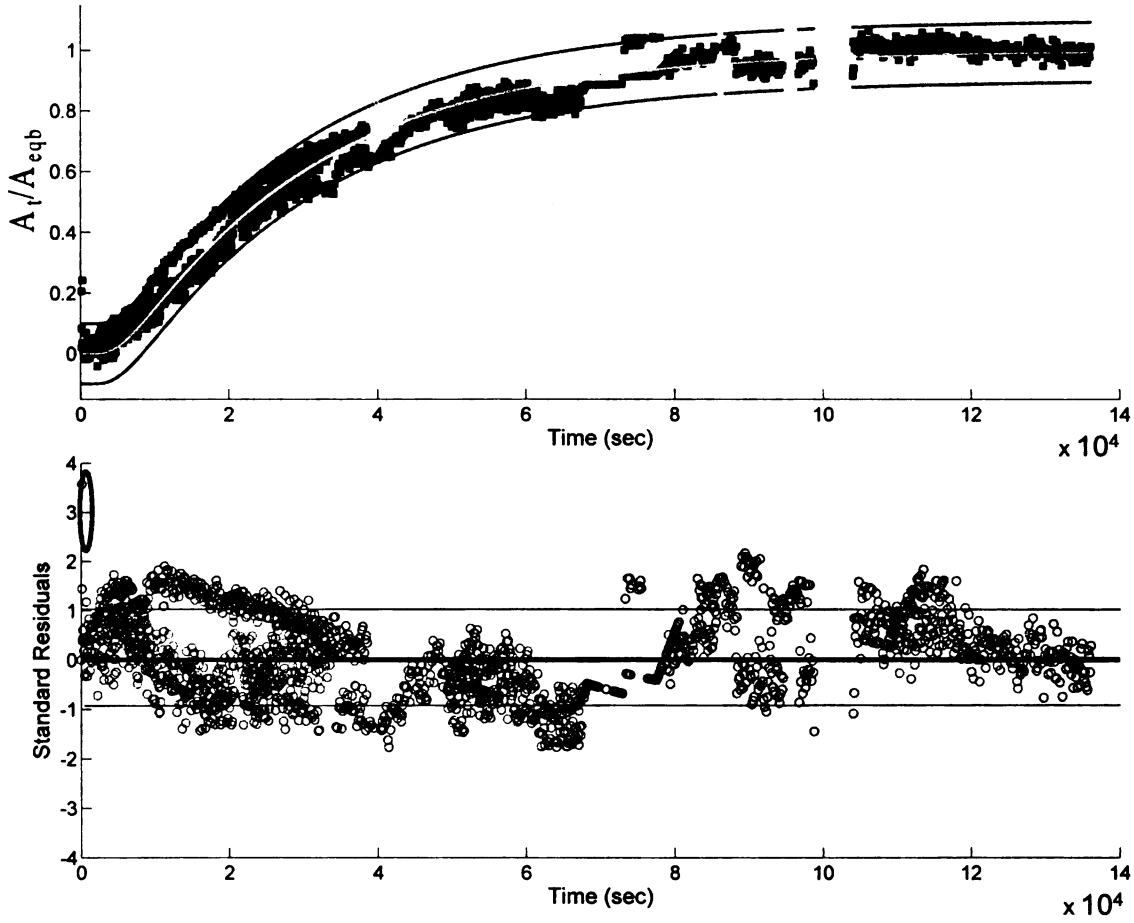


**Figure 4.5a** Normalized eugenol (1514 $cm^{-1}$) absorbance vs time at 16°C.

**Note**: The central line shows the best fit to the dotted experimental values of all the three replications. The outer lines show the prediction interval for the observed experimental values. The confidence interval of the best fit is very narrow to the fitted curve and not clearly visible in the figures. The standard residuals are shown in the graph below with dark line indicating zero residual. The red oval indicates the higher residuals.

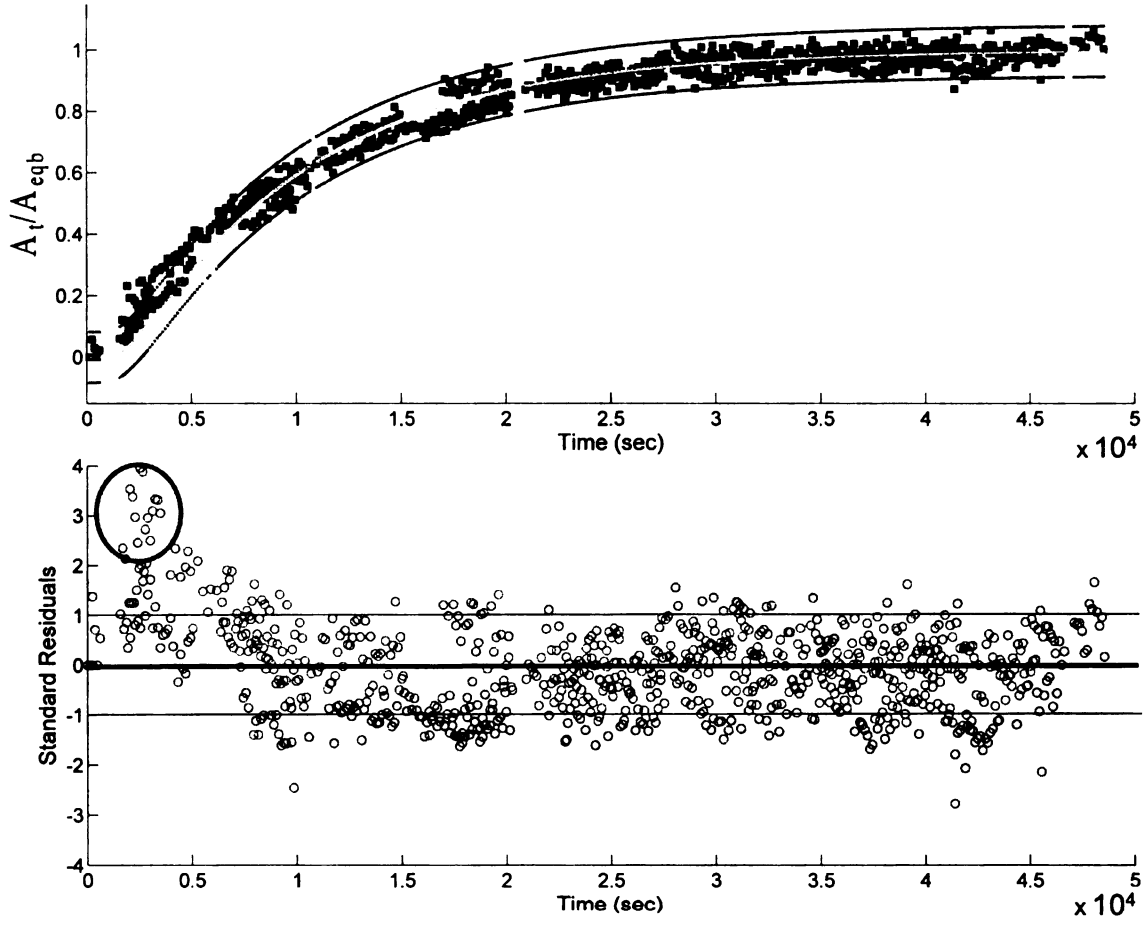


**Figure 4.5b** Normalized eugenol (1514 $cm^{-1}$) absorbance vs time at 23°C.

**Note**: The central line shows the best fit to the dotted experimental values of all the three replications. The outer lines show the prediction interval for the observed experimental values. The confidence interval of the best fit is very narrow to the fitted curve and not clearly visible in the figures. The standard residuals are shown in the graph below with dark line indicating zero residual. The red oval indicates the higher residuals.

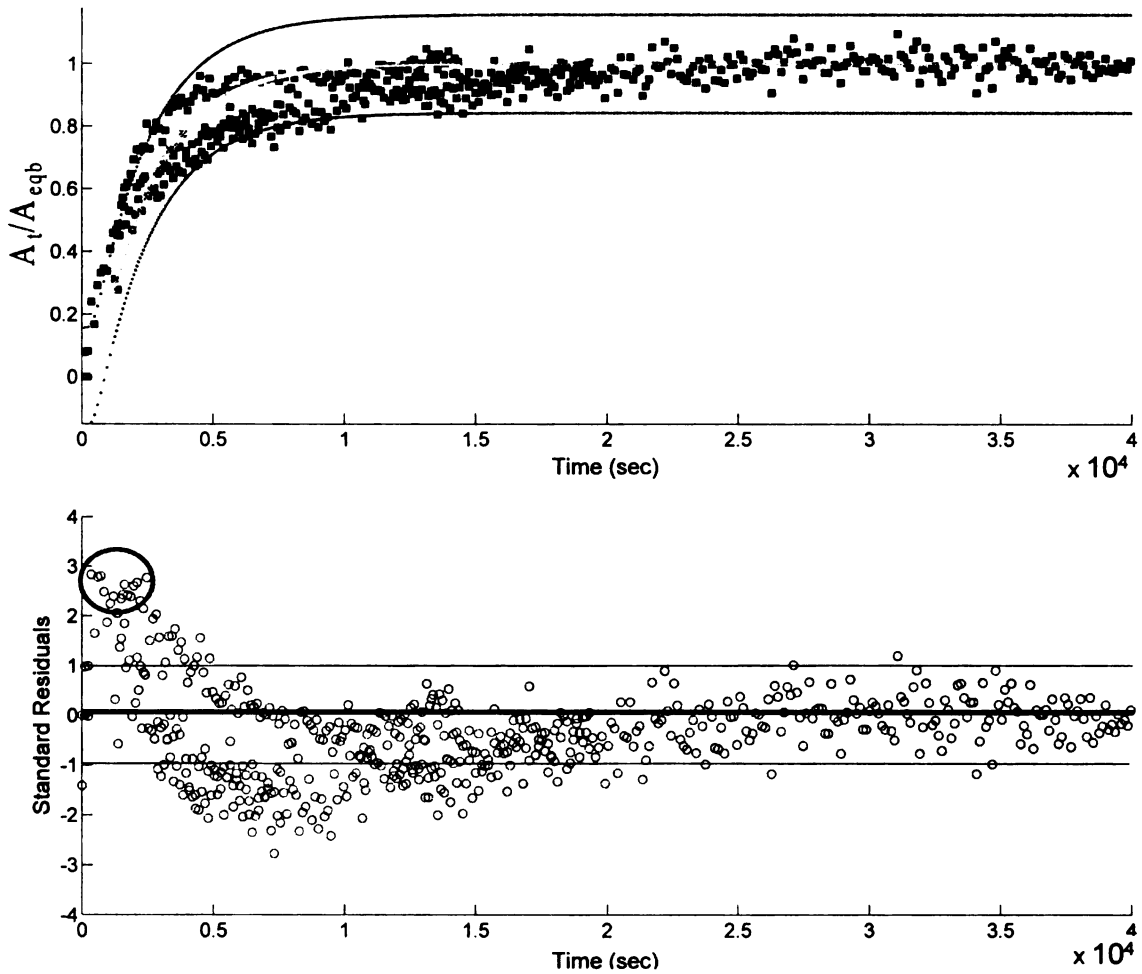


**Figure 4.5c** Normalized eugenol (1514 $cm^{-1}$) absorbance vs time at 40°C.

**Note**: The central line shows the best fit to the dotted experimental values of all the three replications. The outer lines show the prediction interval for the observed experimental values. The confidence interval of the best fit is very narrow to the fitted curve and not clearly visible in the figures. The standard residuals are shown in the graph below with dark line indicating zero residual. The red oval indicates the higher residuals.

In order to determine the effect of initial higher residuals on the *D* value, the experimental data were fitted by replacing the initial higher residual absorbance data by the best-predicted/theoretical values (Figure 4.6). Despite the perfect fit of the initial data, this procedure did not significantly change the *D* values. *D* with perfect initial fit was $3.32 \times 10^{-10}$ $cm^2/sec$ compared to *D* without discarding the initial data of $3.37 \times 10^{-10}$ $cm^2/sec$ obtained at 23°C. Moreover, after running the sensitivity of *D* in equation 3.2 and plotting against time, the value of *D* was most sensitive (highest point of sensitivity curve) in the region of $0.4<A_t/A_{eqb}<0.6$, where the theoretical diffusion curve fits well with the experimental values (Figure 4.7). Hence, the higher residuals in the initial stage did not significantly affect the results for *D*.

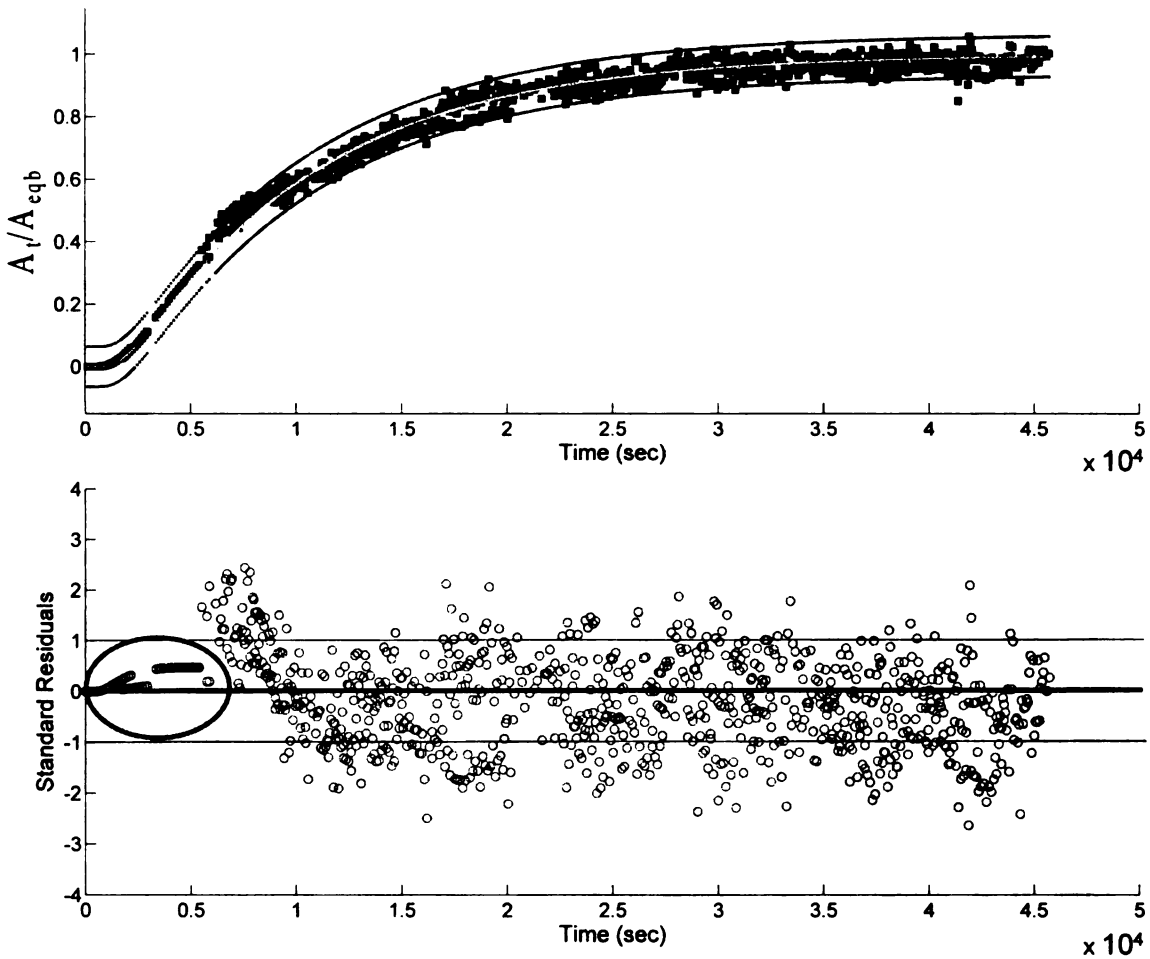


**Figure 4.6** Normalized eugenol (1514 $cm^{-1}$) absorbance vs time at 23°C by replacing initial data with best fit values.

**Note**: The central line shows the best fit to the dotted experimental values of all the three replications. The outer lines show the prediction interval for the observed experimental values. The confidence interval of the best fit is very close to the fitted curve and not clearly visible in the figures. The standard residuals are shown in the graph below with dark line indicating zero residual. The red oval indicates the zero residual obtained after replacing data with best fit values.

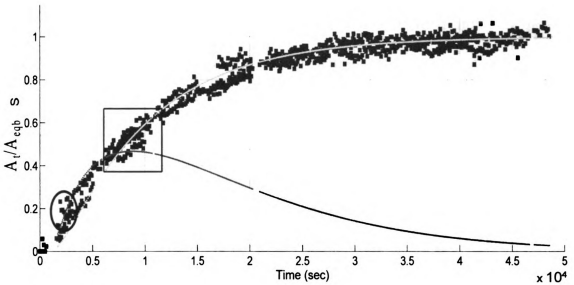


**Figure 4.7** FTIR-ATR normalized eugenol (1514 $cm^{-1}$) absorbance vs time at 23°C and Sensitivity. The central line shows the best fit to the dotted experimental values of all the three replications. The darker line i.e. scaled sensitivity coefficient S vs time is overlapped on ATR values and ATR best fit. The dark oval indicates the initial residuals, while the square indicates the data points in region of highest S.

**Note**: The scaled sensitivity coefficient S and $A_t/A_{eqb}$ have same scale.

### 4.5 HPLC based eugenol/LLDPE diffusion analysis at three different temperatures

Figures 4.8 and 4.9 show the normalized mass gain at three temperatures (16, 23 and 40°C) obtained by two-sided and one-sided HPLC based diffusion process respectively. The insets in the figures show the normalized mass gain at short times or unsteady state of diffusion process. It can be seen that experimental values exhibit Fickian behavior. The central line passing through experimental values is the best fit diffusion curve obtained by using Equation 2.9. The inner lines around the best-fit curve indicate its 95% confidence interval. The outer lines indicate the 95% prediction interval of the observed values. The errors in the HPLC data were within two standard residual values, so good fit of the experimental and predicted values could be established. It was also found that the *D* value in HPLC experiments was most sensitive (highest point of sensitivity curve) in the region $0.5<M_t/M_{eqb}<0.8$ (Figure 4.10). The best fit curve appears to deviate from 95% CI at some points away from experimental values because of the ways both are obtained. The prediction and confidence interval points are obtained at times where experimental data is present and then joined to form a curve. Hence they are not smooth. The best fit curve, on other hand, was obtained by obtaining first the best *D* value and then finding the normalized mass gain in Equation 3.3 with this *D* value and using time intervals much smaller than the actual experimental time intervals. This resulted in smooth fitting curve. The equilibrium mass gain values of eugenol for both two- and one-sided diffusion are given in Appendix C2.

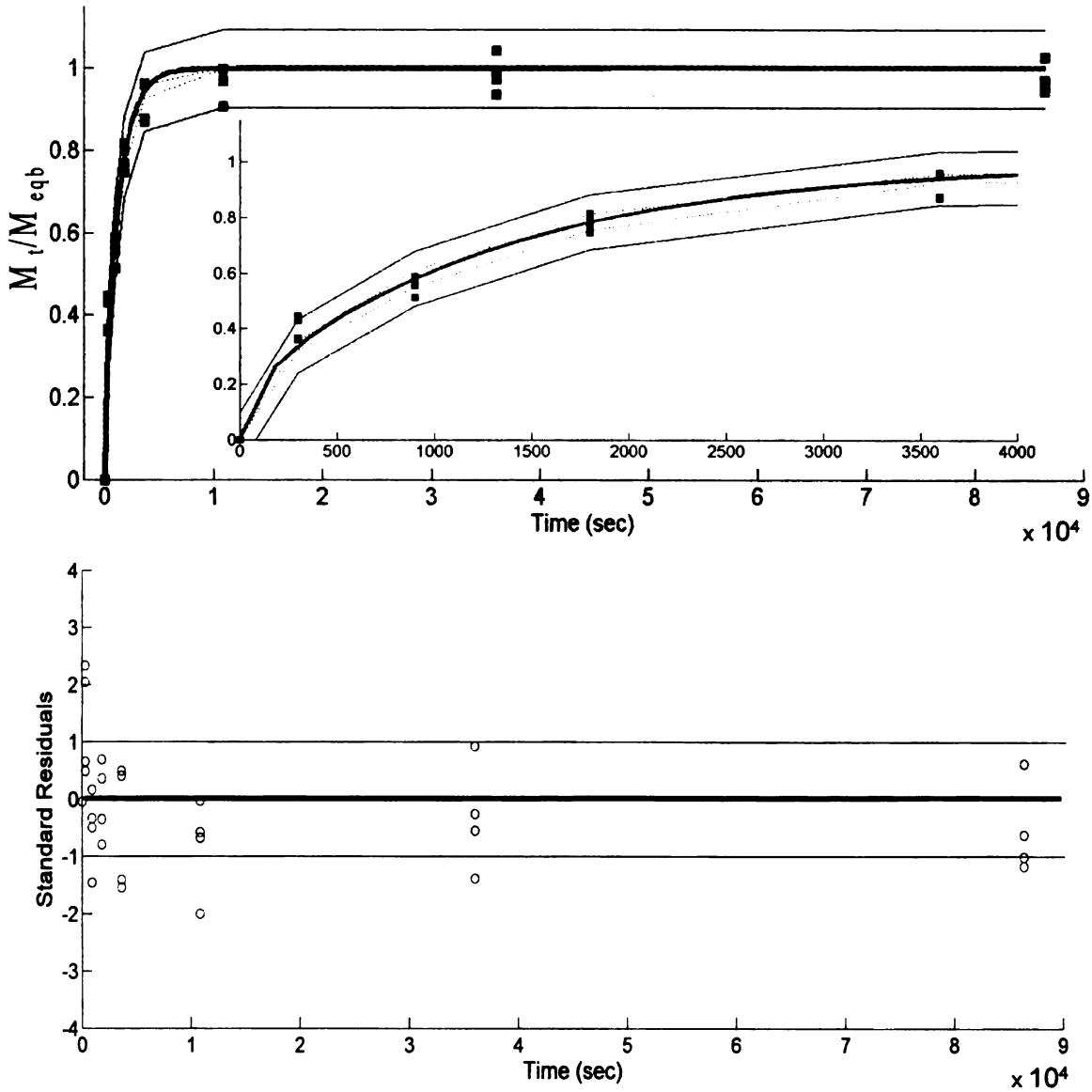


**Figure 4.8a** HPLC two-sided normalized eugenol mass gain vs time at 16°C. The central line shows the best fit to the dotted experimental values. The outer lines show the prediction interval for the observed experimental values. The inner lines around the best fit curve are the confidence intervals for the best fit (the inset has the same axis as larger mass gain graph). The standard residuals are shown in the graph below with dark line indicating zero residual.

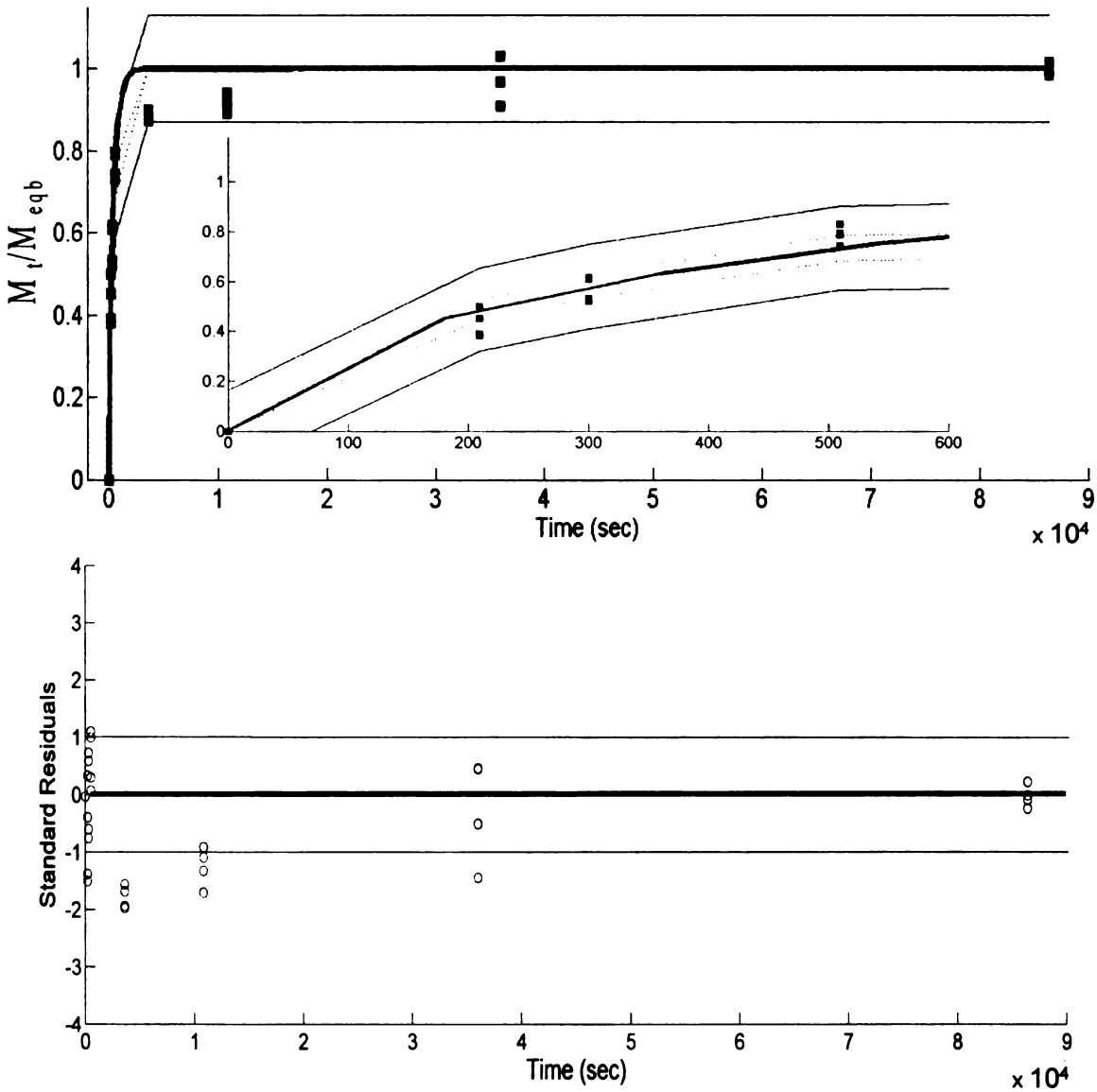


**Figure 4.8b** HPLC two-sided normalized eugenol mass gain vs time at 23°C. The central line shows the best fit to the dotted experimental values. The outer lines show the prediction interval for the observed experimental values. The inner lines around the best fit curve are the confidence intervals for the best fit (the inset has the same axis as larger mass gain graph). The standard residuals are shown in the graph below with dark line indicating zero residual.

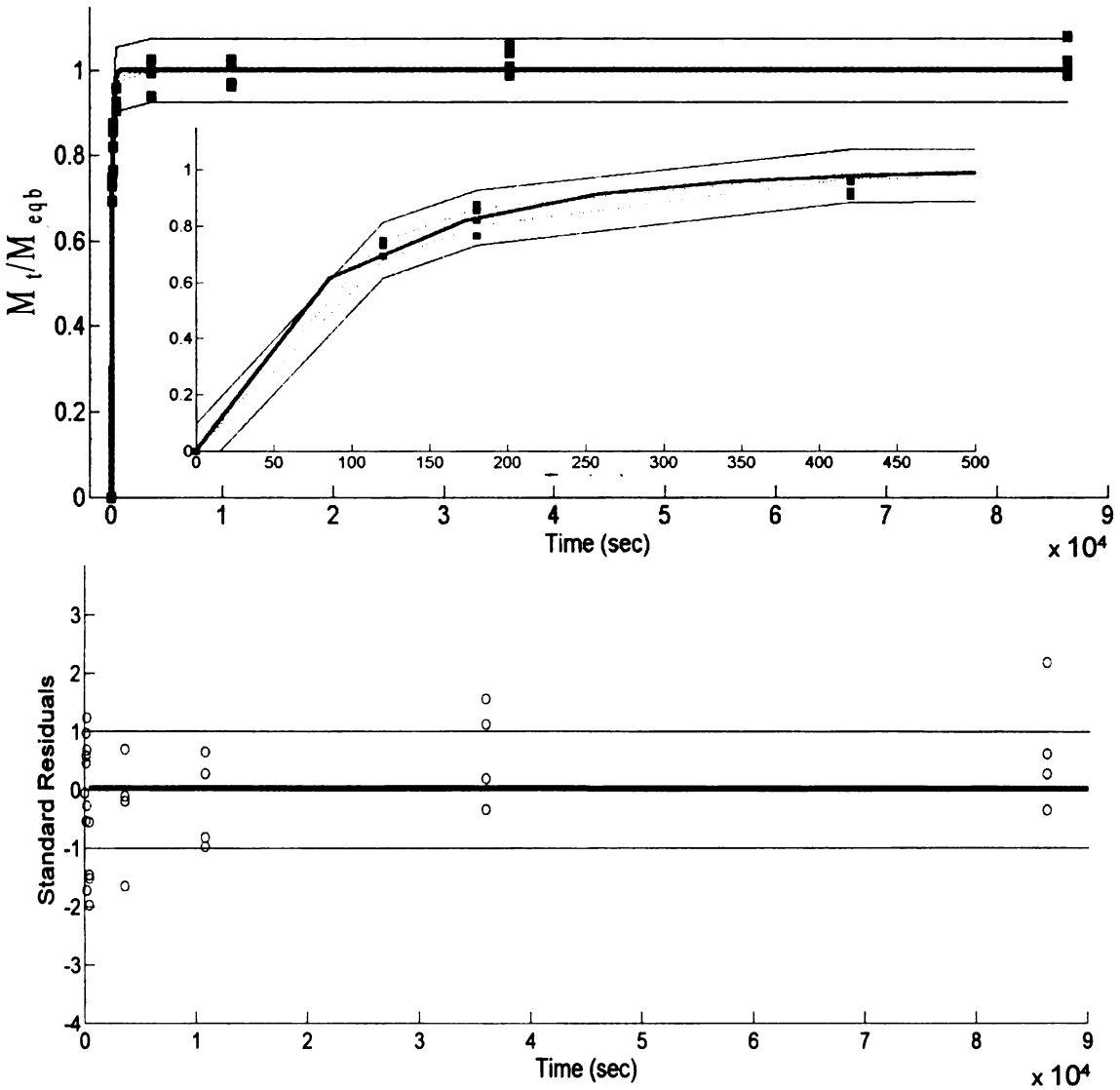


**Figure 4.8c** HPLC two-sided normalized eugenol mass gain vs time at 40°C. The central line shows the best fit to the dotted experimental values. The outer lines show the prediction interval for the observed experimental values. The inner lines around the best fit curve are the confidence intervals for the best fit (the inset has the same axis as larger mass gain graph). The standard residuals are shown in the graph below with dark line indicating zero residual.

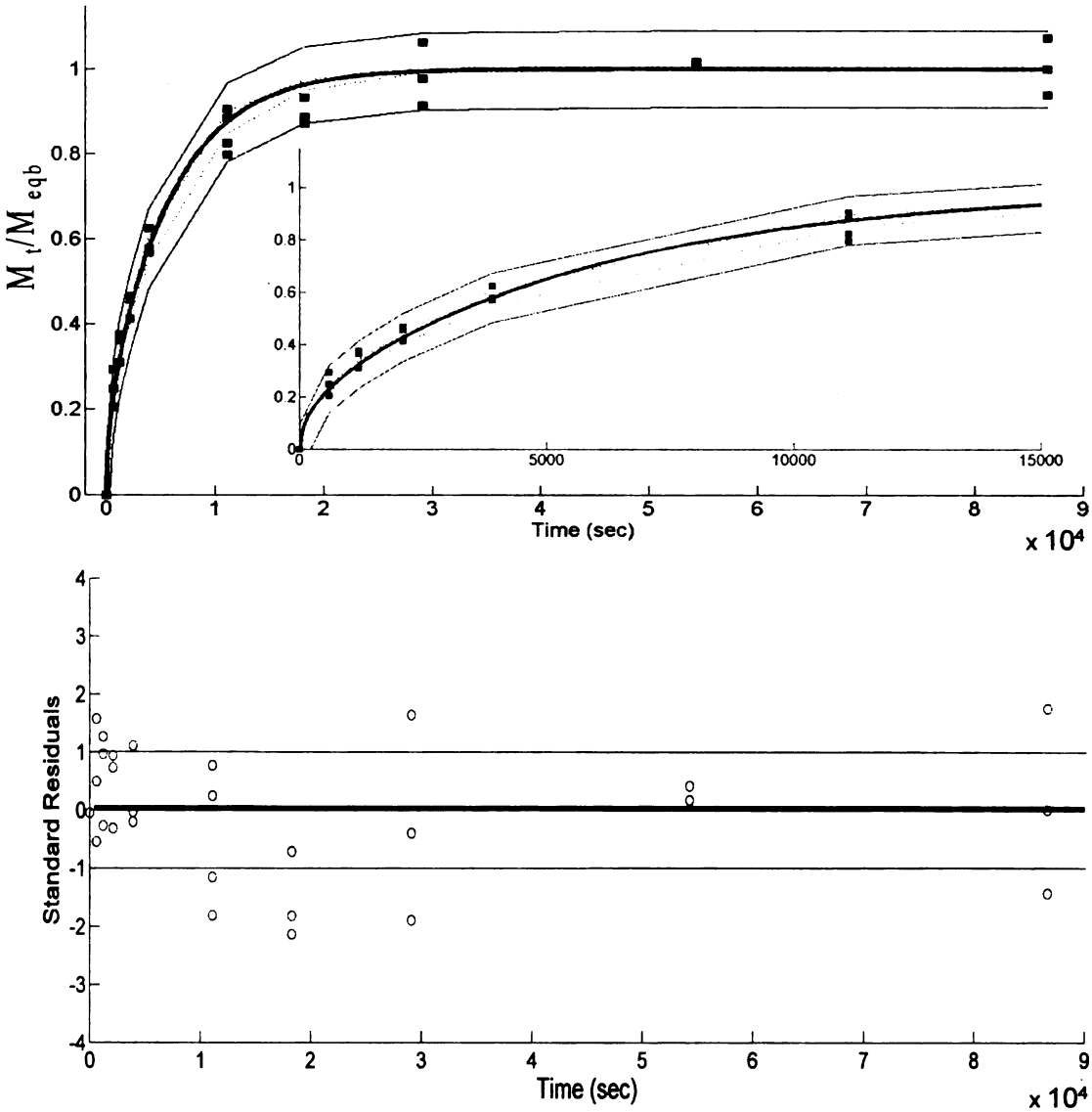


**Figure 4.9a** HPLC one-sided normalized eugenol mass gain vs time at 16°C. The central line shows the best fit to the dotted experimental values. The outer lines show the prediction interval for the observed experimental values. The inner lines around the best fit curve are the confidence intervals for the best fit (the inset has the same axis as larger mass gain graph). The standard residuals are shown in the graph below with dark line indicating zero residual.

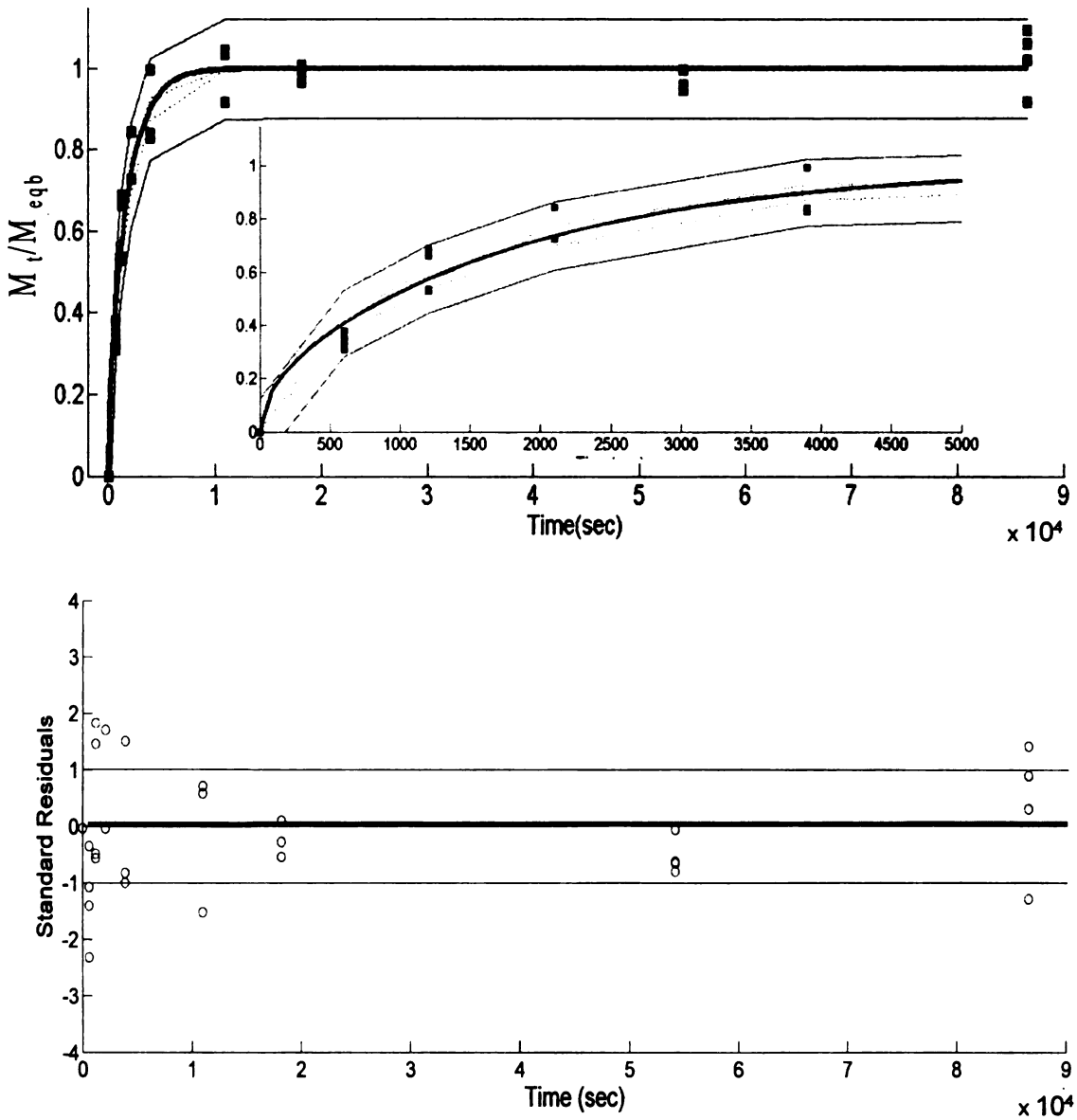


**Figure 4.9b** HPLC one-sided normalized eugenol mass gain vs time at 23°C. The central line shows the best fit to the dotted experimental values. The outer lines show the prediction interval for the observed experimental values. The inner lines around the best fit curve are the confidence intervals for the best fit (the inset has the same axis as larger mass gain graph). The standard residuals are shown in the graph below with dark line indicating zero residual.

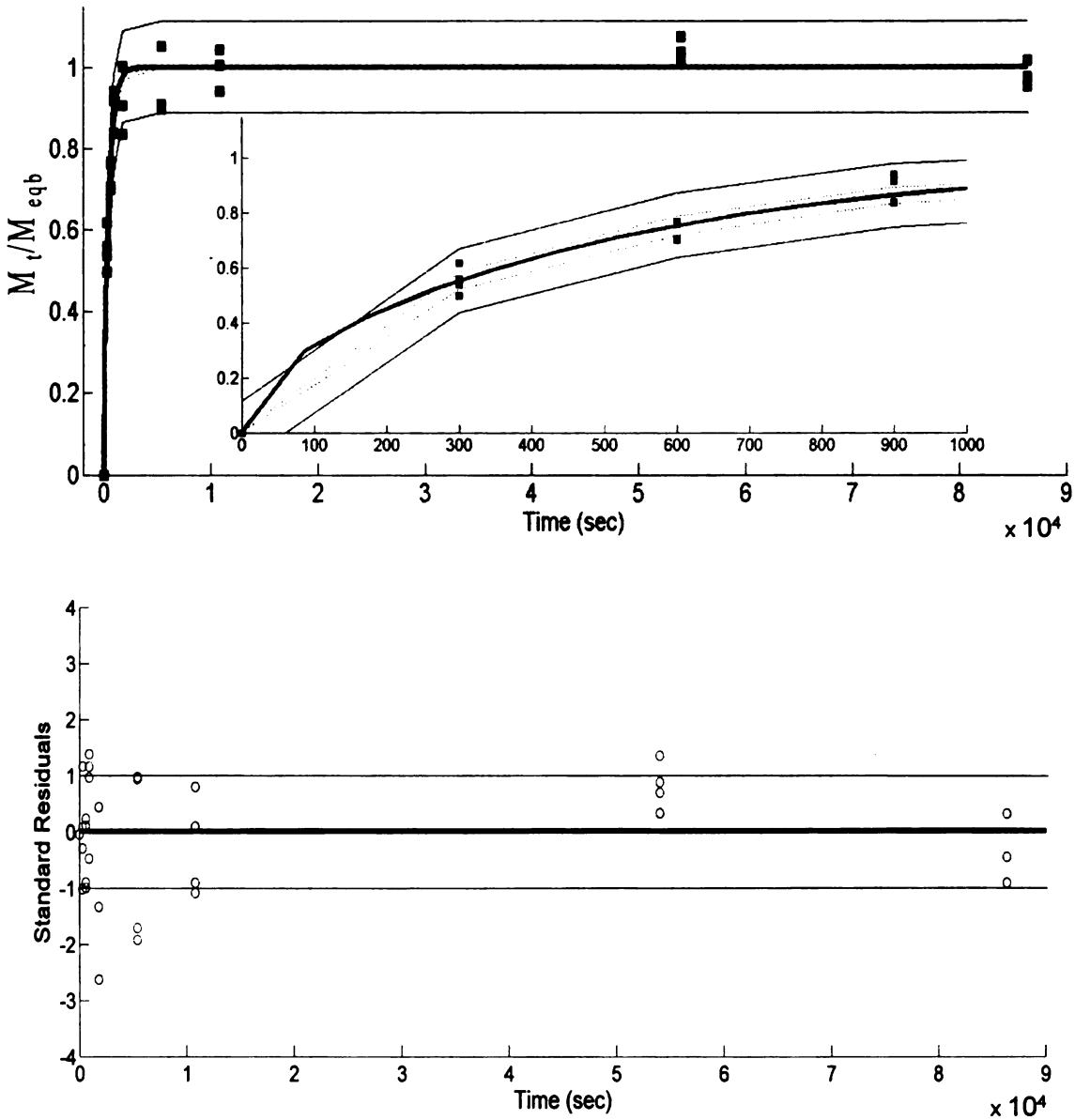


**Figure 4.9c** HPLC one-sided normalized eugenol mass gain vs time at 40°C. The central line shows the best fit to the dotted experimental values. The outer lines show the prediction interval for the observed experimental values. The inner lines around the best fit curve are the confidence intervals for the best fit (the inset has the same axis as larger mass gain graph). The standard residuals are shown in the graph below with dark line indicating zero residual.

As shown in Figures 4.5a, 4.8a and 4.9a that the equilibrium time in case of two-sided HPLC (1 x $10^4$ sec or 2.8 h at 16°C) and one-sided HPLC (3 x $10^4$ sec or 8.3 h at16°C) method was much shorter compared to FTIR-ATR method (10 x $10^4$ sec or 28 h at 16°C). The difference in the equilibrium time in the two-sided and one-sided HPLC experiments was evidently due to the faster sorption of eugenol from the two surfaces of LLDPE exposed in the former compared to one side in the latter process. But the difference in equilibrium time between FTIR-ATR process and one-sided HPLC process was not only due to slower diffusion observed in former process but also contributed by the lag time (approximately zero absorbance till 0.5 x $10^4$ sec or 1.4 h in Fig 4.5a.) This lag time is due to the time required for eugenol to diffuse through the film and come in range of the evanescent field ($d_p$ = 1.25 μm), where it can be detected. The FTIR-ATR model (Equation 2.26) already takes into account the excess time required for eugenol to each evanescent field by incorporation of expression of exponential decay of evanescent field, i.e. $exp(-2\gamma z)$ in equation 2.22. The integration of this expression over entire thickness of the polymer helps determine the $D$ value for the actual polymer thickness (detailed derivation in Appendix F)

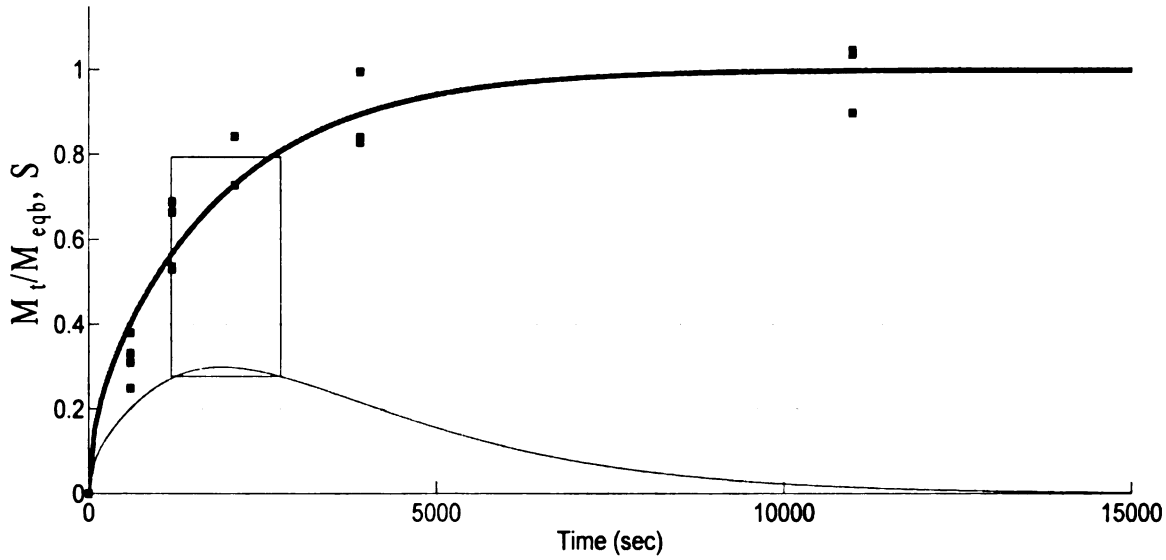


**Figure 4.10** HPLC one-sided normalized eugenol mass gain vs time at 23°C (inset in figure 4.9a). The central line shows the best fit to the dotted experimental values. The lighter line shows scaled sensitivity coefficient S vs time. The rectangle indicates the data points in region of highest S.

**Note**: The scaled sensitivity coefficient S and $M_t/M_{eqb}$ have same scale.

**Table 4.3** Diffusion coefficient (*D*) by FTIR-ATR and HPLC techniques

| **Temperature** | **FTIR-ATR** | | **HPLC** Two-sided | | **HPLC** One-sided | |
|---|---|---|---|---|---|---|
| °C | ***D x $10^{-10}$ ($cm^2$/sec)** | **RMSE** | ***D x $10^{-10}$ ($cm^2$/sec)** | **RMSE** | ***D x $10^{-10}$ ($cm^2$/sec)** | **RMSE** |
| 16 | $1.06 \pm 0.01_{a}$ (1.05 to 1.07) | 0.0683 | $2.96 \pm 0.15_{b}$ (2.66 to 3.27) | 0.0463 | $2.71 \pm 0.13_{b}$ (2.43 to 2.99) | 0.0440 |
| 23 | $3.37 \pm 0.01_{c}$ (3.34 to 3.41) | 0.0448 | $8.86 \pm 0.69_{d}$ (7.44 to 10.28) | 0.0741 | $8.46 \pm 0.60_{d}$ (7.23 to 9.69) | 0.0663 |
| 40 | $13.23 \pm 0.18_{e}$ (12.86 to 13.61) | 0.0631 | $35.11 \pm 1.60_{f}$ (31.85 to 38.37) | 0.0370 | $32.19 \pm 1.87_{f}$ (28.41 to 35.99) | 0.0545 |

* values are expressed as best fit values for three replications ± standard error and ( 95% asymptotic confidence interval ).

RMSE = root mean square error

Note: different subscripts letter between columns and rows indicate statistically significant different values. ($\alpha = 0.05$)

Table 4.3 summarizes the FTIR-ATR and HPLC double and single sided results at three temperatures. The *D* values for two-sided and one-sided HPLC were statistically not significantly different (p=0.05). The FTIR-ATR values were statistically different compared to both single side and two side diffusion process (p=0.05). Eugenol *D* values have been reported to vary in polyolefins (HDPE to LDPE) at 23°C from 1.3 to 10 $x10^{-10}$ $cm^2$/sec [40]. However these values were calculated with the polymer phase in contact with the liquid phase (methanol/ethanol). This contact with the organic liquids may have actually accelerated the loss of eugenol from the film, thereby driving the diffusion coefficient to higher values. A very recent work by Vitrac et al. [102] used the molecular descriptors like Van-der-waal volume, gyration radius and a dimensionless shape parameter in the process of decision tree to estimate *D* values of various compounds in polyolefins. By using a regression tree the *D* value of eugenol in LDPE-LLDPE at 23°C was estimated to be $\log_{10}(-13.9)$ $m^2$/sec or 1.25 x $10^{-10}$ $cm^2$/sec. This value is clearly closer to *D* value estimated by FTIR-ATR technique.

To better understand the significance of eugenol diffusion coefficients we compare it with some other organic compounds; e.g. diffusion of amyl acetate in high density poly(ethylene) (HDPE) showed value of 3.05 x $10^{-9}$ $cm^2$/sec at 33°C (by FTIR-ATR technique) [15], and BHT (I–1076) showed *D* value 2.2 x $10^{-9}$ $cm^2$/sec at 50°C [103]. Cava et al. [104] used FTIR based desorption technique to find the *D* values of limonene (18.5 x $10^{-9}$ $cm^2$/sec), linalool (3.8 x $10^{-9}$ $cm^2$/sec), pinene (9.6 x $10^{-9}$ $cm^2$/sec) and citral (5.5 x $10^{-9}$ $cm^2$/sec) in polyethylene at 22°C. All these values were almost one

order of magnitude higher than $D$ of eugenol in LLDPE which could be expected of the higher volatility (higher partial pressure) than eugenol at the tested temperatures.

The activation energy of diffusion ($E_D$) was calculated by the two methodologies by fitting the Arrhenius equation (Equation 4.1). Activation energy can be defined as the energy required by the permeant molecule to jump across the polymer chains by creating an opening between the chains [103].

$$D = D_0 \exp(-E_D / RT) \tag{4.1}$$

where $D_0$ is the pre exponential factor ($cm^2/sec$), $R$ ( 8.314 kJ/K mol) is the gas constant and $T$ is temperature (K).

$E_D$ values of 76.45, 74.95 and 74.68 kJ/mol for the FTIR-ATR, two-sided HPLC, and one-sided HPLC, were obtained, respectively (Table 4.4 and Figure 4.11). Though the $D$ values of FTIR-ATR and HPLC techniques are not exactly comparable, the close relation of the $E_D$ values shows that a very similar relation of $D$ with temperature by both the techniques was obtained. Activation energy of some saturated hydrocarbons such as n-hexane and n-decane through low density poly(ethylene) (LDPE) film has been reported. $E_D$ depends on penetrant size and shape and seems to increase with n-hexane having a value 67.7 kJ/mol to n-decane having 96.8 kJ/mol [105]. $E_D$ value of toluene diffusion in LDPE was reported to be 87 kJ/mol [106]. Antioxidants like methylester and octadecyester-Irganox 1076 had $E_D$ values of 87 and 104 kJ/mol in LDPE [107].

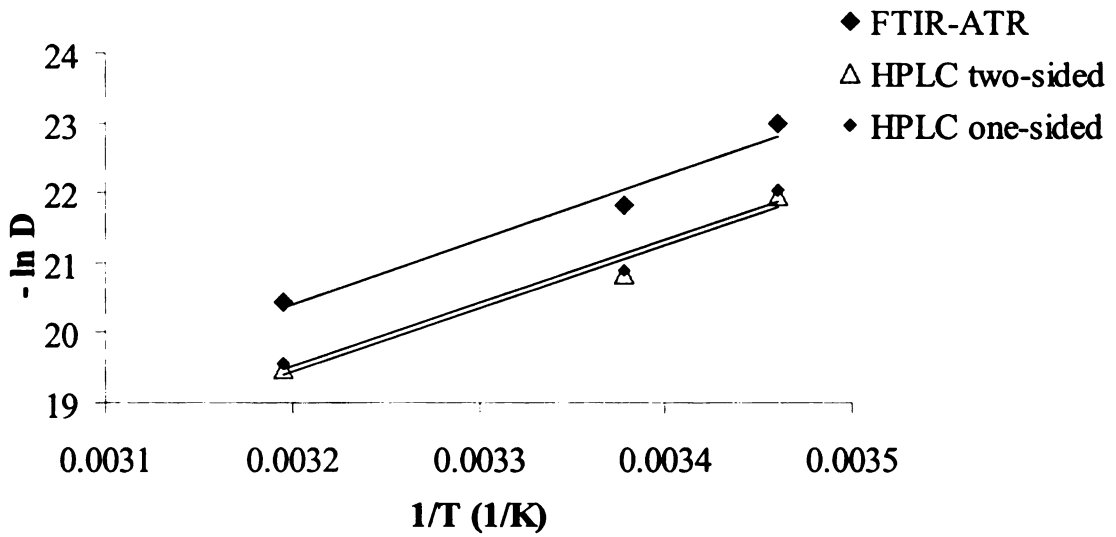


**Figure 4.11** Fit of Arrhenius equation for eugenol/LLDPE system by FTIR-ATR and HPLC methods.

**Note**: the black line indicates the linear relation between negative logarithm of *D* values and reciprocal of temperature.

**Table 4.4** Activation energy ($E_D$) by FTR-ATR and HPLC techniques

| | **FTIR-ATR** | **HPLC** Two-sided | **HPLC** One-sided |
|---|---|---|---|
| $E_D$ (kJ/mol) | 76.45 | 74.95 | 74.68 |
| $D_o$ ($cm^2$/sec) | 8216.50 | 12112.58 | 10084.96 |
| $R^2$ | 0.9707 | 0.9769 | 0.9707 |

Although the higher variation of *D* values by HPLC method, this technique was developed for quantification and it has been considered a conventional technique for

many years. FTIR on the other hand was developed mainly for identification, although it is now being used for quantification. The *D* values were of the same order of magnitude in all the three different experiments for all three temperatures. But the higher value of *D* for two-sided and one-sided HPLC compared to FTIR-ATR based value is not well understood and may be due to the inherent difference in the two measuring techniques. *D* value of $8.86 \times 10^{-10}$ and $8.46 \times 10^{-10}$ $cm^2/sec$ was observed for two-sided and one-sided HPLC based diffusion process respectively, as against $3.37 \times 10^{-10}$ $cm^2/sec$ obtained in ATR result at 23°C. Higher values of *D* in case of amyl acetate sorption in LDPE by gravimetric measurement using saturated vapor compared to FTIR-ATR results with liquid have also been reported by Balik et al. [15].

A possible source of error leading to higher *D* values in HPLC based results could be the inability to efficiently clean eugenol from the polymer surface, resulting in higher concentrations than those in the film. Additional steps like weighing of the film and extraction may contribute to the higher error seen in HPLC based values. Since the commercial LLDPE film was mono-oriented, a possible chance of error in FTIR-ATR based values may actually be due to the non-uniform distribution of crystallites in the film, giving rise to more complex depth profile of the attenuated radiation. On the contrary, the lower *D* values in FTIR-ATR indicating slower transfer of eugenol across LLDPE film may well be due to differential crystallite distribution which might not be accounted for in the HPLC techniques. This discussion can only be verified in future work by performing depth profiling experiments with the LLDPE film.

A possible error in eugenol absorbance change may be due to the measurement error in $A_{t=0}$. $A_{t=0}$ was the IR absorbance value measured as soon as eugenol was in

contact with the LLDPE film (eugenol could be seen entering and exiting the flow cell through small glass tube at inlet and outlet of flow cell). But this absorbance value was obtained after performing 35 scans, which meant that eugenol was already in contact for ~1 min. Another source of error in $A_{t=0}$ is that the LLDPE film and crystal contact would not have been stable when eugenol had just entered the cell. This was evident from the fact that air bubbles were observed exiting the glass tube at the outlet of the flow cell when the IR measurement scans had started. So, if the actual $A_{t=0}$ value is lower than that which is expected to have been obtained if the contact was perfect, it may be responsible for higher residual in the initial phase until the contact became stable. A similar problem of polymer film/crystal contact stability has been discussed by Yi et al. [35], who have also suggested a mathematical correction applicable in cases where peak ratioing is performed.

It is also evident that it is not possible to continuously monitor the entire diffusion process in the HPLC (also known "pat and dry") as in FTIR-ATR technique, especially at higher temperatures. In the FTIR-ATR technique, monitoring of the spectrum throughout the diffusion process did not indicate any anomalous changes like wavelength shift [17] in absorbance peaks, indicating there was no polymer penetrant interaction (see figures D1 to D3 in Appendix D). Also, though the LLDPE peaks were overlapped by eugenol peaks, we did not observe any slow or abrupt decrease in LLDPE absorbance at any stage in the diffusion process, indicating there was no significant swelling in the film. Figure 4.12 shows the increase in absorbance, observed in the eugenol peak (1514 $cm^{-1}$) and adjacent LLDPE peak (1462 $cm^{-1}$) over time.

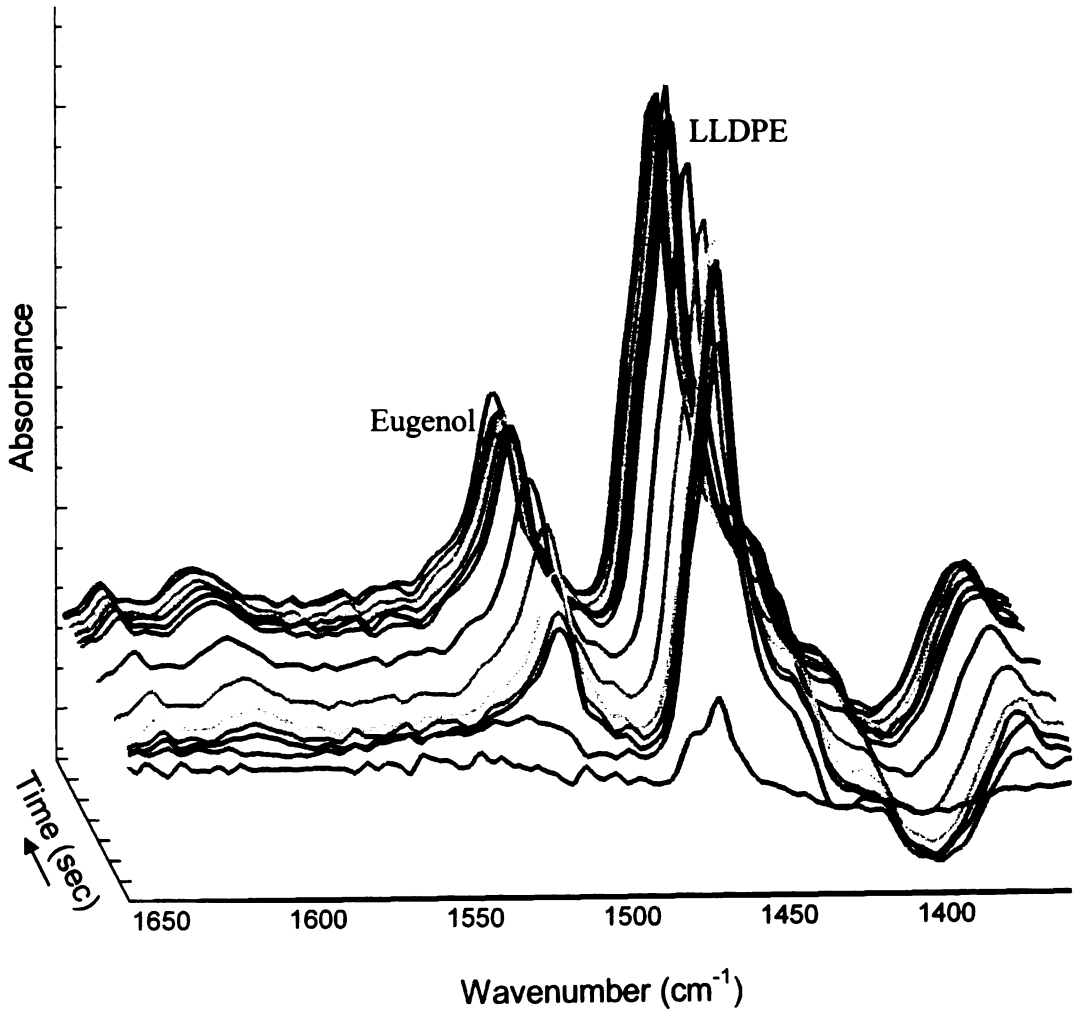


**Figure 4.12** Increase in eugenol (1514 $cm^{-1}$) and LLDPE (1462 $cm^{-1}$) absorbance over time at 40°C.

Figure 4.13 shows the increase in the OH stretching bond (Table 3.1) absorbance as the diffusion proceeds. The larger arrow shows the direction of increase in absorbance of OH stretching bond with time, for the entire diffusion process. The smaller arrow

indicates higher relative increase of the 3520 $cm^{-1}$ region of the OH peak towards the end of the process, which may be due to the formation of eugenol clusters in the polymer film or due to the contact of eugenol with the ATR crystal, as the film gets saturated.

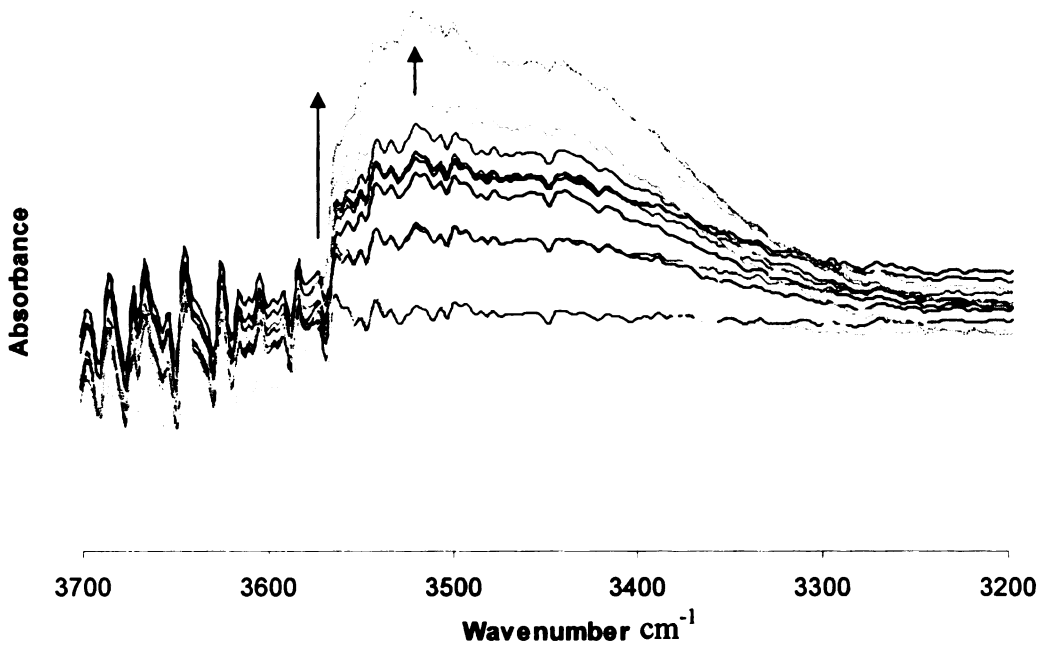


**Figure 4.13** Absorbance of OH stretching bond in eugenol.

### 4.6 FTIR-ATR based eugenol/EVA diffusion analysis

Figure 4.14 shows the overlapped spectrum of EVA and eugenol. The arrows pointing downwards indicate the fall in absorbance of EVA peaks over time. This decrease in EVA absorbance is the result of the swelling of the film as soon as it came in contact with eugenol. The decrease in absorbance is because of the reduction in the polymer density with swelling, thereby, resulting in lesser number of polymer molecules within given evanescent detection field. The upward pointing arrows indicate the increase in eugenol concentration over time. Due to the high swelling of EVA film, a simple

Fickian model of diffusion could not be fit to the data, however some information on the interaction of eugenol with EVA could be monitored over time.

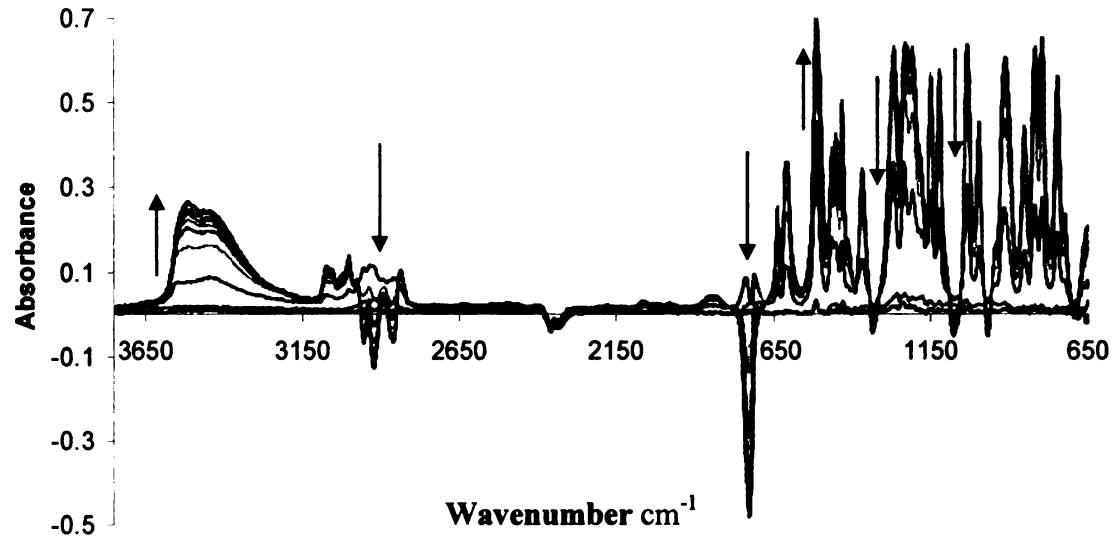


**Figure 4.14** Eugenol diffusion in EVA. Arrows pointing down indicates some of the EVA peaks, and arrows pointing up indicate increase in eugenol concentration over time.

On close observation of these peaks (Figure 4.15) it was seen that the fall of –C=O stretching peak absorbance in EVA followed a trend, in which at shorter times the absorbance peak shifted to 1724 $cm^{-1}$. After this initial shift, the absorbance peak shifted and continued to fall at 1728 $cm^{-1}$. This shift to lower wavenumber (higher frequency) at shorter times may have been due to the higher energy required for –C=O bond stretching in EVA. Higher energy may have been required due to hydrogen bonding between EVA (-C=O bond) and eugenol (-OH bond) at shorter times. After the increase in eugenol concentration, hydrogen bonding within eugenol (-OH bond) may have been predominant, causing the –C=O bond in EVA return to 1728 $cm^{-1}$.

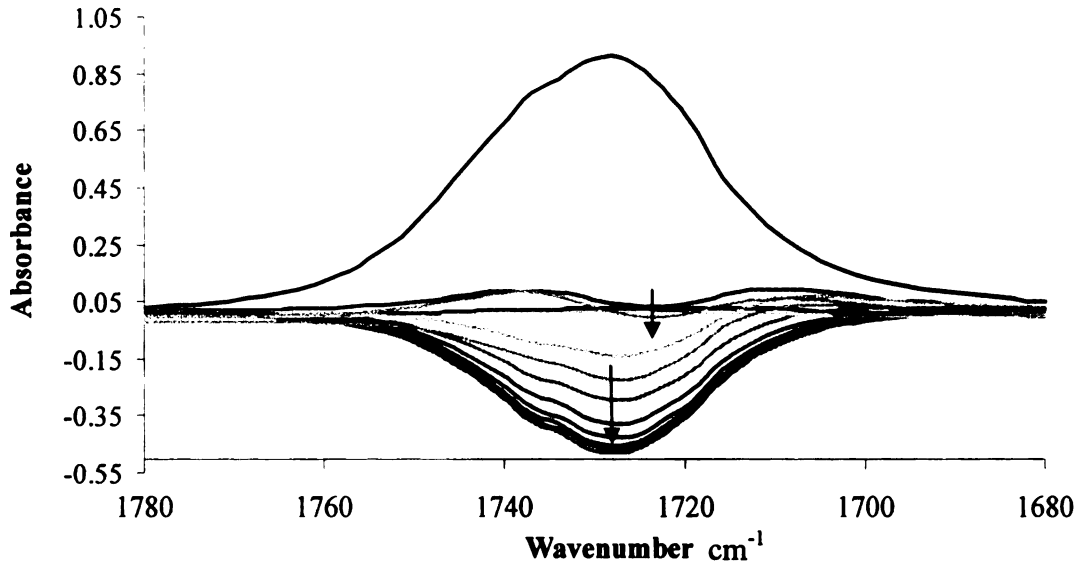


**Figure 4.15** EVA (1728 $cm^{-1}$) peak of C=O stretching bond over time. The arrows indicate the shift in wavelength of the absorbance peak over time.

The presence of hydrogen bonding can also be verified on observation of (-OH stretching) in eugenol (Figure 4.16a) in which the maximum absorbance region shifts from 3448 $cm^{-1}$ at shorter times to 3523 $cm^{-1}$ at longer times when eugenol concentration is high and hydrogen bonding within liquid eugenol (clustering) may be predominant. Similar shift in eugenol 1514 $cm^{-1}$ peak to 1504 $cm^{-1}$ indicates that eugenol has been divided in two fractions i.e. clustered/bound (by hydrogen bonding) eugenol and free eugenol. Due to the heavy swelling observed in EVA/eugenol system we could not fit the Fickian curve to the experimental results. However, to have an estimate of mass transfer of eugenol through EVA, the Fickian equation gave a *D* value of $7.73 \pm 0.22 \times 10^{-9}$ $cm^2$/sec with asymptotic 95% confidence interval from (7.28 to 8.18)

x $10^{-9}$ $cm^2$/sec. Also, from Figure 4.17 we can see that equilibrium reached very soon (2000 to 33.3 mins).

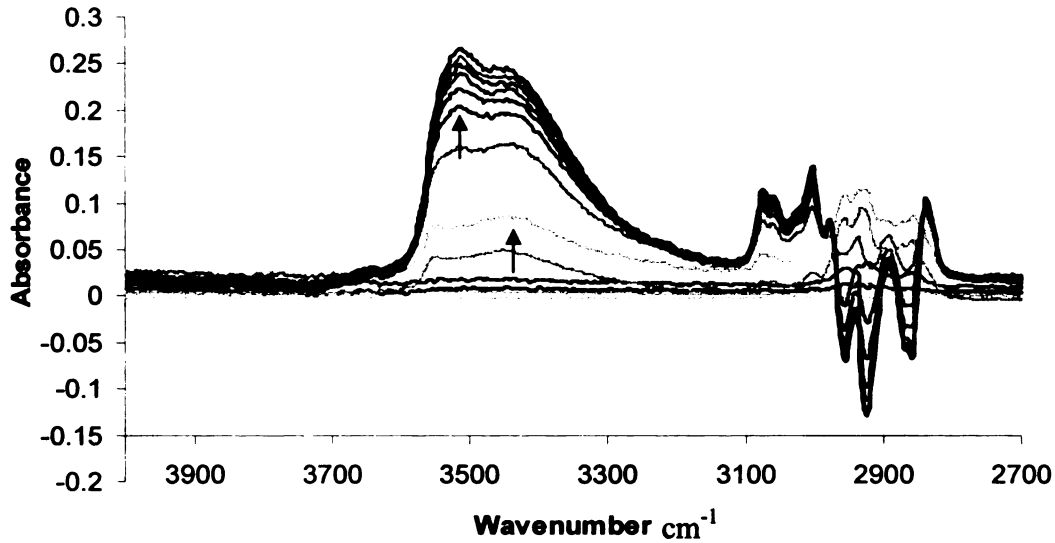


a)

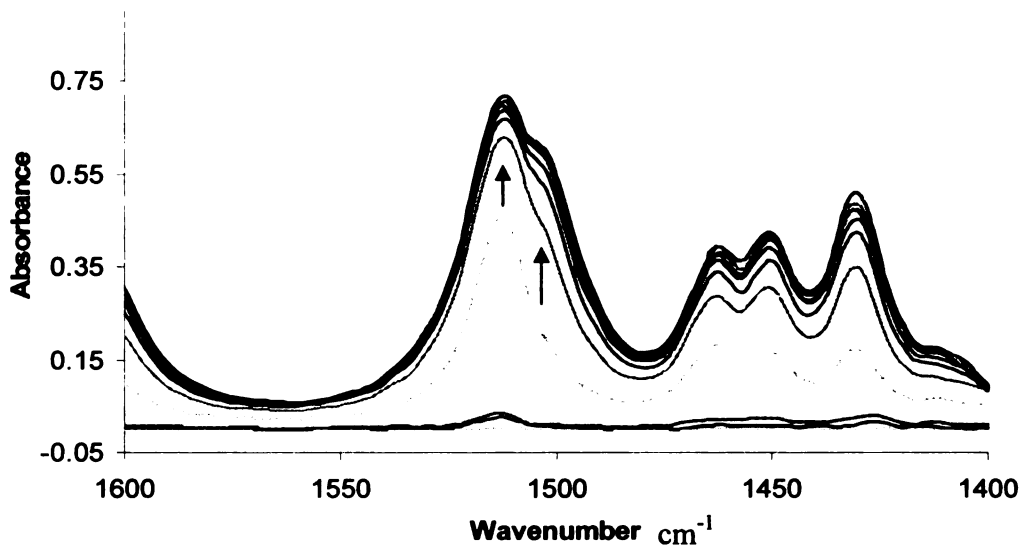


b)

**Figure 4.16** a) Absorbance of OH stretching bond and b) –C=C- benzene ring stretching of eugenol in EVA over time. The arrows indicate shift in wavelength of the absorbance peak over time.

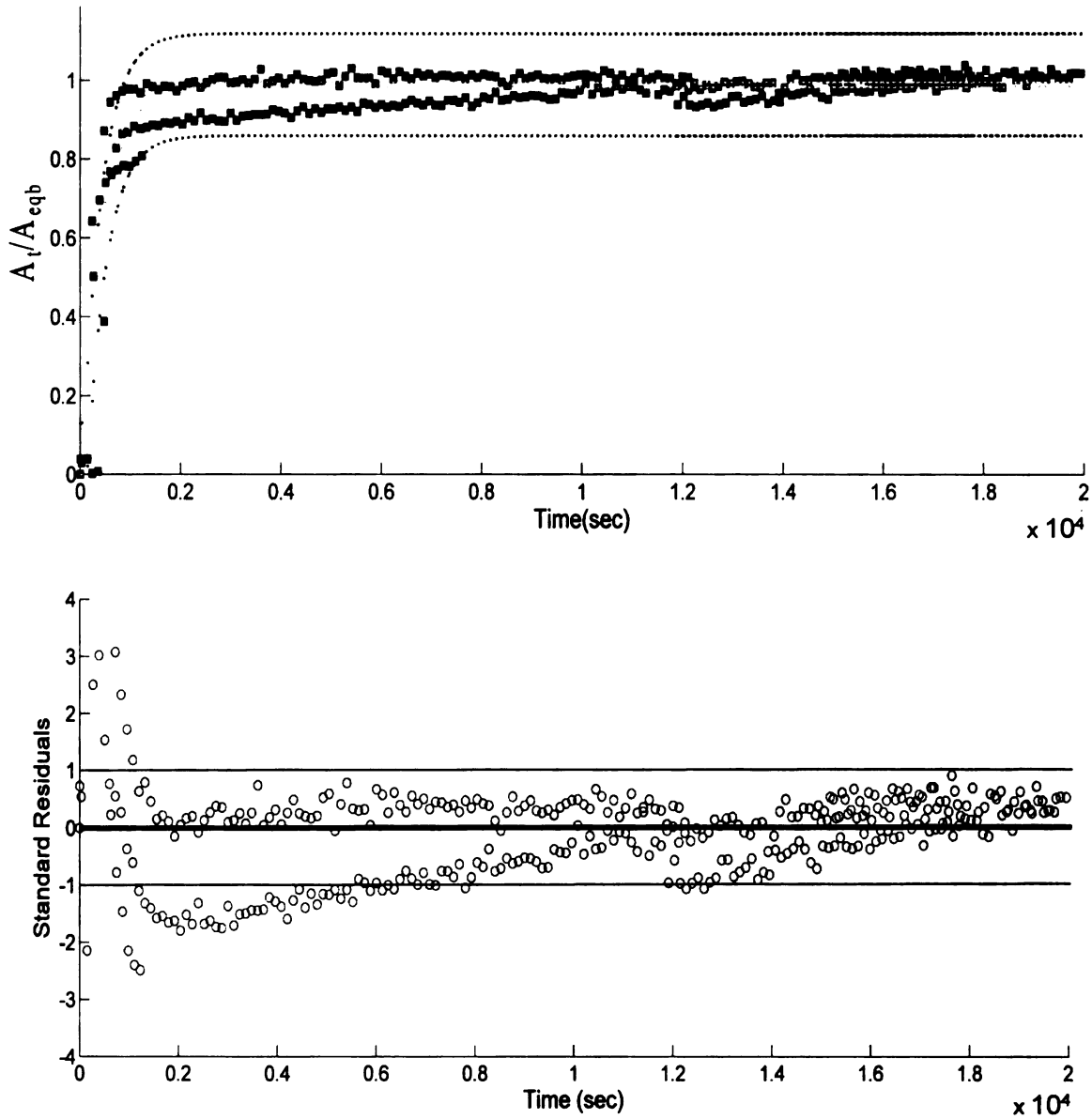


**Figure 4.17** Normalized eugenol (1514 $cm^{-1}$) absorbance vs time at 23°C in EVA.

**Note**: The central line shows the best fit to the dotted experimental values of all the three replications. The outer points show the prediction interval for the observed experimental values. The confidence interval of the best fit is very close to the fitted curve and not clearly visible in the figures. The standard residuals are shown in the graph below with dark line indicating zero residual.

### 4.7 Some potential applications of *D* values of eugenol obtained from this research

Since eugenol is found in many spices, its loss from food products, also known as scalping, may lead to organoleptic effects. The *D* values obtained in this study can be used to estimate the rate of loss of eugenol from food products into the package material. As a comparison eugenol rate loss from food ($D$ = 3.37 to 8.86 x $10^{-10}$ $cm^2$/sec @ 23°C) would be much slower than limonene, which has $D$ = 1.85 x $10^{-8}$ $cm^2$/sec as determined by Cava et al. [104]. The mass gain values shown in Appendix C2, also help suggest that the maximum sorption of eugenol in LLDPE package would be 0.8 mg/g of LLDPE or 800 ppm. The mass gain values, *D* values and the activation energy of eugenol/LLDPE system may hence help predict the material and conditions for packaging of eugenol and eugenol/clove containing foods.

Clove oil, usually containing 85 to 90% wt/wt eugenol, is considered Generally Recognized as Safe (GRAS) as a substance added directly to human food (21 CFR 184.1257). Eugenol is GRAS in animal feed (21 CFR 582.60) and isoeugenol is cleared for use in human food (21 CFR 172.515). Both compounds are listed as synthetic flavoring substances and adjuvant. Eugenol (not clove oil) is used as a component in dental cement for temporary fillings (21 CFR 872.3275) [108]. Even though eugenol is not established as GRAS due to inadequate data, its one of the active component offered in over-the-counter drugs (21 CFR 310.545). Moreover, its indirect use through clove oil as strong antioxidant and antimicrobial (section 2.8), may prove its potential as active component in active packaging.

For example, a commonly used antioxidant BHT is added at 500 ppm (0.05 %) in LDPE for its protection from degradation [109] while in active packaging application for

protection of Asadero cheese was reported to be added to ~1% (8 mg/g) levels. This amount accounted for the loss during manufacturing and the quantity required to protect the cheese [110]. Since eugenol concentration that can remain in the film is not more than 0.08 % or 0.8 mg/g (Appendix C2), the remaining concentration from the film is likely to be released in the food. Phoopuritham et al. [90] found that clove oil showed comparable but slightly lesser antioxidant properties than BHT, while it showed almost same DPPH radical scavenging activity. Hence, the concentration of eugenol as antioxidant that may be added to the film is comparable to the levels of BHT. Hence, it could be considered that eugenol shows very good potential to be released as an active component to food. The *D* values and mass gain values are however likely to change with the polymer/food system to be studied. It is expected as the affinity between eugenol and the food system in contact increases, the rate of eugenol should increase. Although FTIR-ATR in this study was used to measure the sorption of eugenol in LLDPE, it can also be utilized to study its desorption in various food simulants.

# Chapter 5

# Conclusions

In this study, a FTIR-ATR system and methodology to study the sorption of organic compounds through commercially available polymer films has been developed. This system was used to study diffusion in case where peak ratioing could not be performed. FTIR-ATR proved to be an excellent technique not only for diffusion measurement, but also in studying various interactions between the organic compound and the polymer.

## 5.1 Outcomes from the study

Firstly, the eugenol flow circuit was designed and different parts were configured. A continuous flow system enabling constant eugenol temperature, and a flow pressure to achieve better contact of the polymer film with the ATR crystal was achieved.

MATLAB® codes were developed for analyzing the experimental values. The MATLAB® programs were used to perform non linear regression analysis in both; the Fickian mass uptake equation and the modified Fickian equation for the case of FTIR-ATR measurements. The use of MATLAB® program enabled the measurement of various parameters like the diffusion coefficient, equilibrium mass uptake/absorbance, confidence intervals for theoretical curve as well as prediction intervals for experimental values and standard error in the predicted values. It was also possible to study the residuals of the theoretical and experimental fit.

To determine the various parameters affecting the outcomes of the study, preliminary runs were carried out. An absorbance peak at 1514 $cm^{-1}$ (-C=C- stretching) was chosen to study eugenol diffusion over time. Eugenol *D* values varied from 2.45 ± 0.05 to 4.90 ± 0.04 x $10^{-10}$ $cm^2$/sec for flow range of 0 to 11 ml/min at 23°C. It was found that best results could be achieved with eugenol flow rate of 8 ml/min. The change in angle of penetration of the IR beam from 45° to 39° was performed to increase IR depth of penetration. However, it did not enable better results and infact increased the errors involved in the measurement.

After the initial studies, the technique was used to find the diffusion coefficient of eugenol through LLDPE and EVA film. Eugenol diffusion in LLDPE followed a Fickian behavior and the *D* values were in the range of 1.05 ± 0.01 and 13.23 ± 0.18 x $10^{-10}$ $cm^2$/sec through the temperature range tested (16 to 40°C). Eugenol diffusion in EVA was accompanied by swelling of EVA, which could be easily observed by monitoring of 1728 $cm^{-1}$ –C=O stretching in EVA. It was also possible to monitor the hydrogen bonding between EVA and eugenol, resulting in two different population of diffused eugenol (bound and free) within EVA.

The higher residuals in the experimental and theoretical fit, in the initial times of diffusion process seen in FTIR-ATR experiments were attributed to the poor contact between the crystal and LLDPE film. However, after performing a sensitivity analysis of the Fickian diffusion equation, it was ascertained that the higher residuals were observed in the region where the sensitivity of *D* was not very significant, thereby had a very minimal effect on the results.

To compare the FTIR-ATR results, a more conventional technique based on the use of HPLC was performed. A standard permeation vial and specially designed aluminum permeation cell enabled measurement of two-sided and one-sided diffusion of eugenol in LLDPE film, respectively. The diffusion coefficients found by HPLC technique compared favorably with the FTIR-ATR results since they were in the same order of magnitude, but actually higher. In case of two-sided diffusion *D* values varied from 2.96 ± 0.15 to 35.11 ± 1.60 x$10^{-10}$ $cm^2$/sec, while in one-sided it varied from 2.71 ± 0.15 to 32.29 ± 1.87 x$10^{-10}$ $cm^2$/sec over at temperature range of 23 to 40°C. Activation energy, 76.45, 74.95 and 74.68 kJ/mol for the FTIR-ATR, HPLC two-sided, and HPLC one-sided respectively, were calculated for eugenol diffusion through LLDPE.

Unlike HPLC, ATR method helps monitor the entire diffusion process and requires less time to set up and to determine the diffusion coefficient values. Hence, FTIR-ATR technique can also be used in permeant/polymer systems where peak ratioing is not possible.

**5.2 Recommendation for Future work**

From this work we review the background, theory and the potential of FTIR-ATR technique in diffusion analysis. However, there is great scope for future development of this technique in following areas:

1. The FTIR-ATR data can be analyzed with more powerful software enabling the integration of the area under the absorbance peaks and their deconvolution for more accurate results.

2. The technique can be used not only in case of sorption experiments, but also mass transfer processes like desorption, migration and release of components from the polymer film. Also multi-component sorption/desorption can be studied by this technique.
3. The use of variable angle attachment helps change the depth of penetration of the IR radiation, thereby, it enables the use of this technique in measuring mass transfer in multilayer films.
4. By use of a polarizer, it is also possible to measure the crystallinity in polymer films, and also monitor the effect of permeant diffusion on polymer crystallinity.

## Appendices

**Appendix A1.** Processing data obtained from IR Solution® software.

A1. Visual Basic based program to import FTIR-ATR readings into Excel™ spreadsheet.

A2. Spreadsheet displaying data obtained from program in Appendix A1.

**Appendix B.** MATLAB Programs

B1a. To fit FTIR-ATR data to Fickian diffusion model

B1b. Non linear regression program for FTIR-ATR Fickian diffusion model

B2a. To fit HPLC data to Fickian diffusion model

B2b. Non linear regression program for HPLC Fickian diffusion model

B3a. Sensitivity analysis of FTIR-ATR based Fickian diffusion model

B3b. Sensitivity analysis of HPLC based Fickian diffusion model

**Appendix C.** FTIR-ATR and HPLC results

C1. Table C1 Diffusion coefficients and equilibrium absorbance in each run for FTIR-ATR experiment at different temperatures.

C2. Table C2 Equilibrium mass gain in HPLC two-sided and one-sided experiments at different temperatures.

**Appendix D.** Figures (D1 to D3) LLDPE peak absorbance at different wavenumbers over time.

**Appendix E.** Figures (E1 and E2) Eugenol chromatogram obtained from HPLC and eugenol calibration curve.

**Appendix F.** Detailed derivation of the FTIR-ATR diffusion model

## Appendix A1

## Visual Basic based program to import FTIR-ATR readings into Excel™ spreadsheet

```
Sub LDPE()
Application.ScreenUpdating = False

'Reading path for files to be opened
myPath = Sheets("Frontend").Cells(2, 3).Text

'Reading number for files to be opened
'All files are stored with consecutive numbers
'Example LLDPE1.txt to .. LLDPE350.txt

myNumbers = Sheets("Frontend").Cells(4, 3).Value

'Reading Target wavenumbers that need to be read (1514 etc.)
Target1 = Sheets("Frontend").Cells(5, 3).Value
Target2 = Sheets("Frontend").Cells(6, 3).Value
Target3 = Sheets("Frontend").Cells(7, 3).Value
For i = 1 To myNumbers

 'Setting File Name to be opened
    myFile = Sheets("Frontend").Cells(3, 3).Text & i
    filnm = myPath & "\" & myFile

  'Opening the file
    Workbooks.OpenText Filename:=filnm, DataType:=xlFixedWidth

 'Counting number of entries in file
    myEntries = Application.WorksheetFunction.CountA(Range("A:A"))

 'Locating the values
        For j = 1 To myEntries
        If Cells(j, 1) = Target1 Then
            Value1 = Cells(j, 2)
        Else
            If Cells(j, 1) = Target2 Then
                Value2 = Cells(j, 2)
            Else
                If Cells(j, 1) = Target3 Then
                    Value3 = Cells(j, 2)
                Else
                End If
            End If
        End If
        Next j

'Closing the data file
    ActiveWorkbook.Close
```

```
 'Pasting the relevant values in Data Sheet
    Worksheets("Data").Cells(i + 3, 1) = myFile
    Worksheets("Data").Cells(i + 3, 2) = i
    Worksheets("Data").Cells(i + 3, 6) = Value1
    Worksheets("Data").Cells(i + 3, 7) = Value2
    Worksheets("Data").Cells(i + 3, 8) = Value3

'Releasing Values
Value1 = 0
Value2 = 0
Value3 = 0
Next i
Worksheets("Data").Select
Range("A1").Select
Application.ScreenUpdating = True
End Sub
```

**NOTE: All words in bold are just for the explanation of different commands and are not part of the MATLAB program.**

## Appendix A2

### Spreadsheet displaying data obtained from program in Appendix A1.

The following spreadsheet displays the data calculations performed. Absorbance values at three wavenumbers, though we need only 1514 $cm^{-1}$ could be obtained from program in Appendix A1. These values are enlisted in columns A, B and C. As the values are negative, the lowest negative value was added to all other, to obtain positive values in columns D, E and F. Time is noted in mins, seconds and square root of second in adjacent columns. The initial absorbance value $A_o$ is subtracted from all the values for 1514 $cm^{-1}$ wavenumber in column G. Then time vs column G data is input in MATLAB program (Appendix B1a) to obtain diffusion coefficient and also $A_{eqb}$ (Equilibrium absorbance) value. To obtain a normalized curve, data in column G is divided by $A_{eqb}$ value to obtain column H.

| | Scaling factor | | | | | | | | Ao | Aeqb from MATLAB | |
|---|---|---|---|---|---|---|---|---|---|---|---|
| | 0.463437 | | | | | | | | 0.021 | 0.3278 | |
| Values from Appendix A1 program | | | | | | | D | E | F | G | H |
| A | B | C | | Time | Time | Time | Peak | Peak | Peak | At-Ao | (At-Ato)/Aeqb |
| 2912.51 | 1033.85 | 1514.12 | Sr. no. | mins | Sec | sqrt | 2912.5 | 1033.9 | 1514.1 | | |
| 0.38366 | -0.46347 | -0.45779 | 0 | 2 | 120 | 10.954 | 0 | 0 | 0 | 0 | 0 |
| 0.41983 | -0.44658 | -0.43676 | 1 | 4 | 240 | 15.492 | 0.8833 | 0.0169 | 0.0267 | 0.0057 | 0.0172413 |
| 0.4147 | -0.44839 | -0.43854 | 2 | 29 | 1740 | 41.713 | 0.8781 | 0.015 | 0.0249 | 0.0039 | 0.0118081 |
| 0.40464 | -0.44129 | -0.43487 | 3 | 31 | 1860 | 43.128 | 0.8681 | 0.0221 | 0.0286 | 0.0075 | 0.0229979 |
| 0.41718 | -0.43447 | -0.42643 | 4 | 33 | 1980 | 44.497 | 0.8806 | 0.029 | 0.037 | 0.016 | 0.04873 |
| 0.43192 | -0.43128 | -0.42288 | 5 | 35 | 2100 | 45.826 | 0.8954 | 0.0322 | 0.0406 | 0.0195 | 0.059572 |
| 0.69316 | -0.29055 | -0.27728 | 50 | 172 | 10320 | 101.59 | 1.1566 | 0.1729 | 0.1862 | 0.1651 | 0.5037575 |
| 0.72836 | -0.23231 | -0.22131 | 100 | 282 | 16920 | 130.08 | 1.1918 | 0.2311 | 0.2421 | 0.2211 | 0.6744744 |
| 0.74768 | -0.21107 | -0.19311 | 150 | 418 | 25080 | 158.37 | 1.2111 | 0.2524 | 0.2703 | 0.2493 | 0.7605238 |
| 0.78333 | -0.18855 | -0.17749 | 200 | 534 | 32040 | 179 | 1.2468 | 0.2749 | 0.2859 | 0.2649 | 0.8081748 |
| 0.79096 | -0.17085 | -0.16104 | 250 | 634 | 38040 | 195.04 | 1.2544 | 0.2926 | 0.3024 | 0.2814 | 0.8583426 |
| 0.83528 | -0.12784 | -0.11807 | 300 | 970 | 58200 | 241.25 | 1.2987 | 0.3356 | 0.3454 | 0.3243 | 0.9894286 |
| 0.8062 | -0.11828 | -0.10912 | 345 | 1060 | 63600 | 252.19 | 1.2696 | 0.3452 | 0.3543 | 0.3333 | 1.0167257 |
| 0.81588 | -0.12 | -0.11323 | 346 | 1062 | 63720 | 252.43 | 1.2793 | 0.3434 | 0.3502 | 0.3292 | 1.0041998 |
| 0.80055 | -0.1307 | -0.12111 | 347 | 1064 | 63840 | 252.67 | 1.264 | 0.3327 | 0.3423 | 0.3213 | 0.9801638 |
| 0.80595 | -0.12766 | -0.11525 | 348 | 1066 | 63960 | 252.9 | 1.2694 | 0.3358 | 0.3482 | 0.3272 | 0.9980253 |
| 0.81358 | -0.11646 | -0.11137 | 349 | 1068 | 64080 | 253.14 | 1.277 | 0.347 | 0.3521 | 0.331 | 1.0098771 |
| 0.82159 | -0.11699 | -0.11316 | 350 | 1070 | 64200 | 253.38 | 1.285 | 0.3464 | 0.3503 | 0.3292 | 1.0044225 |

## Appendix B1a

## To fit FTIR-ATR data to Fickian diffusion model

```
clear all % To clear MATLAB workspace of any previous data

load ATR23.dat % Load file 'ATR23' to MATLAB workspace
global L % To use thickness L of polymer film for both programs B1a and
B1b.
beta=[0.4 0.9]; % Estimate of [(Diffusion coefficient D x 10^-10)&
Absorbance at equilibrium Aeqb].

L=2.5e-03; % (cm) Thickness of the Polymer film
t=ATR23(:,1)'; % (sec) First column in file ATR23 gives time 't'
A=newalldata23(:,3)'; % Experimental absorbance values 'A' in third
column of file ATR23

[beta,resids,J] = nlinfit(t,A,@myfuntwoparametersATR,beta); %nlinfit
function used takes program to function program Appendix B1b through
command @ myfuntwoparametersATR

ci=nlparci(beta,resids,J); % to find asymptotic confidence interval and
residuals
[Apred, delta] =
nlpredci('myfuntwoparametersATR',t,beta,resids,J,0.05,'on','curve'); %
to find confidence interval for predicted absorbance values 'Apred'
[Apred, deltaobs] =
nlpredci('myfuntwoparametersATR',t,beta,resids,J,0.05,'on','observation
'); % to find prediction intervals for the observed values

SS=0;
for i = 1:length(Apred)
    SS = SS + resids(i)^2;  % Sum of Squared error
end

n = length(Apred);
p = length(beta);
nu = n-p;  % degree of freedom
MSE = SS/nu; % Mean squared error
rmse = sqrt(MSE); % Root mean squared error
covmat = inv(J'*J)*MSE;
stderr_beta = sqrt(covmat(1,1)); % To obtain standard error in beta(
diffusion coefficient)
standardresiduals = resids/rmse; % To obtain Standard residual

asyCImax1 = Apred+delta;
asyCImin1 = Apred-delta;
predCImax1 = Apred + deltaobs;
predCImin1 = Apred - deltaobs;

figure
hold on
```

```
h1(1) = plot(t,A,'s','MarkerFaceColor', [0 0 1]); % To plot
experimental absorbance values with time
h1(2) = plot(t,Apred,'r', 'LineWidth',2);%'r', 'LineWidth',2); % To
plot predicted absorbance values with time
h1(3) = plot(t,asyCImax1,':'); % To plot upper CI as dotted line
h1(4) = plot(t,predCImax1,'-'); % To plot upper PI as solid line
plot(t, asyCImin1,':'); % To plot lower CI as dashed line
plot(t, predCImin1,'-');  % To plot lower PI as dashed line

figure
hold on
h1(1) = plot(t,resids,'*'); % To plot residuals with time
xlabel('Time (sec)');
ylabel('Residuals');

figure
hold on
h1(1) = plot(t,standardresiduals,'*'); % To plot standard residuals
with time
xlabel('Time (sec)');
ylabel('Standard Residuals');

% to get output of program

beta % Multiply final result of D by 10^-10 to get actual values
ci
MSE
rmse
stderr_beta
```

**NOTE: All words in bold are just for the explanation of different commands and are not part of the MATLAB program.**

## Appendix B1b

## Non linear regression program for FTIR-ATR Fickian diffusion model

```
function Apred = myfuntwoparametersATR(beta,t) % The calculations from
this program are returned back to program Appendix B1a. The nlinfit
function is used to obtain Apred(predicted absorbance values)

b1 = beta(1); % Predicted best fit difusión coefficient
b2 = beta(2); % Predicted equilibrium absorbance

global L

nt=length(t);
n=100; % Number of terms in the infinite series
n1=1.5; % Refractive index of polymer
n2=2.43; % Refractive index of ATR crystal
angle=pi/4; % Incident angle of IR rays.
wavenumber=1514.12; % Wavenumber of (-C=C-) stretching in eugenol
lambda=1/wavenumber; % Wavelength
gamma=(2*n2*pi*sqrt((sin(angle))^2-((n1/n2)^2)))/lambda % gamma or the
decay coefficient

% Solution toward the infinite series or summation in Fickian diffusion
model
for i=1:nt
for j=0:n
f(j+1)=((2*j+1)*pi)/(2*L);
g(j+1)=((-b1*10^(-10))*(2*j+1)^2*pi^2*t(i))/(4*L^2);
h(j+1)=(exp(g(j+1))*(f(j+1)*exp(-2*gamma*L)+(-1)^j*(2*gamma))/
((2*j+1)*(4*gamma^2+f(j+1)^2)));
end
yha(i) =b2*(1-8*gamma/(pi*(1-exp(-2*gamma*L)))*sum(h));
end
Apred = yha; % Predicted absorbance values
```

**NOTE: All words in bold are just for the explanation of different commands and are not part of the MATLAB program.**

## Appendix B2a

## To fit HPLC data to Fickian diffusion model

```
clear all % To clear MATLAB workspace of any previous data
load HPLC40.dat % Load file HPLC40 to MATLAB workspace
global L % To use thickness L of polymer film for both programs B2a and
B2b.
L=2.0e-03; % Thickness of the Polymer film in cm
beta= [2 0.5] % Estimate of [(Diffusion coefficient x 10^-10)& (Mass
gain at equilibrium x 10^-3)]

t=newHPLC40(:,1); % First column in file HPLC40 gives time 't' in sec
M=newHPLC40(:,3)'; % Experimental mass gain values 'M' in third column
of file HPLC40

[beta,resids,J] = nlinfit(t,M,@myfuntwoparametersHPLC,beta); %nlinfit
function used takes program to function program Appendix B1b through
command @ myfuntwoparametersATR

ci=nlparci(beta,resids,J,0.05) % to find asymptotic confidence interval
and residuals
[Mpred, delta] =
nlpredci('myfuntwoparametersHPLC',t,beta,resids,J,0.05,'on','curve');
to find confidence interval for predicted mass gain values 'Mpred'
[Mpred, deltaobs] =
nlpredci('myfuntwoparametersHPLC',t,beta,resids,J,0.05,'on','observatio
n'); % to find prediction intervals for the observed mass gain values
'M'

% To find predicted mass gain values 'M_an' at time intervals shorter
than experimental time intervals.

b1=beta(1); % predicted best fit difusión coefficient (from Appendix
B2b)
b2=beta(2); % predicted equilibrium mass gain (from Appendix B2b)
t_ana=0:t(Nt)/1000:t(Nt); % new time 't_ana' starting 0 to total
experimental time length 'Nt' with interval of 'Nt/1000'
Nt_ana=length(t_ana);
for i=1:Nt_ana
for j=0:n
h_ana(j+1)=8/((2*j+1)^2*pi^2)*exp((-b1*10^(-
10))*(2*j+1)^2*pi^2*t_ana(i)/(4*L^2)); % L^2 for two-sided and 4*L^2
for one-sided diffusion process
end
M_an(i)=(b2*10^(-03))*(1-sum(h_ana));
end


SS=0;
for i = 1:length(Mpred)
    SS = SS + resids(i)^2;     % Sum of Squared error
end
```

```
n = length(Mpred);
p = length(beta);
nu = n-p; % Degree of freedom
MSE = SS/nu; % Mean squared error
rmse = sqrt(MSE); % Root mean squared error
covmat = inv(J'*J)*MSE;
stderr_beta = sqrt(covmat(1,1)); % To obtain standard error in beta
(diffusion coefficient)
standardresiduals = resids/rmse; % To obtain Standard residual

asyCImax1 = Mpred+delta;
asyCImin1 = Mpred-delta;
predCImax1 = Mpred+deltaobs;
predCImin1 = Mpred-deltaobs;

figure
hold on
h1(1) = plot(t,M,'s','MarkerFaceColor', [0 0 1]); % To plot
experimental mass gain values with time
h1(2) = plot(t_ana,M_an,'r', 'LineWidth',3); % To plot predicted mass
gain values with time
h1(3) = plot(t,asyCImax1,':'); % To plot CI as dotted line
h1(4) = plot(t,predCImax1,'-'); % To plot upper PI as solid line
plot(t, asyCImin1,':'); % To plot lower CI as dashed line
plot(t, predCImin1,'-');  % To plot lower PI as dashed line

figure
hold on
h1(1) = plot(t,resids,'*'); % To plot residuals with time
xlabel('Time');
ylabel('Residuals');

figure
hold on
h1(1) = plot(t,standardresiduals,'*'); % To plot standard residuals
with time
xlabel('Time');
ylabel('Residuals');

% To get output of program

beta % Multiply final result of diffusion coefficient by 10^-10 and
Mass at equilibrium by 10^-3 to get the actual values
ci
MSE
rmse
stderr_beta
```

**NOTE: All words in bold are just for the explanation of different commands and are not part of the MATLAB program.**

## Appendix B2b

## Non linear regression program for HPLC Fickian diffusion model

```
function Mpred = myfuntwoparametersHPLC(beta,t) % The calculations from
this program are returned back to program Appendix B2a. The nlinfit
function is used to obtain Mpred(predicted mass gain values)

b1 = beta(1); % predicted best fit difusión coefficient
b2=beta(2); % predicted equilibrium mass gain

global L


% Solution toward the infinite series or summation in Fickian diffusion
model

nt=length(t);
n=100;
for i=1:nt
% time loop
for j=0:n
h(j+1)=1/((2*j+1)^2)*exp((-b1*10^(-10))*(2*j+1)^2*pi^2*t(i)/(L^2)); %
L^2 for two-sided and 4*L^2 for one-sided diffusion process
end
M_ana(i)=(b2*10^(-03))*(1-(8/pi^2)*sum(h));
end
Mpred = M_ana; % Predicted mass gain values
```

**NOTE: All words in bold are just for the explanation of different commands and are not part of the MATLAB program.**

## Appendix B3a

## Sensitivity analysis of FTIR-ATR based Fickian diffusion model

```
clear all % To clear MATLAB workspace
load ATR23.dat % To load file 'ATR23' to MATLAB workspace
beta=3.4e-10; % (cm^2/sec) The difusión coefficient found by program in
Appendix B1a
L=2.5e-03; % (cm) Thickness of polymer film
t=ATR23(:,1)'; % (sec) First column in file ATR23 gives time 't'
A=ATR23(:,3)'; % Experimental absorbance values 'A' in third column of
file ATR23
nt=length(t);
n=100;
n1=1.5; % Refractive index of polymer
n2=2.43; % Refractive index of ATR crystal
angle=pi/4; % IR ray incidence angle
wavenumber=1514.12; % % Wavenumber of (-C=C-) stretching in eugenol
lambda=1/wavenumber; % Wavelength
gamma=(2*n2*pi*sqrt((sin(angle))^2-((n1/n2)^2)))/lambda; % gamma or
decay coefficient

% To get the predicted values at different times by input of diffusion
coefficient value
for i=1:nt
for j=0:n
f(j+1)=((2*j+1)*pi)/(2*L);
g(j+1)=(-beta*(2*j+1)^2*pi^2*t(i))/(4*L^2);
h(j+1)=(exp(g(j+1))*(f(j+1)*exp(-2*gamma*L)+(-1)^j*(2*gamma)))/...
((2*j+1)*(4*gamma^2+f(j+1)^2));
end
yha(i)=1-8*gamma/(pi*(1-exp(-2*gamma*L)))*sum(h);
end
Apred=yha; % 'Apred' are the predicted values as per the best fit

m=0.000001; % A small number to cause a very small increment in value
of beta
newbeta=beta+beta*m; % New beta value


% To get the predicted values at different times by input of the new
diffusion coefficient value
for i=1:nt
% time loop
for j=0:n
f(j+1)=((2*j+1)*pi)/(2*L);
g(j+1)=(-newbeta*(2*j+1)^2*pi^2*t(i))/(4*L^2);
h(j+1)=(exp(g(j+1))*(f(j+1)*exp(-2*gamma*L)+(-1)^j*(2*gamma)))/...
((2*j+1)*(4*gamma^2+f(j+1)^2));
end
yhad(i) =1-8*gamma/(pi*(1-exp(-2*gamma*L)))*sum(h);
end
newApred = yhad;
```

```
derivative=((newApred - Apred)/m); % Sensitivity of FTIR-ATR diffusion
model

figure
hold on
h1(1) = plot(t,A,'s','MarkerFaceColor', [0 0 1]); % Plot of observed
absorbance values
h1(2) = plot(t,Apred,'r', 'LineWidth',2); % Plot of predicted
absorbance values
h1(3) = plot(t,derivative,'-'); % Plot of sensitivity curve
```

**NOTE: All words in bold are just for the explanation of different commands and are not part of the MATLAB program.**

## Appendix B3b

## Sensitivity analysis of HPLC based Fickian diffusion model

```
clear all % To clear MATLAB workspace
load HPLC40.dat % To load file 'HPLC40' to MATLAB workspace
beta=8.46e-10; % (cm^2/sec) The difusión coefficient found by program
in Appendix B2a
L=2.5e-03; % (cm) Thickness of polymer film
t=HPLC40(:,1); (sec) First column in file HPLC40 gives time 't'
M=HPLC40(:,3)'; % Experimental absorbance values 'M' in third column of
file ATR23
nt=length(t);
n=100;

% To get the predicted values at different times by input of diffusion
coefficient value

t_ana=0:t(nt)/1000:t(nt);
Nt_ana=length(t_ana);
for i=1:Nt_ana
for j=0:n
h_ana(j+1)=8/((2*j+1)^2*pi^2)*exp(beta*(2*j+1)^2*pi^2*t_ana(i)/(4*L^2))
;
end
M_an(i)=1-sum(h_ana);
end
Mpred=M_an; % 'Mpred' are the predicted values as per the best fit

m=0.000001; % A small number to cause a very small increment in value
of beta
newbeta=beta+beta*m; % New beta value

% To get the predicted values at different times by input of the new
diffusion coefficient value

for i=1:Nt_ana
% time loop
for j=0:n
h(j+1)=1/((2*j+1)^2)*exp(-newbeta*(2*j+1)^2*pi^2*t_ana(i)/(4*L^2));
end
M_anal(i)=1-(8/pi^2)*sum(h);
end
newMpred=M_anal;

derivative=(newMpred - Mpred)/m; % Sensitivity of FTIR-ATR diffusion
model

figure
hold on
h1(1) = plot(t,M,'s','MarkerFaceColor', [0 0 1]); % Plot of observed
mass gain values
```

```
h1(2) = plot(t_ana,Mpred,'r', 'LineWidth',3); % Plot of predicted mass
gain values

h1(3) = plot(t_ana,derivative,'-'); % Plot of sensitivity curve
```

**NOTE: All words in bold are just for the explanation of different commands and are not part of the MATLAB program.**

## Appendix C1

**Table C1** Diffusion coefficients and equilibrium absorbance in each run for FTIR-ATR experiment at different temperatures.

| Temperature °C | *$D$ x $10^{-10}$ $cm^2/sec$ | Average $D$ x $10^{-10}$ (Standard deviation) $cm^2/sec$ | $A_{eqb}$ |
|---|---|---|---|
| 16 | 0.99±0.01 (0.96 to 1.02) | 1.02 (0.09) | 0.1488 (0.1464 to 0.1511) |
| | 0.96±0.01 (0.94 to 0.98) | | 0.4579 (0.4539 to 0.4618) |
| | 1.13±0.01 (1.10 to 1.15) | | 0.6770 (0.6702 to 0.6839) |
| 23 | 2.76±0.03 (2.69 to 2.83) | 3.20 (0.41) | 0.3278 (0.3252 to 0.3304) |
| | 3.28±0.04 (3.19 to 3.36) | | 0.2181 (0.2163 to 0.2199) |
| | 3.57±0.03 (3.50 to 3.63) | | 0.1988 (0.1939 to 0.1988) |
| 40 | 11.38±0.27 (10.84 to 11.92) | 13.52 (4.24) | 0.0993 (0.0985 to 0.1001) |
| | 18.41±0.27 (17.70 to 19.12) | | 0.1926 (0.1915 to 0.1937) |
| | 10.78±0.22 (10.35 to 11.21) | | 0.1792 (0.1781 to 0.1803) |

* values for diffusion coefficient $D$ are expressed as best fit values for each replications ± standard error and ( 95% asymptotic confidence interval).

$A_{eqb}$ = Eugenol equilibrium absorbance value obtained as best fit value ( 95% asymptotic confidence interval).

## Appendix C2

**Table C2** Equilibrium mass gain in HPLC two-sided and one-sided experiments at different temperatures.

| Temperature °C | HPLC Two-sided $*M_{eqb} \times 10^{-4}$ (mg eugenol/mg polymer) | HPLC One-side $*M_{eqb} \times 10^{-4}$ (mg eugenol/mg polymer) |
|---|---|---|
| 16 | 5.47 (5.31 to 5.63) | 4.14 (4.01 to 4.27) |
| 23 | 5.90 (5.71 to 6.10) | 4.92 (4.72 to 5.13) |
| 40 | 8.00 (7.75 to 8.24) | 6.96 (6.74 to 7.17) |

* values for equilibrium mass gain are expressed as best fit values and (95% asymptotic confidence interval ).

$M_{eqb}$ = Eugenol equilibrium mass gain value.

## Appendix D

**LLDPE peak absorbance at different wavenumbers over time as obtained from IR Solution® software.**

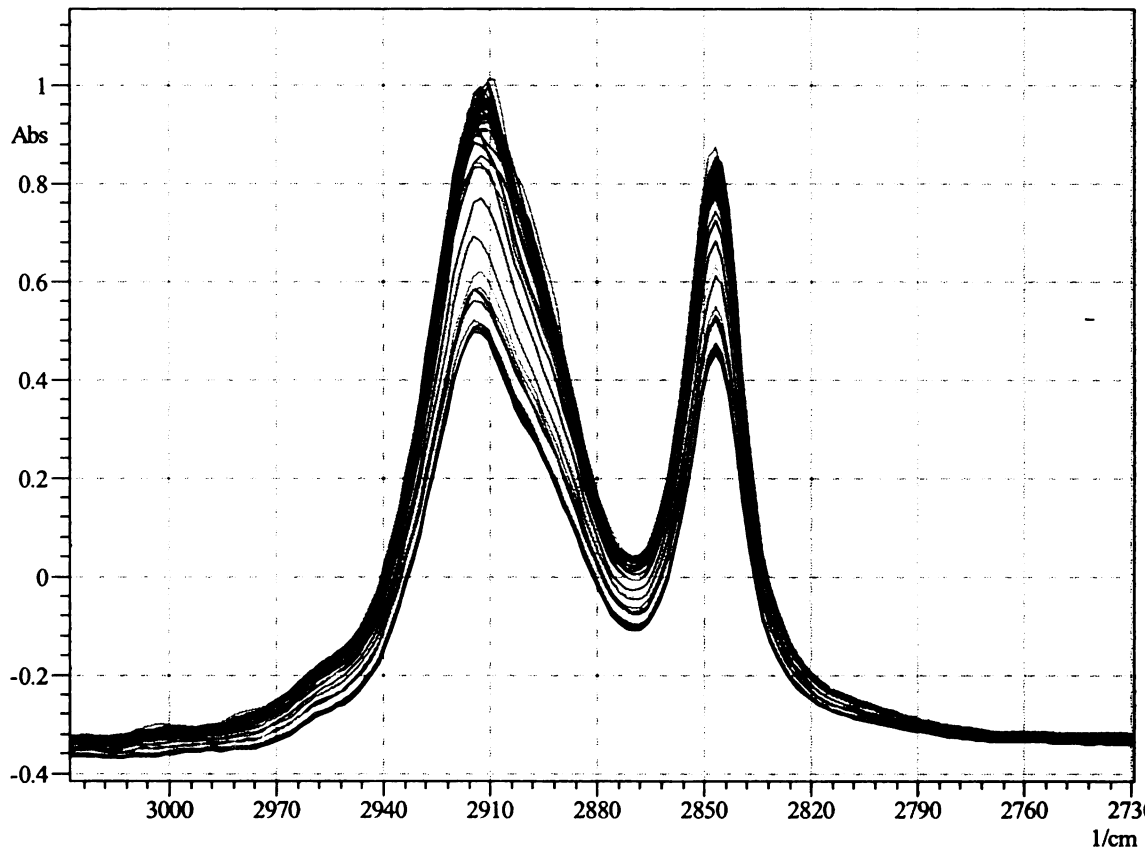


**Figure D1** LLDPE 2912 and 2846 $cm^{-1}$ absorbance over time at 23°C.

**Note:** The peaks do not show any shift in wavenumber

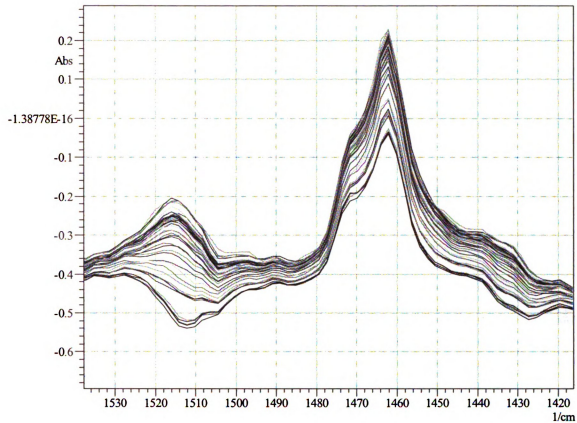


**Figure D2** LLDPE 1462 and eugenol 1514 $cm^{-1}$ absorbance over time at 23°C.

**Note:** The peaks do not show any shift in wavenumber

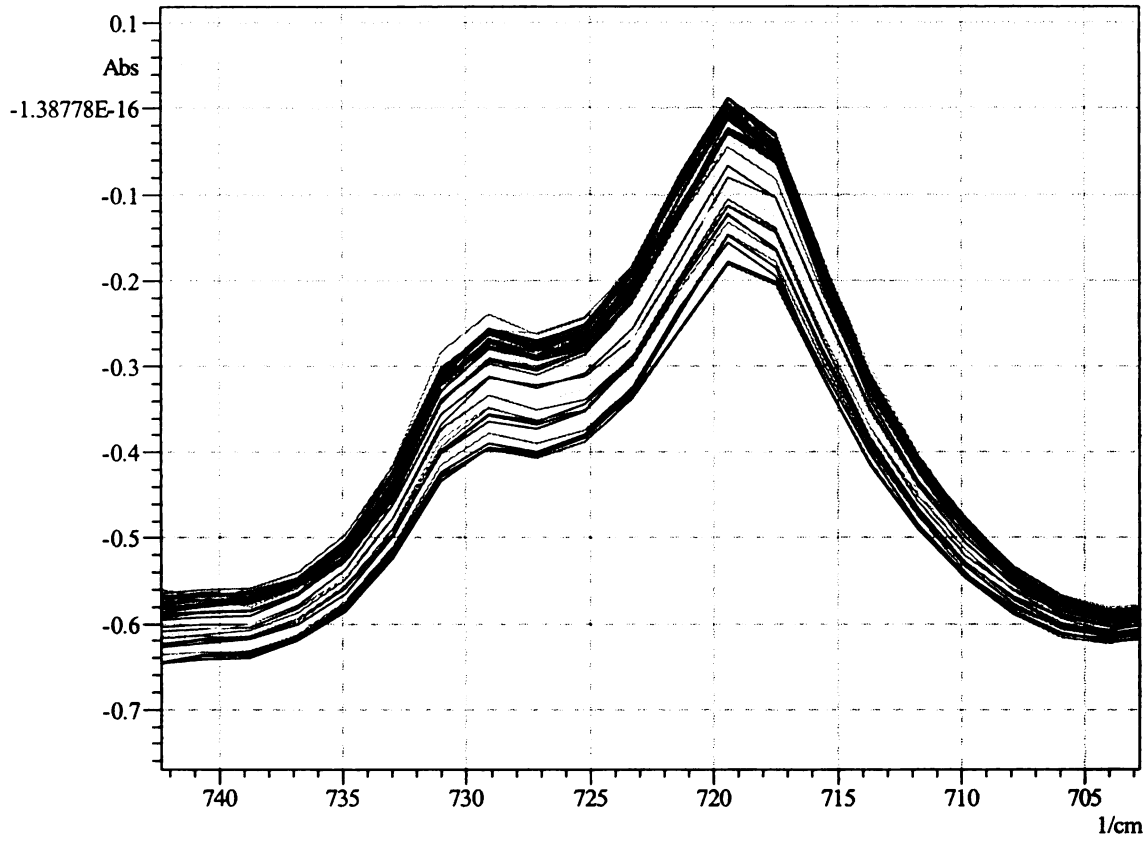


**Figure D3** LLDPE 719 and 729 $cm^{-1}$ absorbance over time at 23°C.

**Note:** The peaks do not show any shift in wavenumber.

## Appendix E

### Eugenol chromatogram obtained from HPLC

An HPLC equipment coupled with a UV detector and equipped with a Nova-Pak® C18 (4 μm) column at 25°C were used to quantify eugenol. A 10μl injection volume and an isocratic elution of 1ml/min flow with methanol: water (85:15) was used. Eugenol elution was found to be 1.5 min.

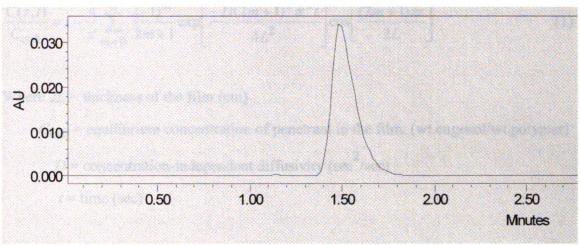


**Figure E1** Eugenol chromatogram obtained from HPLC.

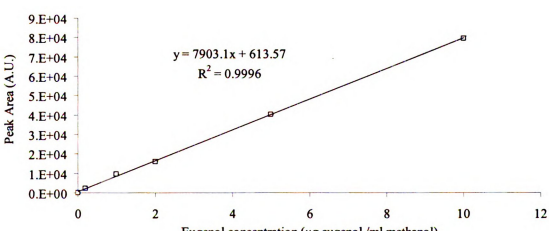


**Figure E2** Calibration curve for HPLC experiments.
**Note**: Error bars are not visible because of very low error values.

## Appendix F

## FTIR-ATR diffusion analysis model

Following is a detailed derivation of the FTIR-ATR diffusion analysis model [111].

Equation 1 is a solution to the boundary conditions for thin film and based on Fick's second law.

$$\frac{C(z,t)}{C_{eqb}} = 1 - \frac{4}{\pi}\sum_{m=0}^{\infty}\frac{(-1)^m}{2m+1}\exp\left[\frac{-D(2m+1)^2\pi^2 t}{4L^2}\right]\cos\left[\frac{(2m+1)\pi z}{2L}\right] \quad (1)$$

Where $2L$ = thickness of the film (cm)

$C_{eqb}$ = equilibrium concentration of penetrant in the film. (wt.eugenol/wt.polymer)

$D$ = concentration-independent diffusivity ($cm^2$/sec)

$t$ = time (sec)

This equation assumes that the initial concentration within the film, $C_{(z=2L,\ t=0)} = 0$, and that no penetrant diffusion occurs at the boundary, z = 0. In FTIR-ATR technique the ATR crystal surface acts as the boundary, z = 0.

In order to derive a single expression relating to IR absorbance to diffusivity, a term K is defined as:

$$K = \frac{A_t}{A_{eqb}} \quad (2)$$

Where, $A_t$ = absorbance at time t

$A_{eqb}$ = absorbance at infinite time.

Substituting the appropriate expression for absorbance yields from equation 2.14 in chapter 2.

$$K = \frac{\int_0^L NeCE_o{}^2 \exp(-2\gamma z)dz}{\int_0^L NeC_{eqb}E_o{}^2 \exp(-2\gamma z)dz} = \frac{\int_0^L C\exp(-2\gamma z)dz}{\int_0^L C_{eqb}\exp(-2\gamma z)dz} \quad (3)$$

This can be re-written as:

$$K = \frac{\int_0^L C\exp(-2\gamma z)dz}{\int_0^L C_{eqb}\exp(-2\gamma z)dz} = \frac{\int_0^L C\exp(-2\gamma z)dz}{B} \quad (4)$$

where $B = \int_0^L C_{eqb}\exp(-2\gamma z)dz$

on integrating B we get,

$$B = \int_0^L C_{eqb}\exp(-2\gamma z)dz = C_{eqb}\left[\frac{1}{-2\gamma}\exp(-2\gamma z)\right]_0^L = \frac{C_{eqb}}{-2\gamma}[\exp(-2\gamma L)-1] \quad (5)$$

$$= \frac{C_{eqb}}{+2\gamma}[1-\exp(-2\gamma L)]$$

Substituting equation 5 in equation 4.

$$K = \frac{\int_0^L C \exp(-2\gamma z) dz}{\frac{C_{eqb}}{+2\gamma}[1 - \exp(-2\gamma L)]} \tag{6}$$

Substituting the expression for $C$ in equation 1 into equation 6.

$$K = \frac{\int_0^L C_{eqb}\left[1 - \frac{4}{\pi}\sum_{m=0}^{\infty}\frac{(-1)^m}{2m+1}\exp\left[\frac{-D(2m+1)^2\pi^2 t}{4L^2}\right]\cos\left[\frac{(2m+1)\pi z}{2L}\right]\exp(-2\gamma z)\right]dz}{\frac{C_{eqb}}{+2\gamma}[1 - \exp(-2\gamma L)]}$$

(7)

On further simplification,

$$K = 1 - \frac{\int_0^L \frac{4}{\pi}\sum_{m=0}^{\infty}\frac{(-1)^m}{2m+1}\exp(g)\cos(fz)\exp(-2\gamma z)dz}{B'} \tag{8}$$

where

$$B' = \frac{1}{2\gamma}[1 - \exp(-2\gamma L)]$$

$$g = \frac{-D(2m+1)^2\pi^2 t}{4L^2} \quad \text{and} \quad f = \frac{(2m+1)\pi}{2L}$$

On placing the terms independent of z outside the integral sign,

$$K = 1 - \frac{4}{\pi B'}\int_0^L \sum_{m=0}^{\infty}\frac{(-1)^m}{2m+1}\exp(g)\cos(fz)\exp(-2\gamma z)dz \tag{9}$$

According to the law of summation of integrals, equation 9 can be re-written as:

$$K = 1 - \frac{4}{\pi B'} \sum_{m=0}^{\infty} \int_0^L \frac{(-1)^m}{2m+1} \exp(g)\cos(fz)\exp(-2\gamma z)dz \tag{10}$$

Placing the terms independent of z outside the integral and re-writing in form of [E].

$$K = 1 - \frac{4}{\pi B'} \sum_{m=0}^{\infty} \frac{(-1)^m}{2m+1} \exp(g)[E] \tag{11}$$

Integrating [E] by parts,

$$[E] = \frac{\cos(fz)\exp(-2\gamma z)}{-2\gamma z}\Bigg|_0^L - \int_0^L \frac{\exp(-2\gamma z) f \sin(fz)}{2\gamma} \tag{12}$$

Again performing integral by parts,

$$\frac{-f}{2\gamma}\int_0^L \exp(-2\gamma z)\sin(fz)dz = \frac{-f}{2\gamma}\left[\frac{\sin(fz)\exp(-2\gamma z)}{-2\gamma}\Bigg| - \int_0^L \frac{\exp(-2\gamma z)}{-2\gamma} f\cos(fz)dz\right]$$

(13)

Substituting equation 13 into 12,

$$[E] = \frac{\cos(fl)\exp(-2\gamma L) - 1}{-2\gamma} + \frac{f\sin(fl)\exp(-2\gamma L)}{(2\gamma)^2} + \frac{-f^2}{(2\gamma)^2}\int_0^L f\cos(fz)\exp(-2\gamma z)dz \tag{14}$$

The remaining integral in above expression is identical to [E], so simplifying,

$$[E]\left(\frac{4\gamma^2+f^2}{4\gamma^2}\right)=\frac{\cos(fl)\exp(-2\gamma L)-1}{-2\gamma}+\frac{f\sin(fl)\exp(-2\gamma L)}{(2\gamma)^2} \tag{15}$$

On multiplying both sides by $\left(\frac{4\gamma^2+f^2}{4\gamma^2}\right)$,

$$[E]=\left[\frac{-2\gamma\cos(fl)\exp(-2\gamma L)+2\gamma+f\sin(fl)\exp(-2\gamma L)}{(4\gamma^2+f^2)}\right] \tag{16}$$

However, from equation 8, $fl=\frac{(2m+1)\pi}{2L}L$

$$\cos(fl)=\cos\left(\frac{(2m+1)\pi}{2L}L\right)=\cos\left(\frac{(2m+1)\pi}{2}\right) \tag{17}$$

For $m$ = odd, $\cos(fl)\sim 0$.

For $m$ = even, $\cos(fl)\sim 0$.

Hence, cos(fl) term can be replaced by zero.

Considering the sine term,

$$\sin(fl)=\sin\left(\frac{(2m+1)\pi}{2L}L\right)=\sin\left(\frac{(2m+1)\pi}{2}\right) \tag{18}$$

For m = odd, $\sin(fl)\sim -1$.

For m = even, $\sin(fl)\sim +1$.

Hence, $\sin(fl)$ term can be replaced by $(-1)^m$.

After making the substitutions for $\cos(fl)$ and $\sin(fl)$ terms,

$$[E]=\frac{1}{(4\gamma^2+f^2)}\left[2\gamma+(-1)^m f\exp(-2\gamma L)\right] \tag{19}$$

From equations 2 and 11, $K$ can be written as:

$$K=1-\frac{4}{\pi B'}\sum_{m=0}^{\infty}\frac{\exp(g)\left[2\gamma(-1)^m+(1)f\exp(-2\gamma L)\right]}{(2m+1)(4\gamma^2+f^2)} \tag{20}$$

Hence, the final expression can be written as:

$$\frac{A_t}{A_{eqb}}=1-\frac{8\gamma}{\pi(1-\exp(-2\gamma L))}\sum_{m=0}^{\infty}\frac{\exp(g)[(-1)^m 2\gamma+f\exp(-2\gamma L)]}{(2m+1)(4\gamma^2+f^2)} \tag{21}$$

where

$$g=\frac{-D(2m+1)^2\pi^2 t}{4L^2} \qquad\qquad f=\frac{(2m+1)\pi}{2L}$$

where $A_t$ and $A_{eqb}$ are the normalized absorbance values at time $t$ (sec) and equilibrium respectively, and $L$ (cm) is the thickness of the polymer. $D$ ($cm^2$/sec) is concentration independent diffusion coefficient and $m$ is number of terms in the infinite series (m=100).

**References**


1. R. Coles, D. McDowell and M. Kirwan ed, Food Packaging Technology. Boca Raton, FL: CRC Press,(2003)

2. A. ElAmin, Plastic packaging growth to benefit from innovation. Breaking News on Food Processing & Packaging. Decision News Media Nov.2008 http://www.foodproductiondaily.com/Packaging/Plastic-packaging-growth-to-benefit-from-innovation

3. N. Cayot, C. Dury-Brun, T. Karbowiak, G. Savary and A. Voilley, Measurement of transport phenomena of volatile compounds: A review *Food Research International* 41 (2008 ), pp. 349–362.

4. S.C. Fayoux, A.-M. Seuvre and A.J. Voilley, Aroma transfers in and through plastic packagings : Orange juice and d-limonene. A review. Part I: Orange juice aroma sorption *Packaging technology & science* 10 (1997), pp. 69-82.

5. R.J. Hernandez and R. Gavara, Plastics Packaging: Methods for Studying Mass Transfer Interactions. Pira International, (1999)

6. Pankaj Kumar, M.S. thesis, Effect of Package configuration on barrier properties and sensory perception of flavor. Michigan State University. 2007

7. A. Brody, E.R. Strupinsky and L.R. Kline, Active Packaging for Food Applications. CRC Press, (2001)

8. M.L. Rooney ed, Active Food Packaging. London: Blackie Academic & Professional,(1995)

9. C.A. Pawlisch, A. Macris and R.L. Laurence, Solute Diffusion in Polymers. 1. The Use of Capillary Column Inverse Gas Chromatography *Macromolecules* 20 (1987), pp. 1564-1578.

10. I.V. Koptyug and R.Z. Sagdeev, Applications of NMR tomography to mass transfer studies *Russian Chemical Reviews* 71 (10) (2002), pp. 789-835.

11. C.M. Leewis, P.H.A. Mutsaers, A.M. de-Jong, L.J. van-IJzendoorn, D.J. Broer and M.J.A. de Voigt, Monomer diffusion assisted preparation of polymer gratings : A nuclear microprobe study *Nuclear Instruments and Methods in Physics Research* B 181 (2001), pp. 367-371.

12. D. Cava, R. Catala, R. Gavara and J.M. Lagaron, Testing limonene diffusion through food contact polyethylene by FT-IR spectroscopy: Film thickness, permeant concentration and outer medium effects *Polymer Testing* 24 (2005), pp. 483–489.

13. J.P. Bobiak and J.L. Koenig, Regions of interest in FTIR imaging applications: Diffusion of nicotine into ethylene-co-vinyl acetate films *Journal of Controlled Release* 106 (2005), pp. 329–338.

14. O.S. Fleming, K.L. Andrew Chan and S.G. Kazarian, High-pressure CO2-enhanced polymer interdiffusion and dissolution studied with in situ ATR-FTIR spectroscopic imaging *Polymer* 47 (2006), pp. 4649–4658.

15. C.M. Balik and W.H. Simendinger III, An attenuated total reflectance cell for analysis of small molecule diffusion in polymer thin films with Fourier-transform infrared spectroscopy *Polymer* 39 (1998), pp. 4723 – 4728.

16. L.M. Doopers, C. Sammon, C. Breen and J. Yarwood, FTIR-ATR studies of the sorption and diffusion of acetone/water mixtures in poly(vinyl alcohol) *Polymer* 47 (2006), pp. 2714 – 2722.

17. Y.A. Elabd, M. Baschetti and T.A. Barbari, Time–Resolved Fourier Transform Infrared/Attenuated Total Reflection Spectroscopy for the Measurement of Molecular Diffusion in Polymers *Journal of Polymer Science* 41 (2003), pp. 2794-2807.

18. J. Esmaiel and N.A. Peppas, Use of ATR-FTIR To Study Interdiffusion in Polystyrene and Poly(vinyl methyl ether) *Macromolecules* 26 (1993), pp. 2175 – 2186.

19. K.C. Farinas, L. Doh, S. Venkatraman and R. Potts, Characterization of Solute Diffusion in a Polymer Using ATR-FTIR Spectroscopy and Bulk Transport Techniques *Macromolecules* 27 (1994), pp. 5220-5222.

20. G.T. Fieldson and T.A. Barbari, Analysis of diffusion in polymers using evanescent field spectroscopy *American Institute for Chemical Engineering Journal* 41 (1995), pp. 795–804.

21. G.T. Fieldson and T.A. Barbari, The use of FTi.r.-a.t.r. spectroscopy to characterize penetrant diffusion in polymers *Polymer* 34 (6) (1993), pp. 1146-1153

22. B.D. Hanh, R.H.H. Neubert and S. Wartewig, Investigation of drug release from suspension using FTIR-ATR technique: part I. Determination of effective diffusion coefficient of drugs *International Journal of Pharmaceutics* 204 (2000), pp. 145–150.

23. U. Hellstern and V. Hoffmann, Diffusion in ultrathin films studied by time resolved FTIR-ATR spectroscopy *Journal of Molecular Structure* 349 (1995), pp. 329-332.

24. P.R. Laity and J.N. Hay, Measurement of water diffusion through cellophane using attenuated total reflectance-fourier transform infrared spectroscopy *Cellulose* 7 (2000), pp. 387–397.

25. P. Morrissey and D. Vesely, Accurate measurement of diffusion rates of small molecules through polymers *Polymer* 41 (2000), pp. 1865-1872.

26. D.A. Mountz, R.F. Storey and K.A. Mauritz, Fourier Transform Infrared/Attenuated Total Reflectance Analysis of Water Diffusion in Poly[styrene-b-isobutyleneb-styrene] Block Copolymer Membranes *Journal of Polymer Science* 43 (2005), pp. 764–776.

27. B. Murphy, P. Kirwan and P. McLoughlin, Study of the impact of penetrant characteristics upon diffusion into Teflon membranes to further assess the performance of an ATR/FTIR sensor *Analytical and Bioanalytical Chemistry* 377 (2003), pp. 195 – 202.

28. B. Murphy, P. Kirwan and P. McLoughlin, Investigation into polymer-diffusant interactions using ATR-FTIR spectroscopy *Vibrational Spectroscopy* 33 (2003), pp. 75 – 82.

29. Ohmana M. Persson D., Leygraf C., In situ ATR-FTIR studies of the aluminium/polymer interface upon exposure to water and electrolyte *Progress in Organic Coatings* 57 (2006), pp. 78–88.

30. A.M. Pereira, M.C. Lopes, J.M.K. Timmera and J.T.F. Keurentjes, Solvent sorption measurements in polymeric membranes with ATR-IR spectroscopy *Journal of Membrane Science* 260 (2005), pp. 174–180.

31. L. Philippe, C. Sammon, S.B. Lyon and J. Yarwood, An FTIR/ATR in situ study of sorption and transport in corrosion protective organic coatings 1. Water sorption and the role of inhibitor anions *Progress in Organic Coatings* 49 (2004), pp. 302 – 314.

32. P. Schmidt, J. Dybal and M. Trchova, Investigations of the hydrophobic and hydrophilic interactions in polymer – water systems by ATR FTIR and Raman Spectroscopy *Vibrational Spectroscopy* 42 (2006), pp. 278 – 283.

33. S. Hajatdoost, C. Sammon and J. Yarwood, FTIR-ATR studies of diffusion and perturbation of water in polyelectrolyte thin films. Part 4. Diffusion, perturbation and swelling processes for ionic solutions in SPEES/PES membranes *Polymer* 43 (2002), pp. 1821-1827.

34. I. Hace, J. Golob and M. Krajnc, Diffusion Coefficient of Diallyl Terephthalate Monomer into Thin Polymer Film *Chemical and Biochemical Engineering* 18 (1) (2004), pp. 73–76.

35. X. Yi, J. Portnoy and J. Pellegrino, Diffusion Measurements Using ATR-FTIR Spectroscopy: Acetone Diffusion in Polypropylene—Use of Penetrant Fluid Pressure to Improve Sample/IRE Contact *Journal of Polymer Science: Part B: Polymer Physics* 38 (2000), pp. 1773–1787.

36. Y. Uda, F. Kaneko and T. Kawaguchi, Guest exchange process in syndiotactic polystyrene thin films measured by ATR – FTIR spectroscopy *Polymer* 45 (2004), pp. 2221 – 2229.

37. Pereira A.M.; Lopes M.C.; Timmera, J.M.K.; Keurentjes, J.T.F., Solvent sorption measurements in polymeric membranes with ATR-IR spectroscopy *Journal of Membrane Science* 260 (2005), pp. 174–180.

38. J. Crank, The Mathematics of Diffusion. New York: Oxford University Press, (1975)

39. H. Fujita, Diffusion in Polymer-Diluent Systems *Fortschr. Hochpolym.-Forsch* 3 (1961), pp. S.1-47.

40. O.-G. Piringer and A.L. Baner ed, Plastic Packaging Materials for Food. Weinheim: Wiley-VCH,(2000)

41. J.W. Robinson, E.M. Skelly Frame and G.M. Frame II, Undergraduate Instrumental Analysis. New York: Marcel Dekker, (2005)

42. C.H. Mannheim and N. Passy, Interaction between packaging materials and foods *Packaging technology & science* 3 (3) (1990), pp. 127-132.

43. R.C. Snyder and C.V. Breder, High-Performance Liquid Chromatographic Determination of 2,4- and 2,6-Toluenediamine in Aqueous Extracts *Journal of Chromatography* 236 (1982), pp. 429.

44. R.C. Snyder and C.V. Breder, New FDA migration cell used to study migration of styrene from polystyrene into various solvents *Association of Official Analytical Chemists* 68 (4) (1985), pp. 770-775.

45. D.R. Jenke, Solute migration through Polypropylene Blend Films *Journal of Applied Polymer Science* 44 (7) (1992), pp. 1223 - 1231.

46. C. Nerín, J. Salafranca, J. Cacho and C. Rubio, Separation of polymer and on-line determination of several antioxidants and UV stabilizers by coupling size-

exclusion and normal-phase high-performance liquid chromatography columns *Journal of Chromatography A* 690 (2) (1995), pp. 230-236.

47. M.H.W. Morelli-Cardoso, E.R. Lachter and D. Tabak, Determination of the Specific Migration of DEHP into Food Simulants Using High Performance Liquid Chromatography *Journal of High Resolution Chromatography* 22 (1) (1998), pp. 70-72.

48. A. O'Brien, A. Goodson and I. Cooper, Polymer additive migration to foods : a direct comparison of experimental data and values calculated from migration models for high density polyethylene (HDPE) *Food Additives and Contaminants* 16 (9) (1999), pp. 367-380.

49. K. O'Callaghan, P.M. Fredericks and D. Bromwich, Evaluation of Chemical Protective Clothing by FT-IR/ATR Spectroscopy *Applied Spectroscopy* 55 (5) (2001), pp. 162A-170A.

50. I.S. Arvanitoyannis and L. Bosnea, Migration of substances from food packaging materials to foods *Critical reviews in food science and nutrition* 44 (2) (2004), pp. 63-76.

51. C. Caner and B. Harte, Effect of high-pressure processing on the migration of antioxidant Irganox 1076 from polypropylene film into a food simulant *Journal of the science of food and agriculture* 85 (1) (2005), pp. 39-46.

52. J.F. Jen and T.C. Liu, Determination of phthalate esters from food-contacted materials by on-line microdialysis and liquid chromatography *Journal of chromatography* 1130 (2006), pp. 28-33.

53. A.S. Silva, J.M. Cruz Freire, R. Franz and P.P. Losada, Time-temperature study of the kinetics of migration of diphenylbutadiene from polyethylene films into aqueous foodstuffs *Food Research International* 41 (2) (2008), pp. 138-144.

54. Harrick N.J., Internal Reflection Spectroscopy. New York: (1979)

55. F.M. Mirabella ed, Internal Reflection Spectroscopy, Theory and Applications. Marcel Dekker,(1992)

56. Popov V.Y. Lavrent'ev V.V., Role of depth of penetration in ATR spectroscopy *Translated from Zhurnal Prikladnoi Spektroskopii* 32 (2) (1979), pp. 336-342.

57. N.J. Harrick and F.K. du Pre, Effective Thickness of Bulk Materials and of Thin Films for Internal Reflection Spectroscopy *Applied Optics* 5 (11) (1966), pp. 1739-1743.

58. Jr. Mirabella F.M., Quantitative Analysis of Polymers by Attenuated Total Reflectance Fourier-Transform Infrared Spectroscopy: Vinyl Acetate and Methyl Content of Polyethylenes *Journal of Polymer Science: Polymer Physics Edition* 20 (1982), pp. 2309-2315.

59. K. Nishikida and R.W. Hannah, Kramers-Kronig Calculation of the Grazing Angle Reflection Spectrum of Barrier Oxide Layer on Aluminum *Applied Spectroscopy* 46 (6) (1992), pp. 999-1001.

60. R.T. Graf, J.L. Koenig and H. Ishida, Optical Constant Determination of Thin Polymer Films in the Infrared *Applied Spectroscopy* 39 (3) (1985), pp. 405-408.

61. L.D. Tickanen, M.I. Tejedor-Tejedor and M.A. Anderson, Concurrent Determination of Optical Constants and the Kramers-Kronig Integration Constant (Anchor Point) Using Variable-Angle ATR/FT-IR Spectroscopy *Applied Spectroscopy* 46 (12) (1992), pp. 1848-1858.

62. J.B. Huang, J.W. Hong and M.W. Urban, Attenuated total reflectance Fourier transform infra-red studies of crystalline-amorphous content on polyethylene surfaces *Polymer* 33 (1992), pp. 5173-5178

63. N.J. Harrick, Internal Reflection Spectroscopy. New York: Interscience Publishers, (1973)

64. V.V. Lavrent'ev, V.Ya. Popov and R.A. Vasenin, Study of diffusion in boundary layers of polymer films by repeated disturbed full internal reflection of IR spectra *Polymer Science U.S.S.R.* 17 (7) (1975), pp. 1869-1872.

65. N.A. Remizov, A.Ye. Chalykha, V.Ya. Popova and V.V. Lavrent'ev, Determination of the diffusion constants of liquids in polymers by sorption and by internal reflection spectroscopy *Polymer Science U.S.S.R.* 24 (8) (1982), pp. 1853-1859.

66. G. Van Alsten J., Diffusion Measurements in Polymers Using IR Attenuated Total Reflectance Spectroscopy *Trends in Polymer Science* 3 (1995), pp. 272-276.

67. E.J. Vorenkamp, J. van Ruiten, F.A. Kroesen, J.G. Meyer, J. Hoekstra and G. Challa, Interdiffusion and adhesion of poly (vinyl chloride) and poly (methyl methacrylate) *Polymer Communications* 30 (1989), pp. 116-120.

68. N.E. Schlotter and P.Y. Furlan, Small Molecule Diffusion in Polyolefins Monitored using the Infrared Evanescent Field *Vibrational Spectroscopy* 3 (1992), pp. 147-153.

69. P.Y. Furlan, Hydrogenated Polybuadiene Morphology and Its Effects on Small Molecule Diffusion *Macromolecules* 25 (1992), pp. 6516-6522.

70. Xu J.R. Balik C.M., Studies of Latex Paint Films Exposed to Aqueous $SO_2$: pH Effects *Journal of Applied Polymer Science* 39 (1990), pp. 1957-1966.

71. R. Xu J. and M. Balik C., Measurement of diffusivities of small molecules in polymers using FT-IR-ATR *Applied spectroscopy* 42 (8) (1988), pp. 1543-1548.

72. M. Balik C. and R. Xu J., Simultaneous measurement of water diffusion, swelling, and calcium carbonate removal in a latex paint using FTIR-ATR *Journal of Applied Polymer Science* 52 (1994), pp. 975-983.

73. G. Van Alsten J. and C. Coburn J., Structural effects on the transport of water in polyimides *Macromolecules* 27 (14) (1994), pp. 3746-3752.

74. S. Banerjee, R.P. Semwal and S. Agarwal, Measurement of Diffusivities of Sulfur Mustard (SM) and Its Analog Oxygen Mustard (OM) in Cured Butyl, Nitrile, and Natural-Rubber Sheets by Weight Gain and FTIR-ATR Methods *Journal of Applied Polymer Science* 57 (1995), pp. 1483-1490.

75. R.P. Semwal, S. Banerjee, L.R. Chauhan, A. Bhattacharya and N.B.S.N. Rao, Study of Diffusion and Sorption of Bis-(2-chloroethyl)sulfide (SM) and Bis-(2-~hloroethyl)ether (OM) Through Polypropylene (PP) and Biaxial-Oriented Polypropylene (BOPP) Films by the FTIR-ATR Spectroscopic Method *Journal of Applied Polymer Science* 60 (1996), pp. 29-35.

76. V.Y. Popov and V.V. Lavrent'ev, Role of depth of penetration in ATR spectroscopy *Journal of Applied Spectroscopy* 32 (2) (1980), pp. 193-198.

77. A.M.L. Tralhão, A.C. Watkinson, K.R. Brain, J. Hadgraft and N.A. Armstrong, Use of ATR-FTIR Spectroscopy to Study the Diffusion of Ethanol Through Glycerogelatin Films *Pharmaceutical Research* 12 (4) (1995), pp. 572-575.

78. S. Hajatdoost and J. Yarwood, ATR-FTIR spectroscopic studies of the structure and permeability of sulfonated poly(ether sulfone) membranes Part 3. Effects of sorption and desorption, and of annealing *Journal of the Chemical Society, Faraday Transactions* 93 (1997), pp. 1613-1620.

79. M.R. Pereira and J. Yarwood, ATR-FTIR spectroscopic studies of the structure and permeability of sulfonated poly(ether sulfone) membranes Part 2.Water diffusion processes *Journal of the Chemical Society, Faraday Transactions* 92 (15) (1996), pp. 2731-2143.

80. S.U. Hong, T.A. Barbari and J.M. Sloan, Diffusion of Methyl Ethyl Ketone in Polyisobutylene: Comparison of Spectroscopic and Gravimetric Techniques *Journal of polymer science. Part B. Polymer physics* 35 (8) (1997), pp. 1261-1267.

81. U. Hong S., A. Barbari T. and M. Sloan J., Multicomponent diffusion of methyl ethyl ketone and toluene in polyisobutylene from vapor sorption FTIR-ATR spectroscopy *Journal of polymer science. Part B. Polymer physics* 36 (2) (1998), pp. 337-344.

82. C. Sammon, J. Yarwood and N. Everall, A FTIR–ATR study of liquid diffusion processes in PET films: comparison of water with simple alcohols *Polymer* 41 (2000 ), pp. 2521–2534.

83. C. Sammon, C. Mura, J. Yarwood, N. Everall, R. Swart and D. Hodge, FTIR-ATR Studies of the Structure and Dynamics of Water Molecules in Polymeric Matrixes. A Comparison of PET and PVC *Journal of Physical Chemistry B* 102 (18) (1998), pp. 3402-3411.

84. Y.A. Elabd and T.A. Barbari, Acetic acid diffusion in polyisobutylene : Probing small molecule structures *Industrial & engineering chemistry research* 40 (14) (2001), pp. 3076-3084.

85. Y.A. Elabd and T.A. Barbari, Separating Solvation from Molecular Diffusion in Polymers *American Institute for Chemical Engineering Journal* 47 (6) (2001), pp. 1255-1262.

86. Y.A. Elabd and T.A. Barbari, Multicomponent Diffusion of Hydrogen-Bonding Solutes in a Polymer *American Institute for Chemical Engineering Journal* 48 (8) (2002), pp. 1610-1620.

87. M. Ohman, D. Persson and C. Leygraf, In situ ATR-FTIR studies of the aluminium/polymer interface upon exposure to water and electrolyte *Progress in Organic Coatings* 57 (2006), pp. 78-88.

88. Kinigakis Panos, Opportunities exist for better food packaging materials. Food and Drug Packaging, (June, 2007)

89. T. Rydlo, J. Miltz and A. Mor, Eukaryotic Antimicrobial Peptides : Promises and Premises in Food Safety *Journal of Food Science* 71 (9) (2006), pp. R125-R135.

90. P. Phoopuritham, M. Thongngam, R. Yoksan and P. Suppakul, Antioxidant and radical scavenging activities of selected plant extracts and possible application in active packaging *15th IAPRI World Conference of Packaging* (2006)

91. N.V. Yanishlieva, E. Marinova and J. Pokorny, Natural Antioxidants from herbs and spices *European Journal of Lipid Science and Technology* 108 (2006), pp. 776-793.

92. S. Fujisawa, T. Atsumi, Y. Kadoma, H. Sakagami and J. Han, Antioxidant and prooxidant action of eugenol related compounds and their cytotoxicity *Toxicology* 177 (2002), pp. 39-54.

93. L. Jirovetz, G. Buchbauer, I. Stoilova, A. Stoyanova, A. Krastanov and E. Schimdt, Chemical Composition and Antioxidant Properties of Clove Leaf Essential Oil *Journal of Agricultural and Food Chemistry* 54 (2006), pp. 6303-6307.

94. R.A. Holley and D. Patel, Review Improvement in shelf-life and safety of perishable foods by plant essential oils and smoke antimicrobials *Food Microbiology* 22 (2005), pp. 273-292.

95. M. Valero and M.C. Salmeron, Antibacterial activities of 11 essential oils against Bacillus Cereus in tyndallized carrot broth *International Journal of Food Microbiology* 85 (2003), pp. 73-81

96. A. Remmal, R. Khadija, T. Bouchikhi, A. Tantaoui-Elaraki and K. Sendide, The Mechanism of Bactericidal Action of Oregano and Clove Essential Oils and of their Phenolic Major Components on Escherichia coli and Bacillus subtilis *Journal of Essential Oil Research* 15 (2003), pp. 356-362.

97. Christelle Marie Laot, M.S. thesis, Spectroscopic Characterization Of Molecular Interdiffusion at a Poly(vinyl pyrrolidone) / vinyl ester interface. Virginia Polytechnic Institute and State University. 1997

98. Pike Technologies, ATR MAX II User Manual. Madison: (2007)

99. R.J. Freund and W.J. Wilson, Statistical Methods. Academic Press, (2003)

100. J.V. Beck and K.J. Arnold, Parameter Estimation in Engineering and Science. New York: John Wiley & Sons, (1977)

101. H. Yasuda and A. Peterlin, Diffusive and Bulk Flow Transport in Polymers *Journal of Applied Polymer Science* 17 (1973), pp. 433-442.

102. O. Vitrac, J. Lezervant and A. Feigenbaum, Decision Trees as Applied to the Robust Estimation of Diffusion Coefficients in Polyolefins *Journal of Applied Polymer Science* 101 (2006), pp. 2167–2186.

103. W. Limm and H.C. Hollifield, Modelling of additive diffusion in polyolefins *Food additives and contaminants* 13 (8) (1995), pp. 949-967.

104. D. Cava, J.M. Lagaron, A. Lopez-Rubio, R. Catala and R. Gavara, On the applicability of FT-IR spectroscopy to test aroma transport properties in polymer films *Polymer Testing* 23 (2004), pp. 551–557.

105. A.A. Asfour, M. Saleem, D. DeKee and B. Harrison, Diffusion of saturated hydrocarbons in low density polyethylene (LDPE) films *Journal of Applied Polymer Science* 38 (8) (2003), pp. 1503 - 1514.

106. M. Saleem, A.A. Asfour, D. DeKee and B. Harrison, Diffusion of organic penetrants through low density polyethylene (LDPE) films: Effect of size and shape of the penetrant molecules *Journal of Applied Polymer Science* 37 (3) (2003), pp. 617 - 625.

107. K. Moller and T. Gevert, An FTIR Solid-state Analysis of the Diffusion of Hindered Phenols in Low-Density Polyethylene (LDPE): The Effect of Molecular Size on the Diffusion Coefficient *Journal of Applied Polymer Science* 51 (1993), pp. 895-903.

108. Center for Veterinary Medicine, Guidance for Industry Status of Clove Oil and Eugenol for Anesthesia of Fish. U.S. Department of Health and Human Services, Food and Drug Administration, http://govdocs.aquake.org/cgi/reprint/2003/813/8130070.pdf

109. J.P.H. Linssen, J.C.E. Reitsma and J.L. Cozijnsen, Migration of Antioxidants from Polyolefins into Ethanolic Simulants *Packaging technology & science* 11 (1998), pp. 241-245.

110. C.D. Soto-Cantú, A.Z. Graciano-Verdugo, E. Peralta, A.R. Islas-Rubio, A. González-Córdova, A. González-León and H. Soto-Valdez, Release of butylated

hydroxytoluene from an active film packaging to asadero cheese and its effect on oxidation and odor stability *Journal of Dairy Science* 91 (2008), pp. 11-19.

111. Kermit.S. Kwan Jr, PhD thesis, The Role of Penetrant Structure on the Transport and Mechanical Properties of a Thermoset Adhesive, Chapter 4. Virginia Polytechnic Institute and State University. 1998